



FACULTY OF SCIENCE AND TECHNOLOGY

## MASTER'S THESIS –REPORT

**Study programme / specialisation:** Engineering Structures and Material Science / Mechanical Systems

**The spring semester, 2022**

**Open / Confidential**

**Author:** Navaneethan S. Kurukkal

.....  
(Signature Author)

**Course coordinator:** Prof. Hirpa G. Lemu

**Supervisor(s):** Prof. Hirpa G. Lemu and Yosef W. Adugna

**Thesis title:** Study of medical image data transformation techniques and compatibility analysis for 3D printing

**Credits (ECTS):** 30

**Keywords:**

Additive Manufacturing, 3D Printing, Reverse Engineering, Medical 3D Printing, Segmentation, 3D Slicer, FreeCAD, MeshLab, Solid Modelling, Femur, DICOM, NRRD

**Pages:** 126

**+ appendix:** 12

**Stavanger, June 21, 2022**

---

## **PREFACE**

The research presented in this thesis is a fulfilment of the Master of Science programme in Mechanical and Structural Engineering with a specialisation in mechanical systems at the University of Stavanger, Department of Mechanical and Structural Engineering and Material Science. The thesis was written during the spring semester of 2022.

I would like to express my gratitude and appreciation to my supervisor, Professor Hirpa G. Lemu, for all the feedback and support throughout this master's thesis and for allowing me to work on this interesting and relevant topic. I would also like to thank Yosef W. Adugna, who also supervised me, for his support, guidance, and input in conducting this thesis.

During the experimentation process, Andreas Skaare (engineer of IMBM laboratory at UiS) provided excellent assistance and expertise in familiarising the scanning process and the relevant software. Thank you for facilitating the use of the different scanners utilised during the experiments.

I would like to thank my friends and fellow students, Jon Erik Karlsen, Usman Shaukat and Cristina Tawede Besin, for their continuous moral support throughout this master's, and especially during the period of the thesis.

Last but not least, I would like to thank my wife, Mayuri Swaminathan, for supporting me throughout the master's studies period and also my sister, brother and parents for their continuous support and motivation.

## ABSTRACT

Various applications exist for additive manufacturing (AM) and reverse engineering (RE) within the medical sector. One of the significant challenges identified in the literature is the accuracy of 3D printed medical models compared to their original CAD models. Some studies have reported that 3D printed models are accurate, while others claim the opposite. This thesis aims to highlight the medical applications of AM and RE, study medical image reconstruction techniques into a 3D printable file format, and the deviations of a 3D printed model using RE. A case study on a human femur bone was conducted through medical imaging, 3D printing, and RE for comparative deviation analysis. In addition, another medical application of RE has been presented, which is for solid modelling. Segmentation was done using opensource software for trial and training purposes, while the experiment was done using commercial software. The femur model was 3D printed using an industrial FDM printer. Three different non-contact 3D scanners were investigated for the RE process. Post-processing of the point cloud was done in the VX Elements software environment, while mesh analysis was conducted in MeshLab. The scanning performance was measured using the VX Inspect environment and MeshLab. Both relative and absolute metrics were used to determine the deviation of the scanned models from the reference mesh. The scanners' range of deviations was approximately from -0.375 mm to 0.388 mm (range of about 0.763mm) with an average RMS of about 0.22 mm. The results showed that the mean deviation of the 3D printed model (based on 3D scanning) has an average range of about 0.46mm, with an average mean value of about 0.16 mm.

# Table Of Contents

<b>Preface</b> .....	<b>i</b>
<b>Abstract</b> .....	<b>ii</b>
<b>Abbreviations</b> .....	<b>v</b>
<b>List of Figures</b> .....	<b>vi</b>
<b>List of Tables</b> .....	<b>ix</b>
<b>CHAPTER 1: Introduction</b> .....	<b>1</b>
1.1. Background .....	1
1.2. Objectives.....	2
1.3. Limitations.....	3
1.4. Methodology .....	3
1.5. Scope of work.....	4
<b>CHAPTER 2: Additive Manufacturing or 3D Printing and Applications in the medical sector</b> .....	<b>6</b>
2.1. Additive Manufacturing or 3D Printing .....	6
2.2. General steps of the AM process.....	8
2.2.1 <i>CAD Model</i> .....	8
2.2.2 <i>Slicing</i> .....	11
2.3. Medical Applications of AM and 3DP.....	15
2.4. Medical Model Accuracy .....	22
<b>CHAPTER 3: Reverse engineering in medical applications</b> .....	<b>27</b>
3.1. Reverse Engineering.....	27
3.2. 3D scanning technologies.....	29
3.3. Medical Imaging.....	32
3.4. Medical applications of reverse engineering.....	33
3.4.1 <i>Dentistry</i> .....	35
3.4.2 <i>Tissue Engineering</i> .....	36
3.4.3 <i>Medical Devices</i> .....	37
3.5. 3D Scanning and Reverse Engineering to Measure Accuracy.....	39
3.6. Medical Application Of Reverse Engineering For Solid Modeling.....	40
3.6.1 <i>Geometric modeling</i> .....	40
3.6.2 <i>Solid modeling using FreeCAD</i> .....	41

<b>CHAPTER 4: Medical imaging, 3d printing, and reverse engineering: compatibility study of human femur bone</b> .....	<b>52</b>
4.1. Segmentation And Preparation Of Medical Image Data.....	53
4.2. Segmentation Of Femur Bone.....	62
4.3. Post-processing.....	63
4.4. 3D Printing Process.....	64
4.5. Reverse engineering.....	67
4.5.1 3D Scanning Of Femur.....	68
4.5.2 Handyscan 700.....	74
4.5.3 Artec EVA-M.....	78
4.5.4 Einscan HX.....	80
4.6. Post processing using MeshLab.....	82
4.7. Deviation Analysis.....	87
<b>CHAPTER 5: Results and Discussion</b> .....	<b>89</b>
5.1. Solid Modelling Results.....	89
5.2. Qualitative analysis.....	92
5.3. Quantitative Analysis.....	94
5.4. VX Inspect results.....	96
5.5. MeshLab Results.....	100
<b>CHAPTER 6: Conclusion</b> .....	<b>104</b>
<b>CHAPTER 7: References</b> .....	<b>107</b>
<b>Appendix A</b> .....	<b>127</b>
<b>Appendix B</b> .....	<b>131</b>
<b>Appendix C</b> .....	<b>135</b>

## ABBREVIATIONS

<b>2D</b>	Two-dimensional
<b>3D</b>	Three-dimensional
<b>3DP</b>	Three-dimensional Printing
<b>AI</b>	Artificial Intelligence
<b>AM</b>	Additive manufacturing
<b>ASTM</b>	American Society for Testing and Materials
<b>CAD</b>	Computer aided drawing
<b>CAM</b>	Computer aided drawing
<b>CMM</b>	Coordinate Measuring Machine
<b>CNC</b>	Computerised numerical control
<b>CT</b>	Computerised tomography
<b>DICOM</b>	Data Imaging and Communications in Medicine
<b>FEA</b>	Finite Element Analysis
<b>FEM</b>	Finite Element Methods
<b>ISO</b>	International Organization for Standardization
<b>LED</b>	Light Emitting Diode
<b>LMD</b>	Laser Metal Deposition
<b>MRI</b>	Magnetic resonance imaging
<b>PLA</b>	Polylactic acid
<b>RE</b>	Reverse engineering
<b>SLS</b>	Selective Laser Sintering
<b>SLM</b>	Selective Laser Melting
<b>STL</b>	Standard Tessellation Language / Standard Triangle Language
<b>VP</b>	Vat photopolymerisation

# LIST OF FIGURES

Figure 1-1 - Objectives Flowchart .....	2
Figure 2-1 – Highlights of some problems with CNC machining .....	7
Figure 2-2 – General process applicable to AM and 3DP .....	8
Figure 2-3 - 3/4 section view of UiS Drillbotics PDM 2022 .....	9
Figure 2-4 – Split model with two components (1 and 2), UiS Drillbotics PDM 2022 .....	10
Figure 2-5 – PDM Slicing errors, UiS Drillbotics PDM 2022.....	10
Figure 2-6 - STL file example (ASCII) .....	12
Figure 2-7 - Single facet and slicing plane .....	13
Figure 2-8 - Visualisation of the slicing process.....	14
Figure 2-9 - GCODE example .....	15
Figure 2-10 - Workflow for creating 3D models from DICOM images.....	17
Figure 2-11 - AM and 3DP Research within Medical Sector (2021-2022).....	18
Figure 2-12 - Implants through AM/3DP research by countries (2021-2022) .....	18
Figure 2-13 - AM/3DP in tissue engineering research by countries (2021-2022).....	19
Figure 3-1 - RE vs. Traditional Design Process.....	28
Figure 3-2 - Reverse Engineering Process .....	29
Figure 3-3 - 3D scanning classification [73, 75].....	30
Figure 3-4 - a) Traditional Workflow vs. b) Digital Workflow for dental applications.....	31
Figure 3-5 - Medical Imaging Modalities .....	33
Figure 3-6 - Medical applications of RE.....	39
Figure 3-7 - Mesh design workbench and imported model in FreeCAD.....	42
Figure 3-8 - Cross-section tool.....	43
Figure 3-9 - Cross-sections of the femur .....	43
Figure 3-10 - Polyline sketch .....	44
Figure 3-11 - Loft created using polyline (wireframe representation).....	45
Figure 3-12 - Sketch using Bezier Curve (before adjustments).....	46
Figure 3-13 - Sketch using Bezier Curve (after adjustments).....	46
Figure 3-14 - Sketch using Cubic Bezier Curve .....	47
Figure 3-15 - Sketch using B-spline curve.....	48
Figure 3-16 - Sketch created using NURBS Curve .....	49
Figure 3-17 - Sketch created by joining points using B-Spline Curves.....	50
Figure 3-18 - Split mesh model of the femur.....	51

Figure 4-1 - Import medical image into 3D Slicer.....	54
Figure 4-2 - Highlighting the lung region using the paint tool .....	55
Figure 4-3 - Highlighting the lung region using the level tracing tool .....	56
Figure 4-4 – Segmentation of the lungs using thresholding .....	57
Figure 4-5 – Level tracing for filling between slices .....	58
Figure 4-6 – Fill between slices segmentation.....	58
Figure 4-7 – 3D visualisation of segmentation conducted by fill between slices.....	59
Figure 4-8 – Smoothened model of lungs (fill between slices) .....	59
Figure 4-9 - Selecting seed and background segment.....	60
Figure 4-10 – Preview of grown segments .....	60
Figure 4-11 – Segmentation of the lungs .....	61
Figure 4-12 – 3D visualisation of the lungs.....	61
Figure 4-13 – Smoothened model of the lungs (grow from seeds).....	61
Figure 4-14 – Mimics environment (segmentation) .....	63
Figure 4-15 - Mesh Analysis in FreeCAD and Prusa slicer.....	63
Figure 4-16 - Fortus 450mc (Industrial FDM 3D printer at UiS).....	65
Figure 4-17 - Initial import and slicing .....	66
Figure 4-18 - Final import and slicing .....	67
Figure 4-19 - 3DP Model of femur .....	67
Figure 4-20 - 3D printed femur model from Embodi3D .....	69
Figure 4-21 - Raw scan data vs post processed model .....	70
Figure 4-22 - 3D printed model vs. scanned model.....	71
Figure 4-23 - Suitable scanning angle of a femur model for Handyscan 700 .....	72
Figure 4-24 - Scanning of femur using CMM .....	73
Figure 4-25 - Handyscan 700.....	74
Figure 4-26 – Initial scan of femur using Handyscan 700.....	74
Figure 4-27 – 3DP model setup of femur for scanning (Handyscan 700) .....	75
Figure 4-28 – Artec EVA-M.....	79
Figure 4-29 – Scanning process using Artec EVA-M .....	79
Figure 4-30 - Einscan HX .....	80
Figure 4-31 - Shining3D Pre-setting.....	80
Figure 4-32 – 3DP model setup of femur for scanning (Einscan HX) .....	81
Figure 4-33 - Alignment of femur scans in Shining3D .....	81
Figure 4-34 - Imported scans in MeshLab .....	82
Figure 4-35 - Points chosen for pre-alignment .....	84



Figure 4-36 - Completed Global Alignment.....	84
Figure 4-37 - Transformation matrices (reference vs transformed).....	84
Figure 4-38 - Merged Model.....	85
Figure 4-39 - Holes fixed using close hole function in MeshLab.....	86
Figure 4-40 - Before and applying remeshing filter to Poisson Reconstructed model.....	87
Figure 5-1 - Final Solid Model of femur.....	89
Figure 5-2 - Final solid model vs. reference model.....	90
Figure 5-3 - Solid model using FreeCAD.....	91
Figure 5-4 - Handyscan 700 model converted directly to solid in Autodesk Inventor.....	91
Figure 5-5 - Feature based comparison of the original CAD model, 3D printed model and CAD models obtained from the different scanning processes.....	92
Figure 5-6 - CMM measurement vs. STL CAD Model digital measurement.....	93
Figure 5-7 - Femur STL model details (top) Scanning points vs. no. of vertices comparison(bottom).....	94
Figure 5-8 – Maximum, minimum and the range of deviation of the scanned models.....	95
Figure 5-9 - Region of maximum and minimum deviation.....	96
Figure 5-10 – Deviations (left) and Box & Whisker plot (right) for Snapshot 1.....	97
Figure 5-11 - Deviations (left) and Box & Whisker plot (right) for Snapshot 2.....	98
Figure 5-12 - Deviations (left) and Box & Whisker plot (right) for Snapshot 3.....	99
Figure 5-13 - Deviations (left) and Box & Whisker plot (right) for Snapshot 4.....	100
Figure 5-14 - Box and whisker plots of deviation data from each scanner.....	102
Figure 5-15 - Box and Whisker plots of Hausdorff distances.....	103

## LIST OF TABLES

Table 2-1 - Various medical applications of AM .....	20
Table 2-2 - Methods employed for accuracy assessments.....	22
Table 2-3 - Research articles studying the accuracy of 3DP medical models .....	23
Table 3-1 - Methods of applying RE and 3D scanning for accuracy assessment of medical models .....	39
Table 4-1 - Printing Parameters for femur bone (FDM Fortus 450mc).....	65
Table 4-2 - 3D scanner Details ( [162–164]) .....	68
Table 4-3 - Post processing of femur scan in VX Elements .....	76
Table 5-1 - FreeCAD vs. Autodesk Model.....	90

# CHAPTER 1: INTRODUCTION

## 1.1. Background

3D printing (3DP) or additive manufacturing (AM) has various applications within many industries. Adding material layer by layer has created many possibilities in the manufacturing industry. Applications include rapid prototyping, low-volume manufacturing, and industries with high levels of customization. In the same sectors that require high levels of customization, the process of acquiring the design information becomes key. In that regard, another process that goes hand in hand with AM and 3DP is reverse engineering (RE).

One such sector that has had many applications of both AM and RE is the medical sector. 3DP enables the production of patient-specific medical devices that are usually not possible using conventional manufacturing methods. Acquiring design information for these purposes is generally conducted through medical imaging or 3D scanning, in essence, RE.

In this regard, a literature study is presented in this report to examine how 3DP and RE technologies are applied in the medical sector. With a particular focus on AM and RE technology, materials and resources used, and applications.

Medical image file formats are not compatible with performing 3D analyses. Therefore, a transformation process is required to obtain a file format that can be used in CAD or finite element software. The significant aspects of moving from a medical image to a 3D printed model have been studied in this thesis.

One of the critical challenges identified in the literature study is the accuracy of 3D printed medical models. The accuracy and inaccuracy of anatomical models used for surgical purposes, teaching, implants, and finite element analysis (FEA) have been reported in various works of literature. This report presents a case study that investigates a 3D printed model created from medical image reconstruction.

Norway is one of the countries with the highest registered incidence of hip fractures in the world. About 60% of the hip fractures are in the femoral neck, a few in the caput, and the rest are in the trochanteric region, called trochanteric, pertrochanteric, or intertrochanteric fractures [1]. As such, the anatomical structure used in this thesis is a human femur bone model.

## 1.2. Objectives

### General Objective

Medical imaging is the process of obtaining information about the body's interior for diagnostic or treatment purposes and can be obtained from different imaging modalities. The general objective of the thesis is to investigate the compatibility of medical images with 3D printing file formats through an accuracy assessment.

The aim is to study the quality of medical image reconstruction as part of the accuracy assessment. The assessment will include both qualitative (visual and subjective) and quantitative (numerical and objective) analyses.

In addition, the RE process will be explored in the medical context for solid modeling and comparative deviation analysis, i.e., as a tool for quality assurance. A flow chart has been presented in Figure 1-1 to visualise the general objective of the thesis.

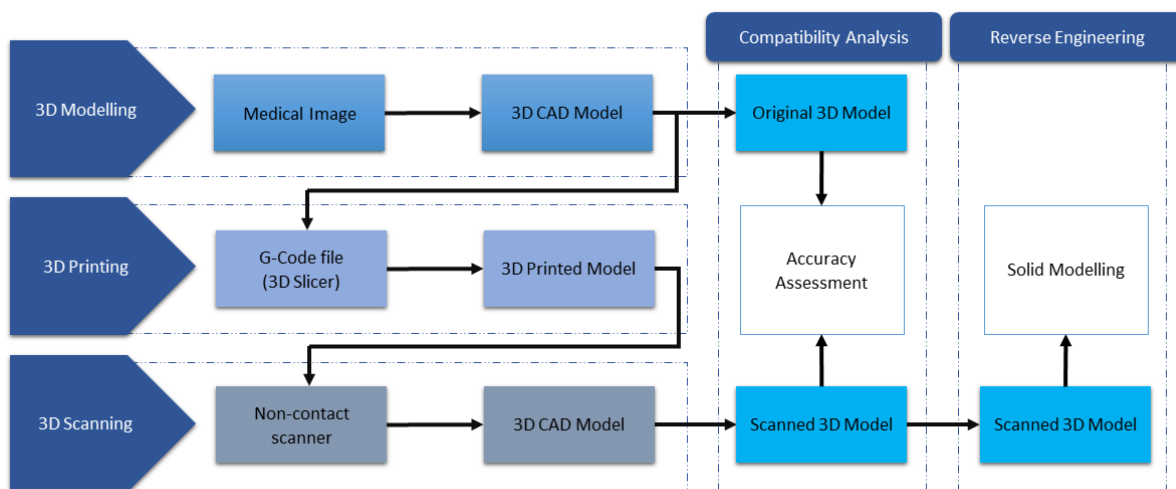


Figure 1-1 - Objectives Flowchart

A medical image will be segmented to extract an anatomical structure model to obtain a 3D CAD model. The CAD model will be used to create a physical representation using 3D printing. The 3D printed model will then be reverse engineered for compatibility analysis through accuracy assessment using non-contact scanning methods. The outcome of the scanning process will be compared with the original CAD model.

## Specific Objectives

The specific objectives of the thesis are as follows:

- 1) A closer review of the application of 3D printing in the medical sector
- 2) A closer review of 3D scanning applications for reverse engineering with a particular focus on medical applications.
- 3) The conversion process of medical image data for 3D printing purposes
- 4) Reverse engineering of an anatomical structure for compatibility analysis

### **1.3. Limitations**

To create a physical model, the first step is medical image acquisition, thereafter segmentation, and then a 3D CAD model is used for 3D printing. The study conducted in this thesis is limited to the second and third steps and not the medical image acquisition process.

The deviation analysis conducted in this thesis considers only deviation caused during 3D printing and the scanning process. Regarding accuracy, the models' deviation from the STL file created from the medical image reconstruction will be considered rather than the medical correctness of the anatomical structure itself.

The most widely used AM technology within the medical sector is fused deposition modeling (FDM) 3D printing. For the studies conducted in this thesis, the 3D printing will be limited to FDM.

### **1.4. Methodology**

An overview of the methodology implemented in the thesis is given below. 3.6 describes in detail the methodology implemented for the experimental work.

- Literature review/study
  - Making use of books, journals, articles, interviews, and other online materials to conduct a literature review
- 3D model from medical image (STL)
  - *Data:*

- medical images from Emobdi3D [2] for trial purposes and
  - medical images from the Stavanger universitetssjukehus for the experiment.
  - **Techniques:** Segmentation using opensource software (3D slicer) for trial purposes and commercial software (Mimics) for the experiment.
- 3D Printing
- **Data:** CAD models from medical image reconstruction (STL)
  - **Techniques:** FDM 3D printer available at UiS (Fortus 450mc)
- 3D Scanning
- **Data:** 3D printed model
  - **Techniques:** 3D scanning with three different scanners available at UiS (Handyscan 700, Einscan HX, and Artec EVA-M)
- Compatibility Analysis
- **Data:** CAD models of 3D printed parts using 3D scanning
  - **Techniques:** Comparative deviation inspection using commercial software (VX Inspect) and open-source software (MeshLab)
- Solid modelling through RE
- **Data:** CAD models of 3D printed parts using 3D scanning
  - **Techniques:** Solid modelling in opensource software (FreeCAD)

## 1.5. Scope of work

This report is divided into two main parts. The first part presents the definition of the thesis, objectives, and the literature study on AM, RE, and medical applications. The second part of this report presents the experimental work conducted to achieve the objectives of this study. In that regard, the thesis layout is as follows:

### ***Part 1 – Introduction and literature review***

- *Chapter 1*

An introduction to the thesis is given in this chapter, together with the purpose and objectives of the studies conducted in this thesis.

- *Chapter 2*

In this chapter, various applications of AM within the medical sector are presented using information gathered from the literature review on medical applications of AM.

The methods used in various accuracy assessments and deviation analyses of medical models are extracted from literature and summarised.

- *Chapter 3*

In this chapter, various applications of RE within the medical sector are presented using information gathered from the literature review on medical applications of RE. The methods used in various accuracy assessments and deviation analyses of medical models using RE and 3D scanning are extracted from literature and summarised.

## ***Part 2 – Experimental work and results***

- *Chapter 4*

This chapter describes in detail the methods, processes, and resources utilized in this thesis for the purposes of 3D printing and RE. In particular, the methodology implemented in the compatibility study of a human femur bone model created using 3D printing will be presented. Furthermore, the methodology implemented during the RE process is presented as well.

- *Chapter 5*

The results obtained from 3D printing and scanning are presented and discussed in this chapter. The results obtained from the solid modelling process are also presented and discussed.

- *Chapter 6*

The conclusions based on the observed results and future works are presented in this chapter.

- *Chapter 7*

The bibliography has been presented in this chapter

## **CHAPTER 2: ADDITIVE MANUFACTURING OR 3D PRINTING AND APPLICATIONS IN THE MEDICAL SECTOR**

In this chapter, various applications of AM within the medical sector are presented using information gathered from various literature on medical applications of AM. An overview of AM and 3D printing is first discussed. The importance of the CAD model and the slicing process for 3D printing is explained.

### **2.1. Additive Manufacturing or 3D Printing**

The advent of 3DP (or AM) has had revolutionary impacts in the field of fabrication and manufacturing. AM makes it possible for on-demand, cost-effective and rapid production of components in comparison to conventional fabrication methods. These qualities have made these technologies a viable alternative in many fields. Creating objects in a successive layer-by-layer fashion through stereolithography has paved the way for greater possibilities in various sectors, including the field of medicine.

AM refers to a group of manufacturing technologies that create physical objects using CAD by joining material in a layer-by-layer fashion. It is different from traditional processes where cutting, drilling, and grinding operations are employed to remove excess or unwanted material from a solid piece of material to create an object [3]. AM is quite lenient in comparison to traditional manufacturing processes for complex geometry fabrication and is one of the core technologies of Industry 4.0.

The American Society for Testing and Materials (ASTM), together with the International Organization for Standardization (ISO), has classified AM technologies as follows [3]: photopolymer vat, material extrusion, powder bed fusion, directed energy deposition, sheet lamination, Material jetting, binder jetting.

Some of the main advantages of AM technologies over traditional manufacturing are [4, 5]:

- Design flexibility – layer-by-layer fabrication enables the fabrication of complex geometry (e.g., organic shapes).



- Cost of geometric complexity – A simple change in design can cause significant production time changes using traditional manufacturing processes. With the use of AM technology, there are no additional costs when implementing complex geometry.
- Dimensional accuracy – current expectations of AM technology require standards to govern the accuracy of finished products. This is mainly because of the shrinkage effects of AM-produced parts and the post-processing when removing support structures.
- Need for assemblage – complex shapes may have to be produced in segments and later assembled with traditional manufacturing. There is no need for that with AM technology. Single parts can be printed in a single go with the aid of support. This also applies to parts with multiple components. In essence, AM technologies make the process somewhat a seamless process.
- Time and cost efficiency in the production run – when it comes to low quantity parts and on-demand fabrication, AM technologies are more suitable.

Some of the problems with CNC machining for components with complex shapes are highlighted in Figure 2-1. Medical models are often made up of organic (complex) shapes. The challenges of manufacturing these models using conventional methods are similar to those highlighted in Figure 2-1. The components displayed are part of the bottom hole assembly used in the Drillbotics project.

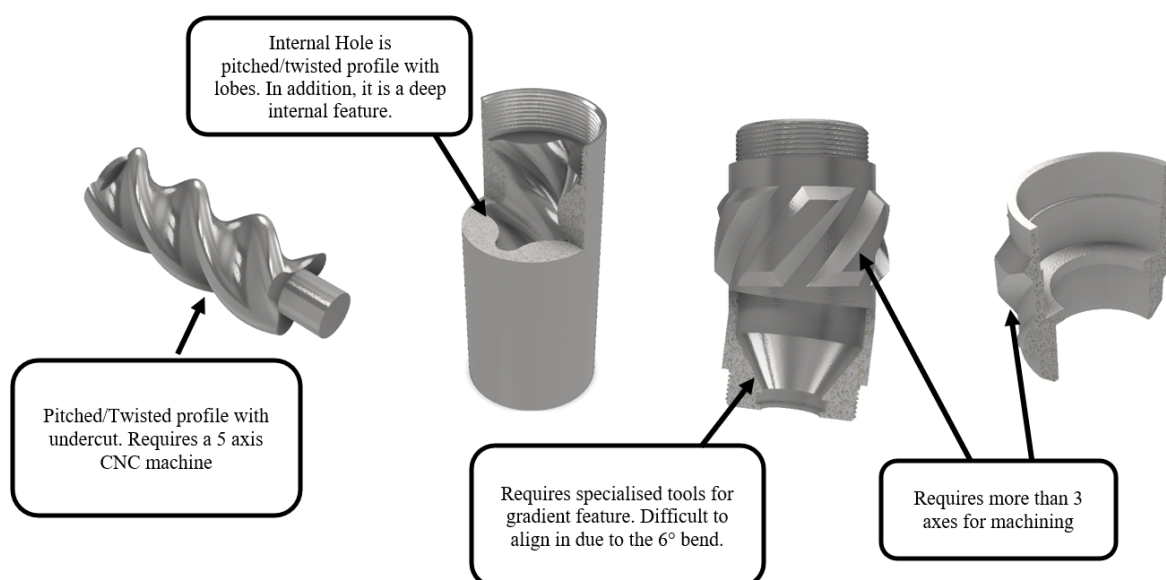


Figure 2-1 – Highlights of some problems with CNC machining

## 2.2. General steps of the AM process

Whether it is for prototyping, model making, or product development, some general steps are taken to produce a 3D printed part (Figure 2-2). The below-mentioned steps might differ slightly between different AM technologies. Each step in this process might have more steps or subprocesses within them, depending on the purpose of 3D printing. E.g., in the case of designing or product development, more steps will lie in the product design process, whereas in the model-making process, there will be more postprocessing. The key aspects of the CAD model and the slicing process will be presented thereafter.

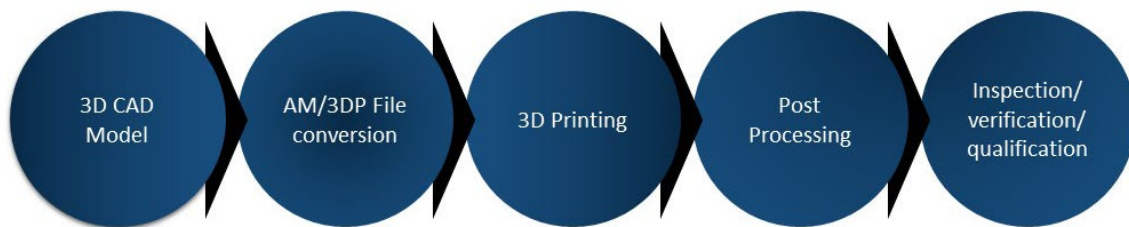


Figure 2-2 – General process applicable to AM and 3DP

The subsections to follow highlight the importance of the CAD file and slicing for 3D printing. In medical applications, a CAD model is required for the printing of an anatomical structure or an ROI extracted during segmentation. The output of the segmentation process is a surface model, essentially a mesh. The quality of the mesh is determined by the segmentation process. The quality of the segmentation can influence the interpolation of the 2D segments to create a 3D model and thus creating errors in the slicing process. It is for this reason that the importance of the CAD file and slicing for 3D printing is emphasized in the sections to follow.

### 2.2.1 CAD Model

The representation of an idea can be in many forms. However, for the process of 3DP, a 3D digital model is required. A 3D digital model can be created or sourced through different avenues. In the design process, concepts and final designs can be created using solid modelling

techniques a CAD software (such as Autodesk Inventor or Solidworks). Alternatively, an already existing object/product can be 3D scanned to get the geometrical information and thus a 3D digital model. If we consider a 3D digital model as the input for the AM process, there are at least three possibilities of input, viz. CAE, RE technology, and haptic-based CAD [5].

A closed, “watertight” model without any gaps is required for preprocessing so that the part can be 3D printed. For 3D printing, problems that can arise in this step are when poor modelling techniques are implemented during the solid modelling process or due to older, poorly developed 3D CAD software. Generally, these can be detected in meshing or slicing software once imported and analyzed.

Example: As part of the Drillbotics project, a positive displacement motor was designed in the CAD software Autodesk Inventor (Figure 2-3). During the design process, separate models were created from a single CAD model using the split function in the software (Figure 2-4, components 1 and 2). During the prototyping phase, the model was to be 3D printed, and this model that was split was then imported into the Prusa slicing software, where an error was encountered.

Using the auto-repair feature was not helpful as the sliced model also turned out to be incorrect. The problem in this model was that the imported component was not “closed” or “watertight” due to the splitting surface in the original CAD model. The problem was solved by importing a solid model where the splitting function was removed.

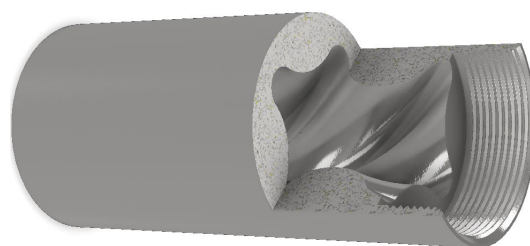


Figure 2-3 - 3/4 section view of UiS Drillbotics PDM 2022

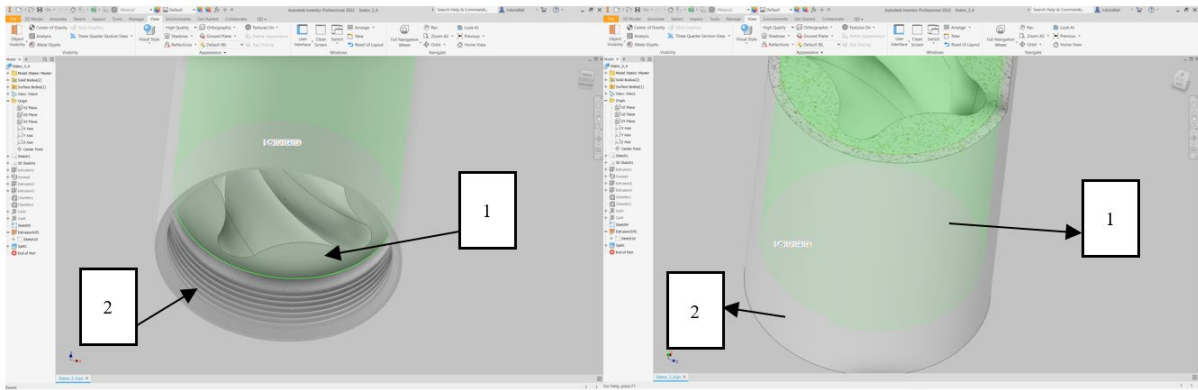


Figure 2-4 – Split model with two components (1 and 2), UiS Drillbotics PDM 2022

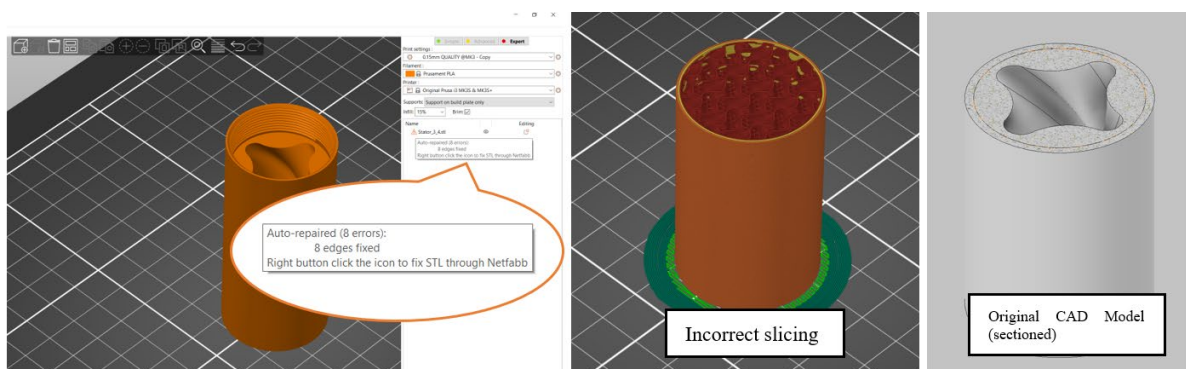


Figure 2-5 – PDM Slicing errors, UiS Drillbotics PDM 2022

In the case of medical images, the CAD file is reconstructed from the segmentation process. If the segmentation process is not conducted correctly or if the post-processing in terms of mesh smoothing and repairing is not conducted correctly, this could lead to errors created during slicing and, in turn, inaccuracies while 3D printing.

### *File Format*

The solid model can be in many different file formats, most of which are unique to a particular brand/franchise of commercial software or open-source software. E.g. for Autodesk Inventor, it is “.ipt,” for Solidworks, it is “.sldpart,” and for FreeCAD, it is “.FCADstd”.

The most common type of file format that 3D models are converted to for 3D printing is STL (Standard Tessellation Language or Standard Triangle Language). It has been the de facto standard for AM and 3DP for over two decades [6, 7]. All solid modelling software allows for the export of local solid models to STL file format. Additional options are also available in CAD software such as Autodesk Inventor and Solidworks, such as ASCII or binary format,

resolution, normal deviation, maximum edge length, and aspect ratio. Other file formats that can be used for slicing are OBJ, AMF, and 3MF. A brief description of these file formats is given below:

- *OBJ (Wavefront file format)* files to store information just like STL with vertices and edges but use polygonal faces together with texture information
- *AMF (Additive Manufacturing File)* makes use of curved triangles to store geometric information
- *3MF (3D Manufacturing formats)* stores 3D model information such as 3D textures, licensing, and signature information

### **2.2.2 Slicing**

3D printers function from numerically controlled apparatuses and require information in a format that the 3D printers' processor can read to print the component. The language used by most standard 3D printers is in GCODE, although some machines use X3G language. X3G is also a 3D printer file used by some desktop printers. The main difference is that GCODE is text-based while X3G is binary.

The CAD model contains a component's geometrical, material, and texture information and cannot be directly imported into slicing software to generate GCODE. They have to be converted to 3D printable file format so the CAD model can be sliced. As mentioned earlier, the STL file format is the standard file format. STL (*ASCII or Binary*) files to store information in the form of normal vectors, and vertices make triangular faces. In Figure 2-6, the general format of the information in an STL file is shown together with an example. STL files do not contain information about colours and textures.

```

solid name
{
  facet normal  $n_i n_j n_k$ 
  outer loop
    vertex  $v_{1_x} v_{1_y} v_{1_z}$ 
    vertex  $v_{2_x} v_{2_y} v_{2_z}$ 
    vertex  $v_{3_x} v_{3_y} v_{3_z}$ 
  end loop
end facet
endsolid name

```

```

3_4_Stator.stl
1 solid ASCII
2 facet normal -5.000000e-01 0.000000e+00 8.660254e-01
3 outer loop
4 vertex 1.212436e+01 0.000000e+00 7.000000e+00
5 vertex 1.039230e+01 0.000000e+00 6.000000e+00
6 vertex 1.212436e+01 -3.000000e+00 7.000000e+00
7 endloop
8 endfacet
9 facet normal -5.000000e-01 0.000000e+00 8.660254e-01
10 outer loop
11 vertex 1.212436e+01 -3.000000e+00 7.000000e+00
12 vertex 1.039230e+01 0.000000e+00 6.000000e+00
13 vertex 1.039230e+01 -3.000000e+00 6.000000e+00
14 endloop
15 endfacet
16 facet normal 8.549119e-01 -0.000000e+00 5.187733e-01
17 outer loop
18 vertex 1.039230e+01 -3.000000e+00 6.000000e+00
19 vertex 1.039230e+01 0.000000e+00 6.000000e+00
20 vertex 1.012070e+01 -3.000000e+00 6.447595e+00
21 endloop
22 endfacet

660060 facet normal -2.290105e-01 4.840496e-01 8.445414e-01
660061 outer loop
660062 vertex 8.979080e+00 -4.931758e+01 -8.422455e+00
660063 vertex 9.216305e+00 -4.965879e+01 -8.162564e+00
660064 vertex 9.361976e+00 -4.965879e+01 -8.123063e+00
660065 endloop
660066 endfacet
660067 facet normal -5.027603e-01 3.293670e-01 7.992180e-01
660068 outer loop
660069 vertex 1.017949e+01 -4.965879e+01 -7.739809e+00
660070 vertex 9.823893e+00 -4.931758e+01 -8.104122e+00
660071 vertex 1.005169e+01 -4.965879e+01 -7.820206e+00
660072 endloop
660073 endfacet
660074 endsolid
660075

```

General format of STL (ASCII)

Information in STL file for stator

Figure 2-6 - STL file example (ASCII)

There are several software platforms available (both commercial and open-source) that can convert CAD models to a file format that can be read by the processor of a 3D printer. The most common open-source slicers are Cura, Slic3r, Prusaslicer, and Octoprint.

Since 3D printing is conducted by adding material layer by layer, the CAD model needs to be sliced, the projected profile needs to be extracted, and motion commands need to be generated so the printer can create the layers. By studying open-source platforms like Pruslicer [8] and Slic3r [9], the algorithm used to create each layer can be deduced. The process of slicing is given hereafter.

The STL file is read to extract the information about each vertex, and this information is stored in different matrices. The maximum height and minimum base locations are determined from the Z coordinates. Thereafter the slicing is done by adding the layer thickness input by the end-user.

- The slicing plane position is given by the equation:  $Z_{SlicingPlane} = Z_{modelMinimum} + slicethickness$ .
- The individual face maximum and minimum z-coordinate values are assessed, i.e.:  $Z_a \leq Z_{SlicingPlane} \leq Z_b$  or  $Z_b \leq Z_{SlicingPlane} \leq Z_c$  or  $Z_a \leq Z_{SlicingPlane} \leq Z_c$
- Once one of the above conditions is fulfilled, the intersecting line can be determined via linear interpolation between the intersecting plane and the intersecting edges of the facet.
- The interpolation is based on the orientation of the triangle. E.g., the Prusa slicer determines the orientation of the facet edge based on the vertices. W.r.t to the slicing plane [10]:
  - The intersecting planes cut two edges
  - One vertex is above the slicing plane while the other two are in-line
  - One vertex is below the slicing plane while the other two are in-line
  - One edge is shared by two triangles, and each has a point either above, below, or in line with the cutting plane
  - All three vertices are in-line with the plane

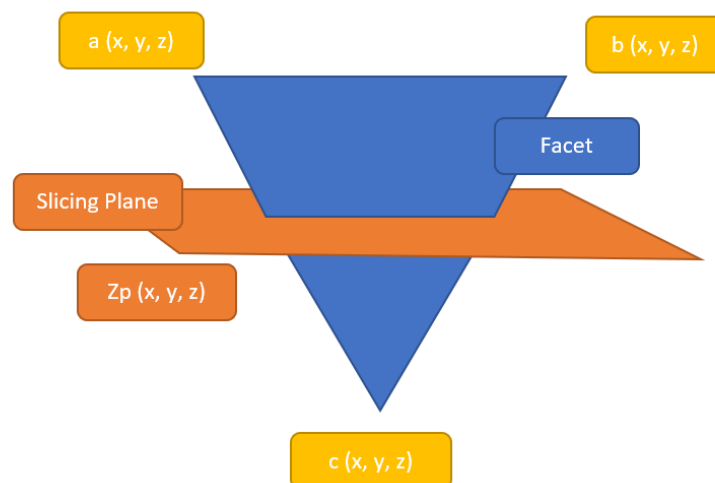


Figure 2-7 - Single facet and slicing plane

A set of intersecting lines are collected using the abovementioned procedure. At this point, there is a general outline of the profile. These lines are then connected to create polygons that become the profile to be printed. This procedure is highlighted in the Slic3r documentation available online [11]. A visualization of this process is shown in Figure 2-8. Once the polygons

are created, they are then converted to GCODE or X3G file format. Thus, the polygons (as can be seen in Figure 2-8) will be used to create the motion path for the printer.

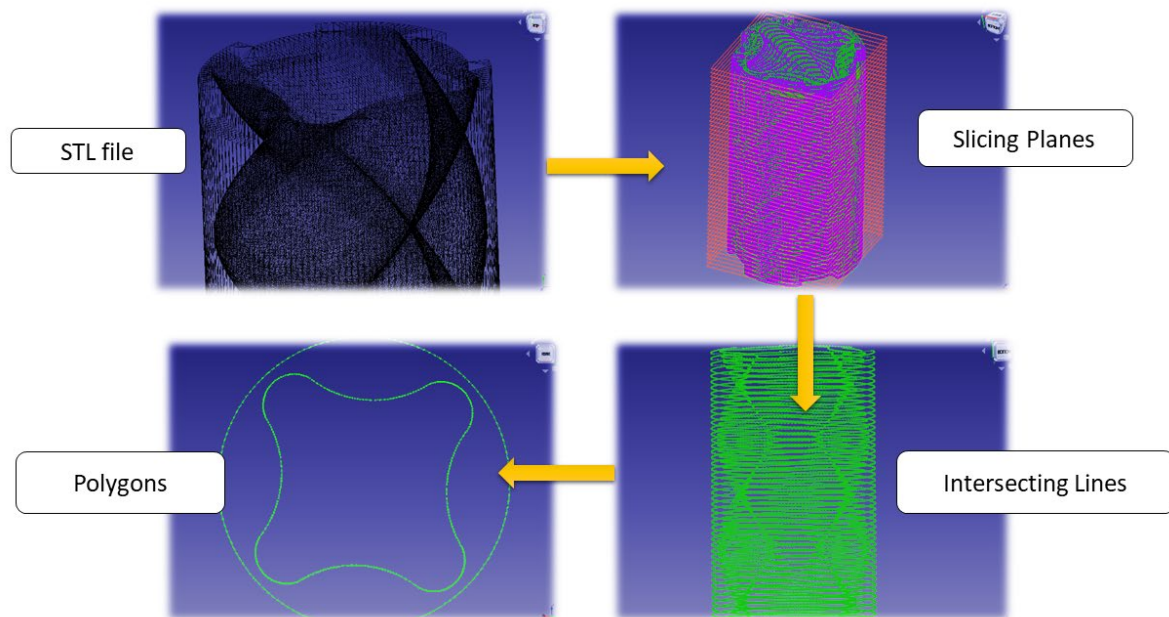


Figure 2-8 - Visualisation of the slicing process

An example of the GCODE that is generated for 3D printing purposes is given in Figure 2-9. Most lines of the code contain code about the motion of the printer tool, i.e., speed and position. For a 3D printer specifically, the code will contain information such as:

- Heating and cooling of the nozzle and print bed
- The setting of nozzle and print bed temperatures
- Auto levelling
- Melting of some plastic before printing (cleaning)



```

1 ; generated by PrusaSlicer 2.3.3+win64 on 2022-04-20 at 07:59:59 UTC
2
3 ;
4
5 ; external perimeters extrusion width = 0.45mm
6 ; perimeters extrusion width = 0.45mm
7 ; infill extrusion width = 0.45mm
8 ; solid infill extrusion width = 0.45mm
9 ; top infill extrusion width = 0.40mm
10 ; support material extrusion width = 0.35mm
11 ; first layer extrusion width = 0.42mm
12
13 M73 P0 R996
14 M73 Q0 S1001
15 M201 X1000 Y1000 Z200 E5000 ; sets maximum accelerations, mm/sec^2
16 M203 X200 Y200 Z12 E120 ; sets maximum feedrates, mm/sec
17 M204 P1250 R1250 T1250 ; sets acceleration (P, T) and retract acceleration (R), mm/sec^2
18 M205 X8.00 Y8.00 Z0.40 E4.50 ; sets the jerk limits, mm/sec
19 M205 S0 T0 ; sets the minimum extruding and travel feed rate, mm/sec
20 M107
21 ;TYPE:Custom
22 M862.3 P "MK3S" ; printer model check
23 M862.1 P0.4 ; nozzle diameter check
24 M115 U3.10.0 ; tell printer latest fw version
25 G90 ; use absolute coordinates
26 M83 ; extruder relative mode
27 M104 S215 ; set extruder temp
28 M140 S60 ; set bed temp
29 M190 S60 ; wait for bed temp
30 M109 S215 ; wait for extruder temp
31 G28 W ; home all without mesh bed level
32 G80 ; mesh bed leveling
33 G1 Y-3.0 F1000.0 ; go outside print area
34 G92 E0.0
35 G1 X60.0 E9.0 F1000.0 ; intro line
36 M73 Q0 S1000
37 G1 X100.0 E12.5 F1000.0 ; intro line
38 G92 E0.0
39 M221 S95

```

```

1999747 ;WIPE_START
1999748 G1 F0640.000
1999749 G1 X113.159 Y102.400 E-0.20030
1999750 G1 X113.606 Y102.106 E-0.12366
1999751 G1 X113.916 Y101.971 E-0.07798
1999752 G1 X114.231 Y101.795 E-0.08328
1999753 G1 X114.682 Y101.613 E-0.11235
1999754 G1 X115.112 Y101.336 E-0.11805
1999755 G1 X115.287 Y101.256 E-0.04439
1999756 ;WIPE_END
1999757 G1 E-0.04000 F2100.000
1999758 G1 Z192.800 F10800.000
1999759 G1 X122.339 Y98.607
1999760 G1 Z192.400
1999761 G1 E0.80000 F2100.000
1999762 ;TYPE:Top solid infill
1999763 ;WIDTH:0.405134
1999764 G1 F2400.000
1999765 G1 X122.690 Y98.958 E0.00791
1999766 G1 X122.950 Y99.482 E0.00932
1999767 G1 X123.281 Y99.774 E0.00705
1999768 G1 X123.466 Y100.004 E0.00471
1999769 G1 X123.588 Y100.246 E0.00432

```

Figure 2-9 - GCODE example

### 2.3. Medical Applications of AM and 3DP

The applications of AM are quite vast. The applications of AM technologies in the field of aerospace [12], automotive [13], construction [14], supply chain [15], food [16], electronics [17], and many other fields [18–21] engineering is quite readily available in various literature.

It is interesting to note that if one searches the database google scholar with key words “3D printing applications” or “additive manufacturing applications,” the number of works of literature that surface related to the applications of AM and 3DP in the medical industry is quite broad. With the aid of CT, MRI, and other scanners, medical practitioners have 3D information of an anatomical part at their disposal. The conversion of this information to a physical object via 3DP has led to many possibilities in terms of research and applications.

Historically speaking, 3DP has its roots in photo sculptures in the 1860s. SLA is similar to the 1950s technology known as “Photo glyph recording” [4]. In terms of milestones and key events, the medical industry's historical developments of 3DP and AM technologies have been compiled by Nestic et al. [22]. A summary of this development is as follows:

- 1984: Invention of SLA 3DP
- 1986: Invention of Selective Laser Sintering (SLS)
- 1988: First commercial SLA 3D printer and bioprinting (micro-positioning of 2 cells)
- 1989: Fused deposition modelling patent
- 1999: Very first 3D printed organ (bladder)
- 2000: First commercial extrusion-based bioprinter
- 2002: Very first early-stage kidney prototype was bioprinted
- 2003: First inkjet bioprinter
- 2005: Open-source initiative RepRap to build a 3DP
- 2007: SLS printer becomes available (metal and plastic)
- 2008: 3D printing of prosthetic leg
- 2009: 3D printing of blood vessels
- 2012: 3D printing of jaw
- 2014: 3D printing of human liver tissue was also the first desk-top bioprinter
- 2015: First implanted 3D-printed bioresorbable scaffold for periodontal repair
- 2018: 3D printing of full human tissue (skin) model
- 2019: 3D printing of heart that contracts that contain blood vessels 3D-printed lung air-sac with surrounding blood vessels
- 2020: 3D printer for personalized medicine M3DIMAKER (FabRx)

Applications of AM technology and 3DP span across various medical sectors, including medical devices, teaching and education, training and simulation, research and preoperative planning, and bio-printing organ replacements. The aspect that works well between AM and medical applications is that medical models are organic in shape, and AM technology allows the fabrication of these models with much more convenience compared to conventional manufacturing methods [23].

The applications of AM technologies in the medical field are within dentistry [24–27], tissue organs and tissue models [28–30], medical devices [31–34], anatomical models [35–37], and pharmaceutical applications [38–40] and others [41–44]. The process of 3D printing medical and physical models is shown in Figure 2-10 [44–47].

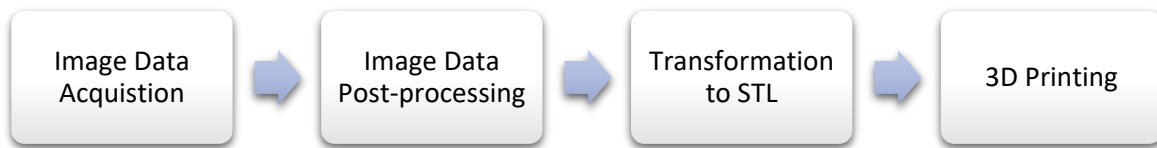


Figure 2-10 - Workflow for creating 3D models from DICOM images

A literature review was conducted to better understand the applications of AM in the medical industry, determine the current research applications and trends, and highlight the challenges encountered with the implementation of AM technology and 3D printing in the medical sector. The medical fields of interest are neurosurgery, cardiovascular, dentistry, tissue organs, medical devices, anatomical models, and pharmaceutical applications.

The Scopus database was used to explore the most recent research material on the specific topics by searching with keywords “additive manufacturing,” “3D printing”, and the respective medical field, which are:

- Tissue engineering
- Pharmaceutical
- Neurosurgery
- Medical Devices
- Implants
- Dentistry
- Cardiology
- Anatomical Models

Additional filters were added to gain open access to journal articles that were published from 2021 to date in English. The number of articles mentioned below has been filtered in this manner and by further filtering articles pertinent to that medical sector. The number of publications for each medical sector for the chosen period of 2021-2022 is shown in Figure 2-11. The global distribution of research articles published in tissue engineering and medical implants based on AM is presented in Figure 2-12 and Figure 2-13. In Table 2-1, some applications have been highlighted together with the various software platforms for CAD and the material that was used for printing.

## AM and 3DP Research within Medical Sector (2021-2022)

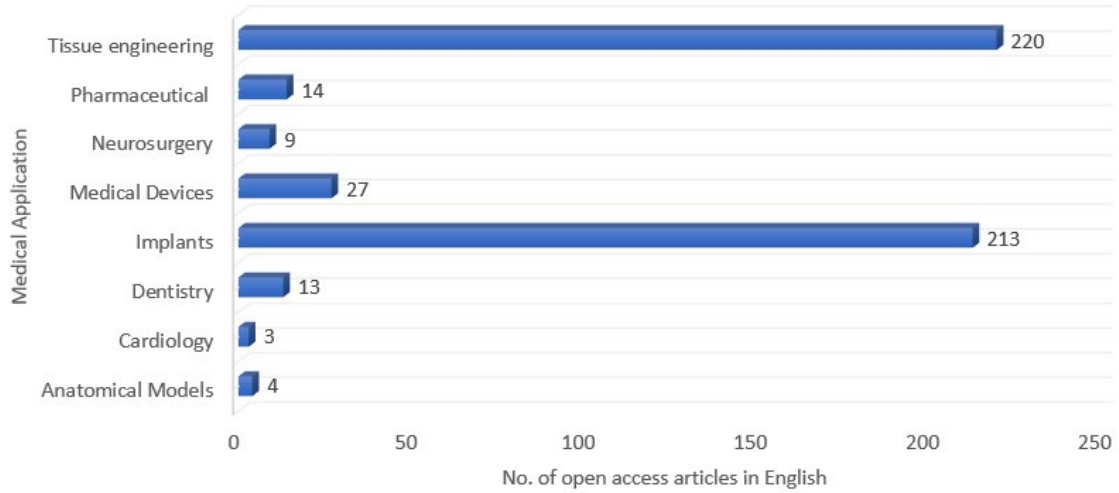


Figure 2-11 - AM and 3DP Research within Medical Sector (2021-2022)

## Implants through AM/3DP research by countries (2021-2022)

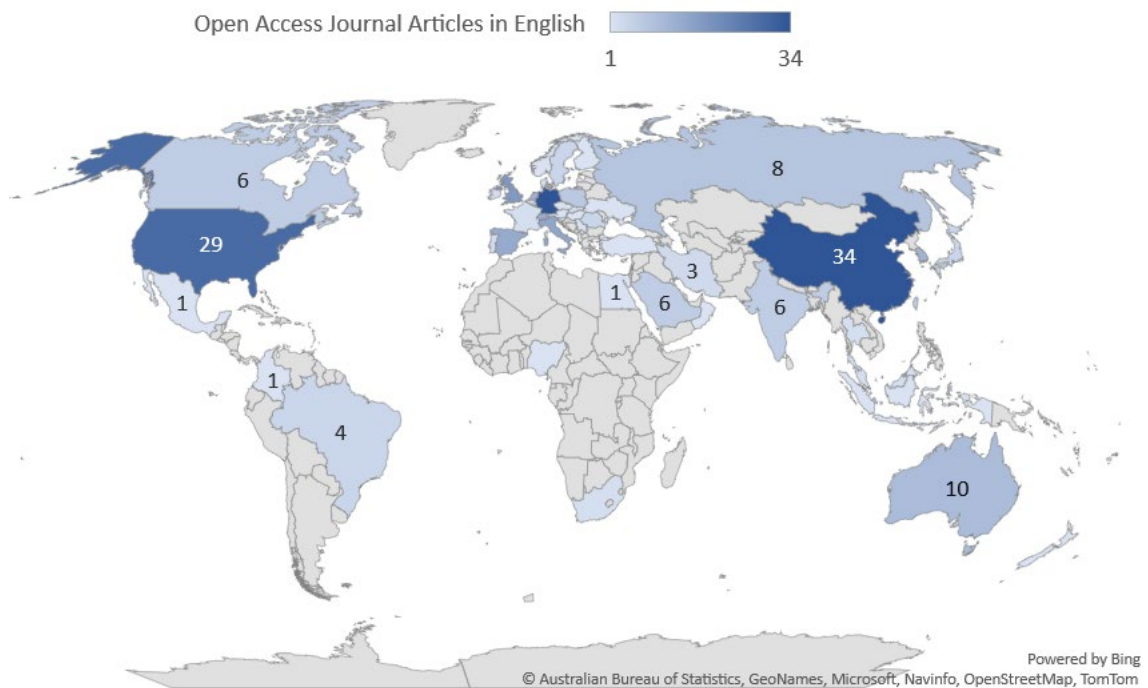


Figure 2-12 - Implants through AM/3DP research by countries (2021-2022)

## Tissue engineering through AM/3DP research (2021-2022)

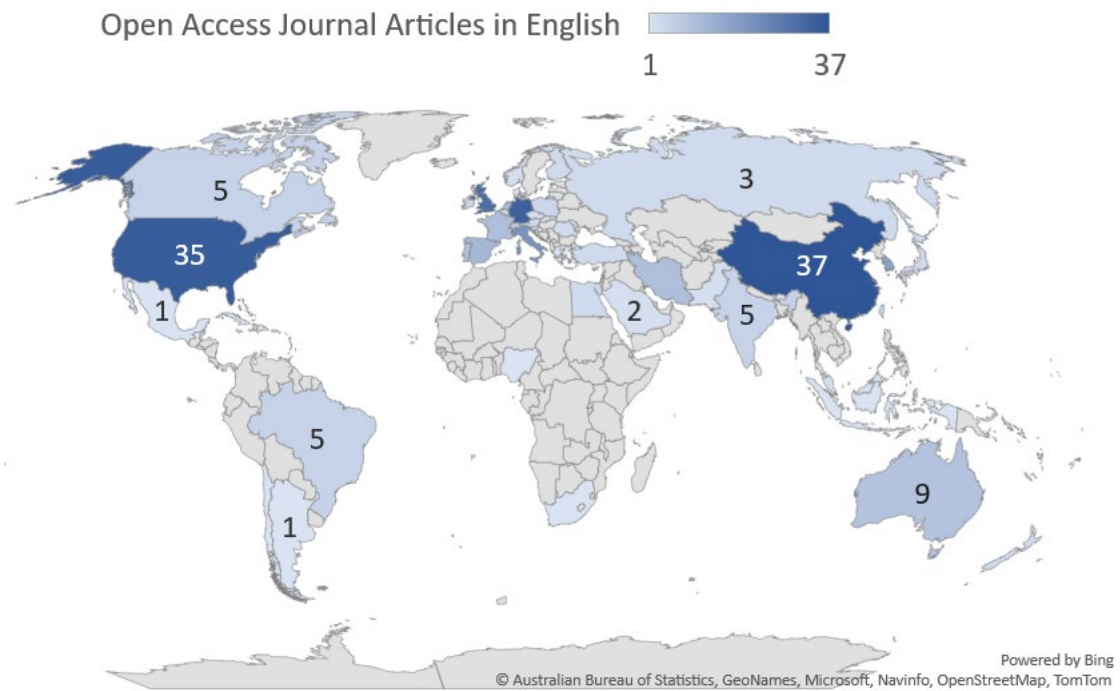


Figure 2-13 - AM/3DP in tissue engineering research by countries (2021-2022)

Figure 2-12 and Figure 2-13 portray the global distribution of areas that have publications in the fields of medical implants and tissue engineering, and AM applications. Countries like the USA and China have the highest number of publications in this regard.

Table 2-1 - Various medical applications of AM

<b>Medical Application</b>	<b>DICOM to STL</b>	<b>Image acquisition</b>	<b>CAD Software</b>	<b>AM Technology / 3DP Method</b>	<b>Printing Material</b>	<b>Reference</b>
Surgical Planning and Anatomy teaching	N/A	Portable 3D scanner (Creaform 3D GO Scan)	VXElements, Geomagic Inc	FDM	ABS with resin support	[48]
	D2P Software	CT scanning	Geomagic Inc	Color jet printing	Gypsum	[49]
	Invesalius	CT scanning	Mashmixer, Magics	SLS	Polyamide	[50]
	N/A	Echocardiographic imaging	N/A	FDM	PLA	[51]
Implants	N/A	N/A	N/A	LMD	Ti-Al-xNb Ternary Alloy	[52]
Medical Device	N/A	Intraoral 3D digital scanner	Meshmixer	3D stereolithography printer	Dental LT Clear Resin Denture Teeth Resin	[53]
	N/A	Intraoral 3D digital scanner	Geomagics control	digital light processing 3D printer	Polymethyl methacrylate	[54]
		Intraoral 3D digital scanner	Model Builder software	Polyjet technology	Ceramic	[55]
		Intraoral 3D digital scanner	Zbrush	Polyjet technology	Polymer material, silicone	[56]
		Intraoral 3D digital scanner	Inlab, Meshmixer, TinkerCAD	Independent Dual extrusion	Polyethylene terephthalate glycol (PETG), thermoplastic filament	[57]

---

Scan 500 device (Interscience)	ExoCad Gateway	Digital light processing printing technology (DLP) Stereolithograph y printing technology (SLA)	Liquid, light- curing (meth)acrylate- based onecomponent material Dimethacrylate- based resins with photo-initiator, and pigments (Meth)acrylated oligomers, (meth)acrylated monomers, photo-initiator	[58]
-----------------------------------	----------------	---	--	------

---

## 2.4. Medical Model Accuracy

A significant challenge with medical 3D printing is the dimensional accuracy of the 3D printed models. When it comes to complex surgeries, creating accurate medical models from DICOM images is a useful technique for surgery planning[59, 60]. The inaccuracy of anatomical models used for surgical purposes, teaching, and implants has been reported in different works of literature [46, 61–67]. Besides the deviation of a 3DP model due to shrinkage and different 3DP methods, other steps in the model acquisition processes can lead to inaccuracies in the model [45, 46]. An overview of some studies that reported 3D printed models as accurate and inaccurate has been presented in Table 2-3. Some of the methods employed to conduct the analyses will be presented in Table 2-2.

Table 2-2 - Methods employed for accuracy assessments

<b>Image Acquisition</b>	<b>DICOM to STL</b>	<b>3DP Technology</b>	<b>Deviation Measurement Method</b>	<b>Deviation Analysis software</b>	<b>Reference</b>
CT	OsiriX Materialise	SLM	Contact and Non-contact 3D scanning	GOM Inspect	[62]
CT	OsiriX	FDM	Physical measurements using digital calipers	N/A	[68]
CT	3D Slicer	N/A	CT	Meshlab	[69]
CT/MRI	Mimics	VP	Calipers and Micrometers	N/A	[70]
CT	Synapse3D	FDM	CT Scanning	N/A	[71]
Cone Beam CT	Mango 3D Slicer STL Model Creator	ColorJet Printing (CJP)	3D Scanning	GOM Inspect	[45]
CT	OsiriX	FDM	Electronic caliper	N/A	[66]



Table 2-3 - Research articles studying the accuracy of 3DP medical models

Objective	Method	Results	Conclusion and Future Works	Reference
Evaluate the accuracy of 3D models across different pathologies to understand spatial relationships and safe pre-surgical planning	3D printing of 7 medical models across different pathologies in VP, with different resins. Compare models with their original CT and MRI DICOMs	All models showed a deviation of less than 1mm dimensional error	In the case where a dimensional error of less than 1mm is acceptable, 3D printing models can be utilized for presurgical planning and other clinical uses. For much higher accuracy requirements, further research must be conducted for improvement.	[70]
Determine the accuracy of femoral head models created by 3D printing	RE using CT scanning of cadaveric femur bones. 3D printed femur models and thereafter measuring the organic bone, and 3D printed bone using digital vernier callipers	The deviation of the femur 3D printed model ranges between - 0.22mm and 0.099mm.	3D printed models are accurate in comparison to their bony cadaveric counterparts and can be used for surgical planning and other medical applications	[68]
To compare the accuracy of 3D printed medical models for Robot-Assisted Partial Nephrectomy	Scan of previously printed medical models with the CT scan of the corresponding model	14 out of the 16 models that were scanned were considered to be valid, i.e., within acceptable ranges of accuracy	3D printed models are anatomically correct and can assist in Robot-Assisted Partial Nephrectomy. The reliability of surgical assistance from 3D	[71]

---

printed models needs to be evaluated

---

Accuracy of consumer-grade FDM printers vs. industrial SLS pinner [66]

CT images of a dry skull were obtained and 3D printed on an FDM and SLS printer with 100, 250, and 500-micrometer layers

The SLS printer produced slightly more accurate models (0.3% deviation) than FDM (0.44%, 0.52%, 1.1% deviations)

Consumer-grade FDM models were concluded to be sufficiently accurate for maxillofacial surgery planning

---

Demonstrate the inaccuracies caused by DICOM to STL conversion [45]

Obtain STL files of converted skull DICOM images from three different institutes. 3DP models and scan them for dimensional analysis using CAD

Significant variations in the 3DP model vs. the original DICOM image.

Research is to be conducted on developing methods for converting DICOM data to a suitable CAD/CAM format for maximum accuracy. Testing of methods of printing to determine the most accurate.

---

Compare the errors obtained from a reference model to a model obtained from varying parameters during the building steps. [63]

3DP print medical model as a base model. Thereafter vary parameters in the model building steps and print models for comparison with the base model.

Standard building processes tend to overestimate the size of the model. High curvature areas display the greatest number of errors.

Modification of the standard building process, particularly segmentation algorithms.

---

Determine the impact of manual and automatic thresholding [65]

Obtain images from cadaver heads and STL models of the bony structure in the head with

Manual thresholding results in better STL models than default thresholding.

Development of new approaches based on pattern recognition and machine learning

---

	manual and automatic thresholding			
Determine the errors obtained from a referee model to a model obtained from varying parameters in all building steps, such as CT protocols and thresholding values. Also, determine errors caused by 3D printing when using an end-implant	Use of pig head to create a reference model and subsequently print models with varying thresholds and CT photos for comparison. CAD software was used to determine the error. The implant was 3D printed to determine printing errors	CT scanning, 3D modelling, and AM errors were determined in the bony structure and the implant that was printed	The use of AM in a clinical setting requires precise tools in the entire process chain for accurately creating patient-specific anatomic geometries. Focusing on each step in the process allows for quality control and assurance protocol that may prevent treatment or restoration	[62]
Determine the accuracy of 3DP liver models.	3DP liver models from CT images. Thereafter CT scans the printed models and conducts dimensional analysis	The most significant deviation was 1.92mm. However, the median deviation was less than the CT slice height	Further work is to be done on the impact of pre-surgical planning based on 3DP medical models.	[69]

The data in Figure 2-11 shows that in the past year or so, there has been quite a significant amount of research regarding AM and 3DP applications in the medical sector, especially within tissue engineering and medical implants. In addition, Figure 2-12 and Figure 2-13 show the global distribution in research within tissue engineering and medical implants. Countries such as China, the USA, Germany, the UK, and Italy have a higher number of publications. In terms of numbers, this is also the case for the other medical applications of AM and 3DP.

This information in Table 2-1 shows the variety of AM technologies and the various materials that have been implemented in different medical applications. An interesting observation that can be made from the information presented here is that the image acquisition process is not always from medical imaging (such as from CT/MRI scans). For clinical studies, the use of 3D scanners is also quite prominent. The use of 3D scanners for medical applications will be discussed in the next chapter.

It can also be observed that commercial software is not the only option for clinical studies and opensource software is quite popular. This applies to CAD software such as TinkerCAD and segmentation software such as 3D slicer, and mesh analysis software such as MeshLab.

The information extracted from the literature and presented in Table 2-2 provides a good overview of the resources used to conduct accurate assessments. The deduction from this information is that the deviation analysis can be conducted using contact or non-contact and comparing physical or digital models. The general trend is to have a reference model created from the original acquisition process and compare it with the 3D printed model, either physically or by creating a digital model of the 3D printed model.

## **CHAPTER 3: REVERSE ENGINEERING IN MEDICAL APPLICATIONS**

This chapter discusses the process of RE and 3D scanning technologies. The purpose is to highlight these processes as they are essential aspects of the methods implemented during the experimental work. Thereafter 3D scanning technologies, medical imaging, and medical applications of RE gathered from various literature are presented. One of the medical applications of RE was found to be RE for solid modelling. The solid modelling process of a human femur is demonstrated in the last subsection.

### **3.1. Reverse Engineering**

Analyzing products to obtain their design information is the reverse engineering process [72–74]. It is the opposite of the traditional forward engineering process, where one starts from a logical design process to create a product. The applications of RE are across various industries such as software, aerospace, defence systems, medical, consumer electronics, automotive, sports equipment, toys, and jewellery [72, 75]. Software reverse engineering spans a range of applications, including embedded systems [76], development and maintenance of user interface software [77], progress and upkeep of large software systems and modernization of legacy software [78], extraction of platform-independent models [79] and analysis of peer-to-peer protocols [80].

Contrary to the design process that focuses on creativity and originality, the RE process focuses on analysis and assessment to reinvent a product. Figure 3-1 describes the main differences between the traditional engineering design process and the RE process in the context of manufacturing processes.

In the context of software, e.g., it could be extracting source code from an executable file. When it comes to physical objects, RE is the digitization of physical products, i.e., obtaining a 3D surface geometry model to convert them to a CAD model.

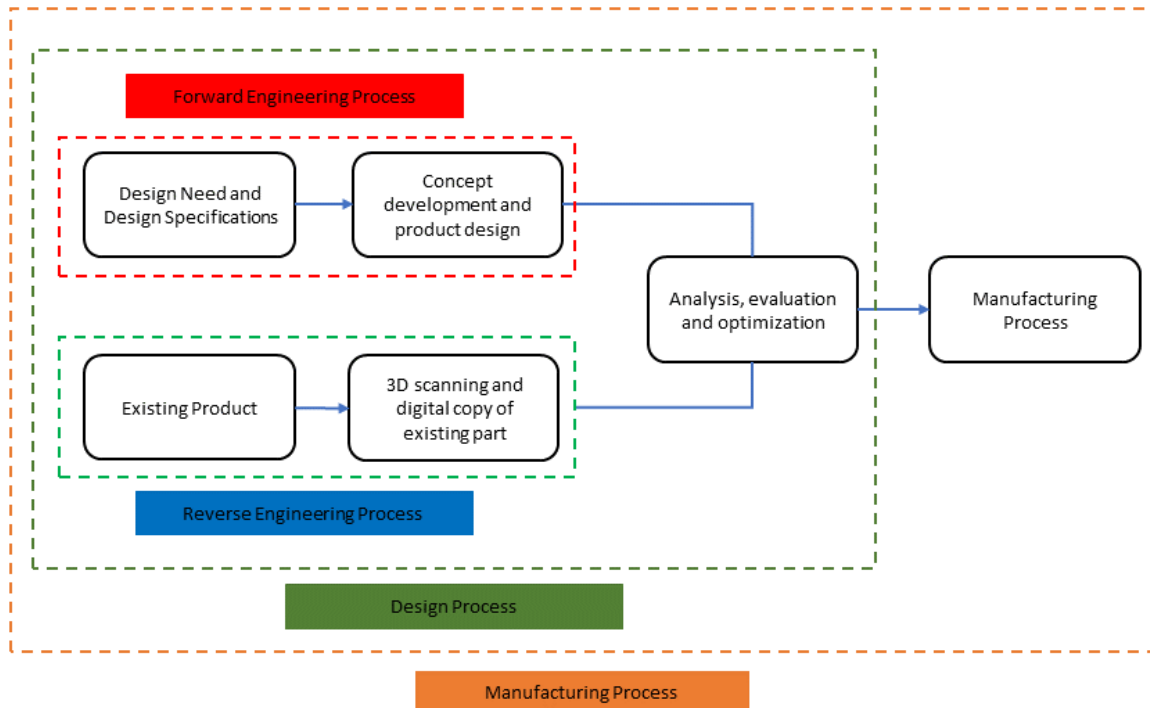


Figure 3-1 - RE vs. Traditional Design Process

Recent applications of RE within product design and spare parts are as follows:

- Product design:
  - New design – especially when product development starts from a physical prototype [75].
  - Modifications – in an iterative design process, modified products often lack CAD information [75].
  - Verification/Quality control – to determine deviations of a design and comparison with the original CAD model. [81]
- Spare parts:
  - Duplication or production of original equipment manufacturer (OEM) parts [75].
  - Reparation or modifications where there is no original design data [72, 73].
  - Model generation of an existing part with no CAD information due to various reasons [72, 73].

## 3.2. 3D scanning technologies

Digitization is possible with 3D scanners to capture a physical object's shape, size, and sometimes colour. The first step of RE is to capture the surface or geometric data of an object of interest. The captured data is then processed and thereafter converted to a 3D model, essentially creating a digital copy. Having a digital copy allows for further modelling. The process is quite standard and is displayed in Figure 3-2. Modern The data generated from modern-day scanners is compatible with software for designing and analysis. A general classification of 3D scanning techniques was compiled by Bidanda et al. [75] and Fernandes et al. [73]. A summary of this classification can be seen in Figure 3-3.

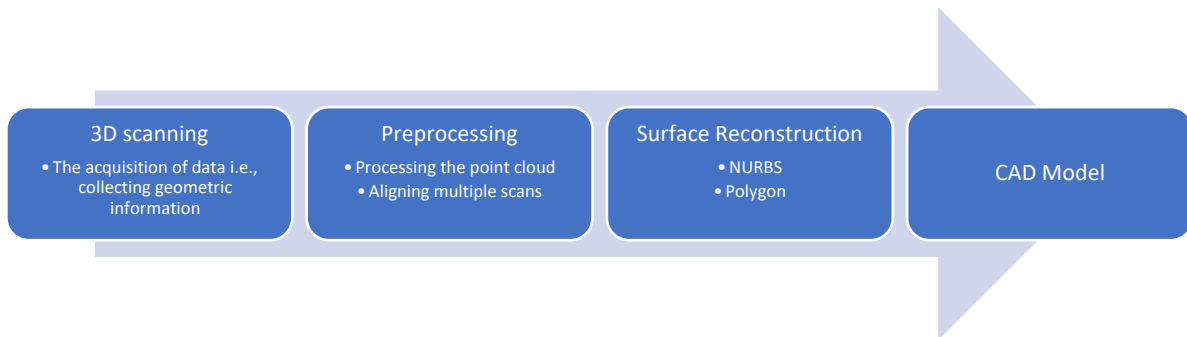


Figure 3-2 - Reverse Engineering Process

In all scanning tools, a physical mechanism is always utilized for scanning. However, scanning technologies can be broadly described based on whether there is physical contact with the object of interest or not [72]. In this regard, scanners can be either contact, non-contact or hybrid technology.

Contact methods make use of a physical probe to move along the surface of an object to capture the details. These could be either manual measurement, coordinate measuring machines (CMM), or Numerical Control (NC)-based machines. However, these techniques are more time-consuming and meant for objects with simple geometric shapes [75, 81]. Moreover, the probes must maintain a certain contact pressure to accommodate very soft materials and tactile features [73, 82]. The sensing of a contact probe can be either point-to-point or analogous (continuous).

Non-contact methods do not make any physical contact but rather use projecting energy sources such as light, laser, sound, magnetic fields or X-rays [72, 73, 75]. Regarding larger, more complex parts with various curvatures and free-form shapes, non-contact scanners are the preferred method. The

surface information is determined by capturing the return of this emitted energy (either transmitted or reflected).

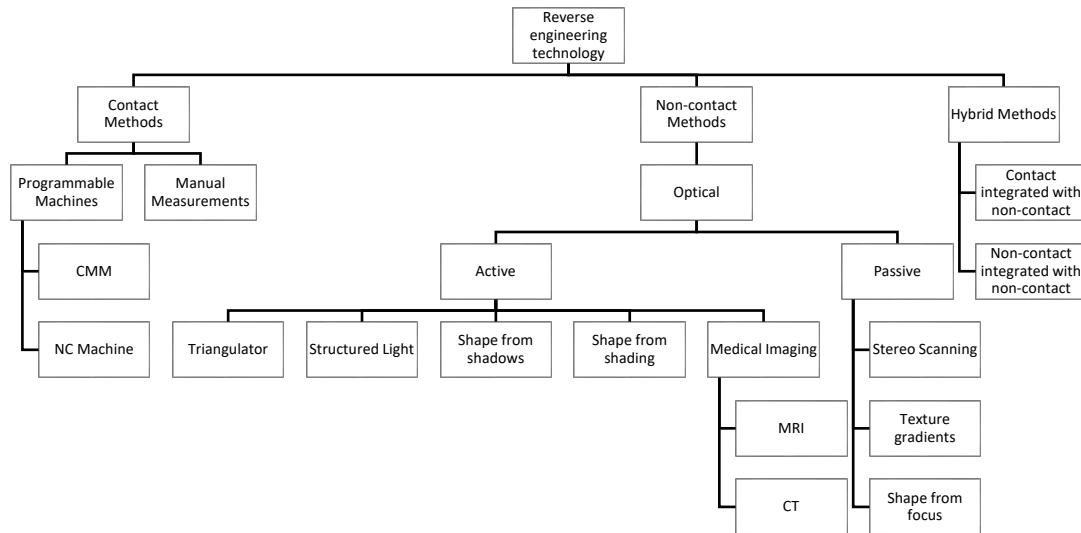


Figure 3-3 - 3D scanning classification [73, 75]

An object must usually be prepared such that it can be scanned. Preparation can be either the mounting or the surface finish, e.g., making use of scanning sprays that are white and are temporary. It is important to choose an appropriate scanning method or technique. This ensures that all features of an object, e.g., holes, slots, pockets, and steps, are captured.

The first step, as seen in Figure 3-2, is the 3D scanning phase. A 3D scanner is utilized to scan an object of interest using an appropriate technique. The data transferred to the relevant software is a point cloud. In other words, the digitization process approximates the object of interest by using discrete points. These are key references of the geometry which will be utilized to define the geometry of the surface.

3D scanners employ different techniques to capture surface details from objects. The techniques differ between active systems and passive systems. The main difference between these systems is that active systems project energy and measure the transmitted or reflected energy to determine the geometry, while passive systems analyse images of the geometry. The physical principles underlying these systems are as follows [73, 83]:

- Active Systems:



- Triangulation
- Time-of-flight or laser pulse
- Interferometry
- Passive Systems:
  - Shape-from-shading
  - Shape-from-motion
  - Passive stereo

### ***3D scanning in healthcare***

The evolution of technology and the integration of digital solutions has transformed diagnostic and treatment planning methods. The use of 3D scanners, e.g., in the field of dentistry, is somewhat revolutionary. This is because 3D scanners are advantageous compared to conventional methods in obtaining oral impressions, e.g., plaster models have several disadvantages [84]. Figure 3-4 displays the change 3D scanning technologies have created in the workflow within orthodontics.

3D scanning has changed record-keeping, cast model acquisition and storage, and other applications such as custom retainers and even surgery simulation. All this has been made possible using extra- and intra-oral scanners [85]. Non-contact 3D scanning (laser) has also been proposed as a viable alternative to CT scanning for accurate evaluations of implant surgery to reduce radiation exposure post-surgery when using a CT scanner [86]. A good overview of the advantages and 3D scanning technologies can be found in the work conducted by Taneva et al. [84].

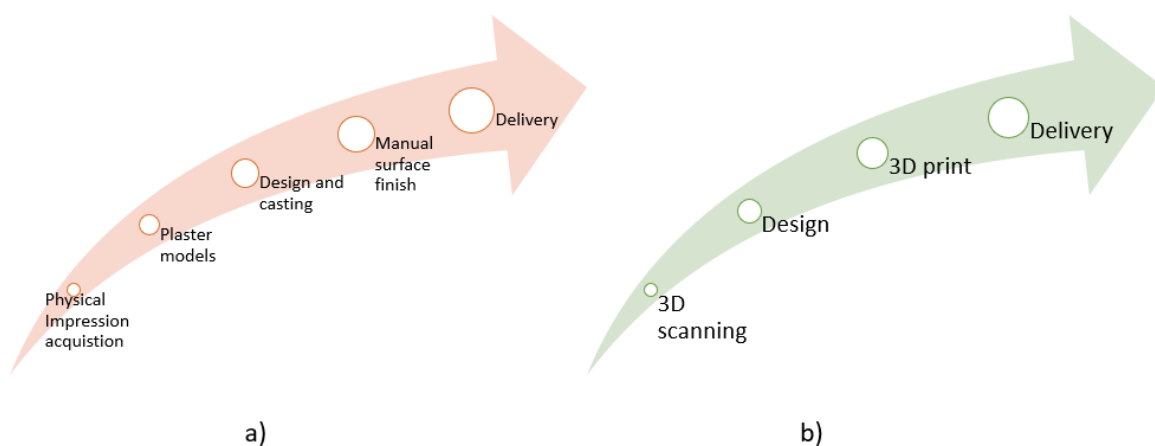


Figure 3-4 - a) Traditional Workflow vs. b) Digital Workflow for dental applications

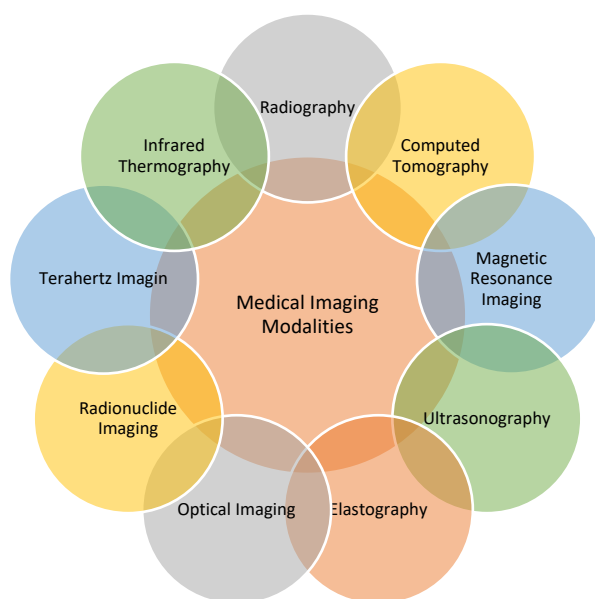
In the field of anatomy teaching, the use of 3D scanning (together with AM technology) has given rise to innovative solutions for visualizing anatomical structures. Di-Donato et al. [48] highlighted the use of 3D scanning tools where digital models of the tongue of the domestic animals were 3D scanned and used in conjunction with practical classes for teaching purposes.

Soodmand et al. [87] conducted an interlaboratory study to compare scanning methods as part of medical image reconstruction. Medical image reconstruction using CT scanning and optical scanning was compared, and the reference model was created using 3D scanning. The results show that the deviation between the CT scanned model and the 3D scanned model is not significant.

### 3.3. Medical Imaging

Medical imaging, as seen in Figure 3-3, is an active system of scanning. Medical practitioners can create images of both the internal and external parts of the body for diagnostic or treatment purposes. The process is known as medical imaging and is a non-invasive procedure to get information about an injury or disease. For quantitative and qualitative assessments, medical images provide information regarding a particular diagnosis and its severity. A medical practitioner conducts the procedure with adequate training.

Analysis of these images enables medical practitioners to solve clinical problems. The most prominent imaging techniques have been displayed in Figure 3-5. The information obtained from these is known as Data Imaging and Communications in Medicine (DICOM) images.



### Figure 3-5 - Medical Imaging Modalities

Several works of literature have provided details of the medical imaging modalities [88–90]. An overview of some of them is mentioned below:

- **Radiography** – the use of X-rays to obtain planar 2D images of anatomical parts. Most applications of this technology involve the analysis of fractures and changes in the skeletal system [88, 89]. Radiography can be either fluoroscopy or projectional radiography [91]. Despite being low cost and widely available, the quality of radiography images has been claimed to be poorer than the quality of images produced by CT and MRI [69].
- **Computed Tomography (CT)** – uses X-rays to obtain 3D images of anatomical parts. Generally made possible with the use of multiple X-ray sources and detectors to obtain a 3D cross-sectional view of the body [88, 89].
- **Magnetic Resonance Imaging (MRI)** – based on the principle of nuclear magnetic resonance, this method is used for morphological imaging (e.g., soft tissue) and functional imaging (e.g., blood flow) [88, 89]. In contrast to CT, MRI radiation is non-ionizing [91].
- **Ultrasonography** – the use of ultrasound (acoustic waves greater than 20kHz) for the use of diagnostic and sometimes therapeutic purposes. For medical applications, the frequency range is between 2.5-12Mhz. Compared to the above procedures, the use of ultrasound means a lack of ionization radiation (which means there will be no biological damage), and it is cheaper than CT and MRI. In addition, this process allows for real-time imaging [91].
- **Elastography** – Mapping the strain and elasticity of tissue for diagnostic purposes. The notion is that hard or stiffer tissue will be unhealthy [91].
- **Optical Imaging** – the working principle is similar to ultrasound but uses light instead of sound. Applications include retinal imaging, cardiovascular imaging, gastrointestinal imaging, and dermatology [88].

### 3.4. Medical applications of reverse engineering

The human body is a complex piece of engineering. As mentioned previously, RE can be seen as a tool for acquiring knowledge when data are deficient for an object. In this regard, the human body is also a mechanism by which components (i.e., body parts, organs, etc.) can be reinvented through RE to be studied where there is a lack of “design data,” and RE can be a great tool for understanding it.

Medical imaging is applicable for obtaining 3D information on internal body parts, and for external scanning parts, 3D scanners are applicable. These technologies allow for capturing data from a patient's body, attached instruments, or models. For medical applications, the process displayed in Figure 3-2 can start with a 3D scanning or a medical imaging process if the aim is to get information about the internal organs. 3D bio-modelling and imaging applications can vary from the fabrication of implants, saw guides, and drill patient-specific guides to patient-specific preoperative 3D medical imaging data [45, 92].

A bibliometric analysis conducted by Haleem et al. [93] displays the increasing trend of researching 3D scanning applications in the medical field. Some of the key findings from this study are as follows:

- 3D scanning is highly compatible with 3D printing and is an excellent support technology for medical applications
- 3D scanning provides information on the upper surface of the human body, while medical imaging provides information on the interior layers of the body [93].
- 3D scanning technologies are applicable across all medical fields
- With basic training, 3D scanning tools are reliable and especially helpful with carrying patient information electronically rather than physically (e.g., moulds).
- 3D scanning is a viable alternative to the laborious task of using a plaster cast for applications within, e.g., orthosis, prosthesis, and dental applications [94].

The research mentioned above was motivated by the need to get information for using 3D scanners for external or outer body parts. From a general perspective, the common uses of RE within the medical field include medical implants, attaining information regarding the patients' external features (shape, size, surface area, or individual body part), and digital models for making use in Virtual Reality and Holographic applications [93]. The availability of a 3D scanner and the process software makes the production of, e.g., implants a rapid process.

A process often associated with RE is AM. There are various applications of RE, especially when combined with AM technologies [75, 81, 95]. The following sections highlight RE applications within dentistry, tissue engineering, and medical devices.

### 3.4.1 Dentistry

It is common even for a routine check-up to make use of intra-oral scanners at the dentist. It seems that having 3D scanners and 3D printers at a dentist is relatively standard. Although in the most common routine check-ups, the intra-oral x-ray scanner is used to determine the extent of a damaged tooth. However, the use of RE and 3D scanners span different dentistry sections, such as prosthodontics, oral and maxillofacial surgery, oral implantology, and orthodontics.

3D scanners assist in obtaining surface information for dental preparations. These could be either in vivo or in vitro. The scanned information is then used for either restorations or implants. Recent applications of RE within dentistry have been within dental implants [96, 97], medical devices [98], dental restorations [99], and FEM on dental implants [100].

In traditional processes, dental impressions have been taken through plaster models. However, using 3D scanners has made it possible to acquire digital impressions. It has also been seen that there is no significant difference, and the digital model has acceptable levels of dimensional accuracy and likeliness as the plaster model [101]. Other dental devices include the fabrication of dental prostheses, implants, and surgical guides using RE [102–104].

RE has been implemented as a new method to compare medical models obtained from different 3D scanning techniques. One study conducted by Ausiello et al. [105] displayed this process. The 3D model of simulated human teeth was first scanned using Cone Beam Computed Tomography (CBCT). The same 3D model was then laser scanned. The laser-scanned model was used to compare the model obtained via CBCT. Another study conducted with a similar purpose was conducted by Zhou et al. [106], where the analysis and measurement of dental casts were conducted, and 3D scanning was tested as an alternative to gypsum casts. Similar studies were done by Carneiro Pereira et al. and Liu et al. [107, 108], where the viability of digital casts and the angles and distance between dental implants were studied. These studies demonstrate using non-contact laser 3D scanning as a viable alternative to CT scanning for dimensional verification.

RE has also been implemented for analysis within dentistry. Martorelli et al. [109] used 3D models of the human mandible, which were created using the process of RE. The motivation is to recreate 3D models that have the same or somewhat similar mechanical properties to the human mandible. The 3D model was then subjected to experimentation with appropriate loading conditions in the validation process to determine the load-displacement relationship. In essence, RE was utilized here

to determine the design information of the human mandible in both the surface layout and the strength. There are other studies conducted with the same purpose, i.e., FEA analysis and fatigue analysis [110, 111]. These studies demonstrate using non-contact laser 3D scanning as an option to obtain geometrical information for analysis purposes.

The advancement of material technology has given rise to the use of composite materials in dental devices. RE has allowed for the analysis of these composite materials. This can be seen in the work conducted by Ilie [112], where it was suggested that RE is a viable method for designing in the future by analyzing already clinically tested materials. In the case of this study, the materials analyzed were resin-based composites.

Together with CAD tools, RE tools allow for kinematic analysis and virtual design in dentistry. In particular, this allows for having a virtual articulator. Having a virtual articulator reduces the need for a physical articulator, which is mechanical, while still enabling practitioners to simulate real patient data and conduct analysis [113, 114].

### **3.4.2 Tissue Engineering**

A solution to address problems related to tissue repair and organ replacement in the regenerative medicine field is tissue engineering. 3D cellular structures (also known as scaffolds) provide an effective platform for new tissue development, mainly by providing mechanical support during the development phase [115, 116]. The structural makeup of scaffolds is quite complex. In this regard, RE has a huge role to play as structural information for modeling purposes can be extracted using scanning methods. In the work conducted by Pina et al. [117], there is mention of the different strategies that could be applied to develop scaffold designs for tissue engineering and regenerative medicine for different organs and tissues. The article highlights the various implementations of 3D scanning and RE for 3D printing hydrogel scaffolds.

In their work, Wang et al. [116] discuss the distinction between parametric design and generating vascular scaffold models using the process of RE. The route of parametric design without the use of AI and machine learning is said to be almost impossible due to the complex nature of vascular scaffolds. However, for batch processing of models that are quite similar, the use of parametric design together with AI and machine learning is said to be relevant.

The use of reverse-engineered models is relevant for patient-specific vascular scaffolds and is not generally used for extensive quantity modeling where there is structural similarity. The workflow of 3D model reconstruction of these models is as described in Figure 2-10, where the DICOM images are obtained from either MRI or CT images. The general conclusion is that parametric design is quicker while RE models are more personalized and provide high anatomical compatibility [116].

The process of RE has also been implemented in bone tissue engineering [118, 119]. Again, the usefulness of RE is within the design and fabrication of scaffolds, in this case, bone tissue scaffolds. Once CT information of a bone is obtained, it is then transferred to CAD software to conduct the design and analysis. One such example is as mentioned by Yao et al. [120], where animal spinal specimens were used to investigate design and construction techniques using the RE process. Another application in this regard was demonstrated by Fucile et al. [121], where RE was adopted to develop nanocomposite structures. In the work done by Wang et al. [122] the RE process was implemented for bone tissue engineering, and eventually, the models were imported for computational fluid dynamics (CFD) to determine the flow field around a cell.

### **3.4.3 Medical Devices**

Asmaria et al. [123], discussed how the implementation of RE can be a national strategy to overcome a nation's debt, especially when most of the debt is caused by the imports of medical devices. The study was conducted in Indonesia, where an aneurysm clip (a high-demand medical tool in Indonesia) was reverse-engineered from design to biomechanical simulation. Also, in South Africa, where there are several resource constraints, there have been efforts to implement RE as a substitute for importing expensive medical equipment [124].

Recently the application of RE during the COVID 19 pandemic has been quite relevant. With soaring demands for personal protective equipment (PPE) and ventilators, and other critical medical devices, supply chains started to collapse. RE posed as a solution to these shortages, and there have been many reported cases of developing equipment in-house in hospitals to meet the high demand [125–128].

These applications are more related to supply chain processes, however, they still show the relevance of RE in the medical context. It can be said that the process of RE has both direct and indirect applications within the medical industry.

Surgical guides are significant tools used in dental treatments as they improve many aspects of the surgical process [60]. These devices are designed and fabricated from a CAD model created using intra-oral 3D scanners. 3D scanning is used to gain intra-oral surface information. RE has been used to determine the accuracy of the surgical guide, again with the aid of 3D scanning. One such case is the work done by Giordano et al. [86], where the process of RE was used to evaluate the accuracy of surgery guides in dental implants. In this regard, RE is a valuable tool in accuracy evaluation or quality control. Other applications of RE to determine the accuracy or trueness are mentioned in the work done by Liang et al. and Lo Russo et al. [129, 130].

As mentioned before, one of the possibilities RE provides in the medical sector is developing customized healthcare products. This allows for patient-specific implants and prosthetics. In their work, Noor et al. [131] demonstrate how a customized bone fracture implant (developed from RE) reduces the stress and movement between the fractured bone and the implant in comparison to the implant developed from a generic model. Apart from the design and fabrication processes, RE has also been used in verification processes. One such case is mentioned by Kloesel et al. [132], where the RE process was used to verify the fit of a medical device in a patient. Other applications include the use of RE within hand orthotics [133] and in soles [134].

Having gone through the various literature on the applications of RE in the medical sector, these are some of the conclusions that can be made:

- The process of RE has both direct and indirect applications in the medical industry. Direct applications that work on patients for surgery, clinical studies and research. Indirect applications that support the supply chain processes in the medical industry
- 3D scanning is an excellent support technology for medical applications
- 3D scanning is a viable alternative for obtaining impressions within, e.g., orthosis, prosthesis, and dental applications
- The process of RE can be implemented for analyses such as FEA and CFD.
- RE has a considerable role to play in tissue engineering in developing accurate structural models for tissue scaffolds.
- RE tools allow for kinematic analysis and virtual design

Some of the typical medical applications of RE are identified, having gone through the various literature, and displayed in Figure 3-6.



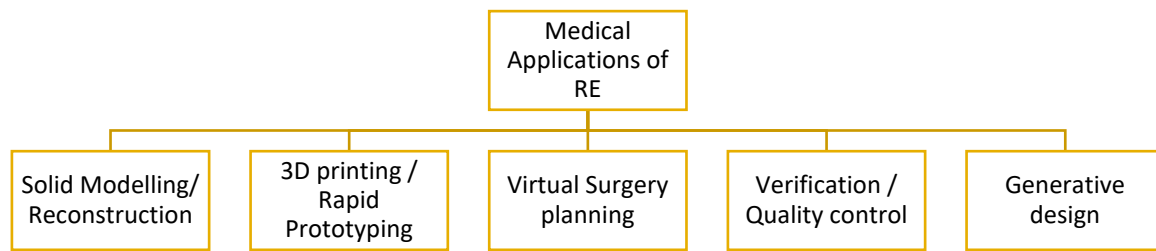


Figure 3-6 - Medical applications of RE

### 3.5. 3D Scanning and Reverse Engineering to Measure Accuracy

As shown in Figure 3-6, the process of RE together with 3D scanning has been implemented for dimensional verification applications. From the literature studied for medical applications of RE, the methods employed for accuracy assessment have been extracted and presented in Table 3-1

Table 3-1 - Methods of applying RE and 3D scanning for accuracy assessment of medical models

Objective	3D scanning	Mesh processing	Mesh Inspection	Reference
Determine the accuracy of medical models	Non-contact 3D scanner (experiment) CT (reference)	Geomagic studio MeshLab	Geomagic	[87]
Accuracy of digital impressions from intraoral scanners	Intraoral scanners Non-contact 3D scanners	Geomagic studio	GOM Inspect	[135]
Evaluate the accuracy of the intraoral scanner to analyse the alignment	Intraoral scanner (experiment) CT scanning (reference)	N/A	GOM Inspect	[108]
Evaluate surface curvature vs. 3D	Industrial Non-contact 3D scanners and	N/A	GOM Inspect	[136]

scanning accuracy of dental casts	intraoral 3D scanners			
Evaluating measurement methods of mandible model created using AM	Non-contact 3D scanners	Geomagic	GOM Inspect	[137]
Estimate the accuracy of mandible models created by AM	Non-contact 3D scanners (Experiment) CMM (reference)	N/A	GOM Professional	[138]
Creation of an ear database for biometric applications	Non-contact 3D scanner	VX Elements	MeshLab	[139]
Creation of medical models as virtual digital resources	Non-contact 3D scanner	MeshLab	CloudCompare	[140]

### 3.6. Medical Application Of Reverse Engineering For Solid Modeling

As highlighted in Figure 3-6, solid modelling is a medical application of RE. In this subsection, the solid modelling process of a human femur will be conducted. The basis for solid modelling, in this case, is an STL file that was obtained from 3D scanning as a reference. Thus, highlighting the medical application of the RE process for solid modelling.

#### 3.6.1 Geometric modelling

Geometric modelling is commonly used these days with the aid of computational systems, e.g., CAD. The geometry of an object can be described via [141]:

- Wireframe model – shape represented by lines and endpoints
- Surface model – lines, endpoints, and surface information with a mathematical description
- Solid model – lines, endpoints, surface, and information about the volume

A wireframe model does not have any volume or mass information, and that is the main drawback. However, wireframe models allow for quick manipulation that can be done easily. Generally, a wireframe model is first obtained from mesh data (from 3D scanning) and thereafter developed into the surface and solid models. For RE, wireframe models are not suitable since the purpose of RE (e.g., 3D scanning) is the digitization of surface information [75]. Some recent applications of wireframe models for medical applications are within computer vision [142] and deep learning for brain tumour detection [143].

Surface models contain surface information, unlike wireframe models. They may contain volume information if they are closed models. Otherwise, they provide a visual of the topography of a component. In medical applications, a segmentation is first reconstructed into a “water-tight” surface model containing some surface area and volume information, then converted to STL file format for further analyses.

A solid model can be used in a CAD system for various purposes, e.g., machining, FEA, etc. For medical applications, a solid model can be utilised for various purposes, such as for the design of implants and prostheses or quality control, verification, and analysis purposes. This is mainly because solid models provide properties such as mass and volume and can be used in mechanical assemblies.

In the case of either designing or reconstructing medical applications, certain techniques are used to account for the missing information. Not due to insufficient scanned data, but due to missing information in the case where there are defective organs or bones, etc. One such study is mentioned in [144], where current techniques are highlighted for the anatomical reconstruction of defective skulls. The techniques mentioned in this study are mirroring, surface interpolation, deformed template, and sliced-based reconstruction. In general, for medical applications for designing and reconstruction purposes, the techniques that have been mentioned are surface fitting, contour skinning, volume polygonization, and implicit-function interpolation [145].

### **3.6.2 Solid modelling using FreeCAD**

There are several avenues to conduct solid modelling using the STL as a reference file. One way is by using commercial software such as Autodesk (Inventor and Fusion360) or Geomagic, which have functions to convert STL files to solid models, which is one option. Another option is to use the very same software to create surfaces using the STL as a reference and convert the surface model to a solid

model. Alternatively, to use part design tools to create sections and surfaces based on the STL model and then convert that to a solid model.

A method will be proposed to create or design a solid model of the femur using FreeCAD. The process is inspired by the work conducted by Yang et al. [146]. Yang et al. make use of commercial software CATIA and initially create a surface model that is then converted to solid.

The methods proposed in the study in this thesis are different in that different methods, processes and resources are used to create a solid model. In this study, FreeCAD is used. FreeCAD is open-source software that can be used for parametric 3D modelling, mesh manipulation and repair, FEA tools, robot simulation modules, and CAM/CNC workbenches [147]. The method proposed here is direct lofting of cross-sections of the mesh and taking advantage of the FreeCAD workbench to convert individual lofts to solids. Thereafter using Boolean functions to create a single solid model. The procedure will be discussed in detail hereafter.

### Step 1 – Import STL into FreeCAD

- FreeCAD provides the option of importing STL files for manipulation. There exists an entire workbench in FreeCAD to deal with mesh design and repair (Figure 3-7).

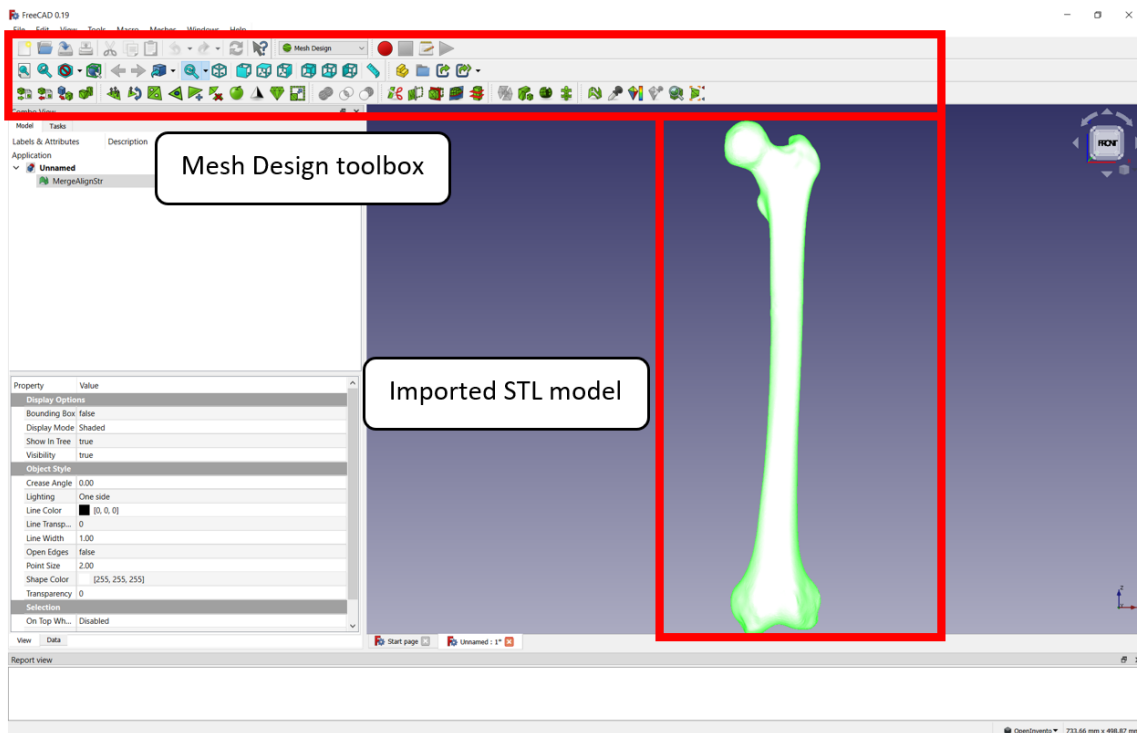


Figure 3-7 - Mesh design workbench and imported model in FreeCAD

## Step 2 – Cross sections of mesh

- A useful tool in the mesh design workbench is the cross-section tool that creates a polyline sketch with the intersection points of the model (Figure 3-8). The options provided are the number of sections, their positions, and their tolerance for connectivity. The sketch is made up of multiple points that are connected with straight lines (Figure 3-10). So the entire sketch is made up of a multitude of just edges and points.

Using this tool, several sections of the femur model can be, as seen in Figure 3-9.

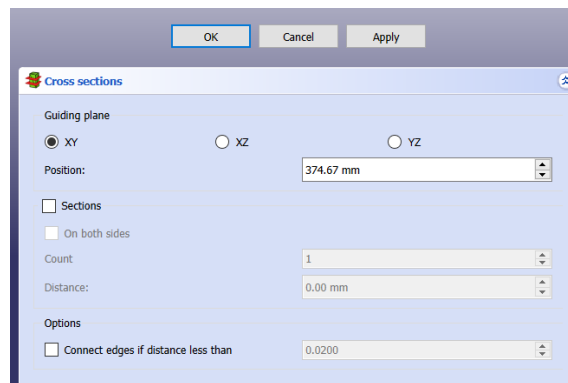


Figure 3-8 - Cross-section tool

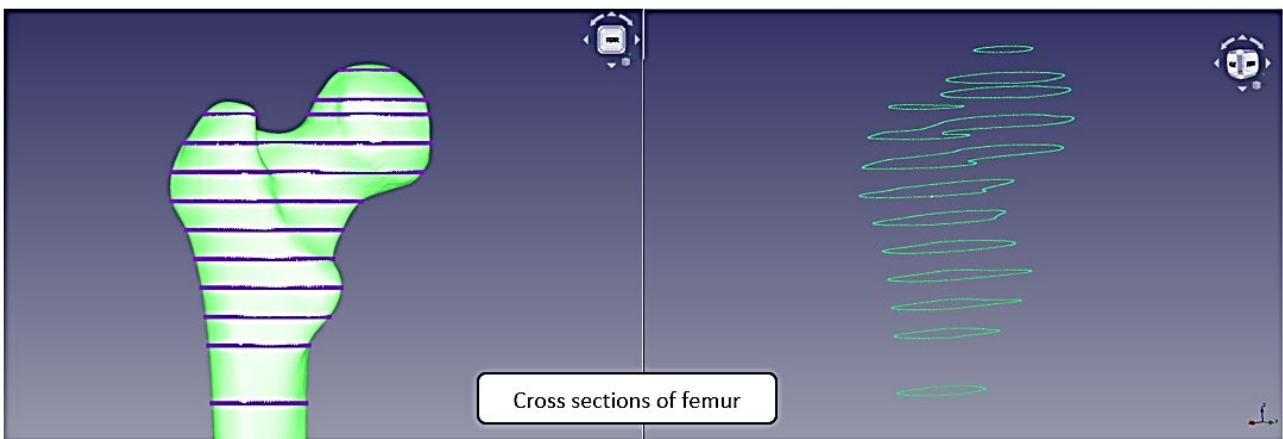


Figure 3-9 - Cross-sections of the femur

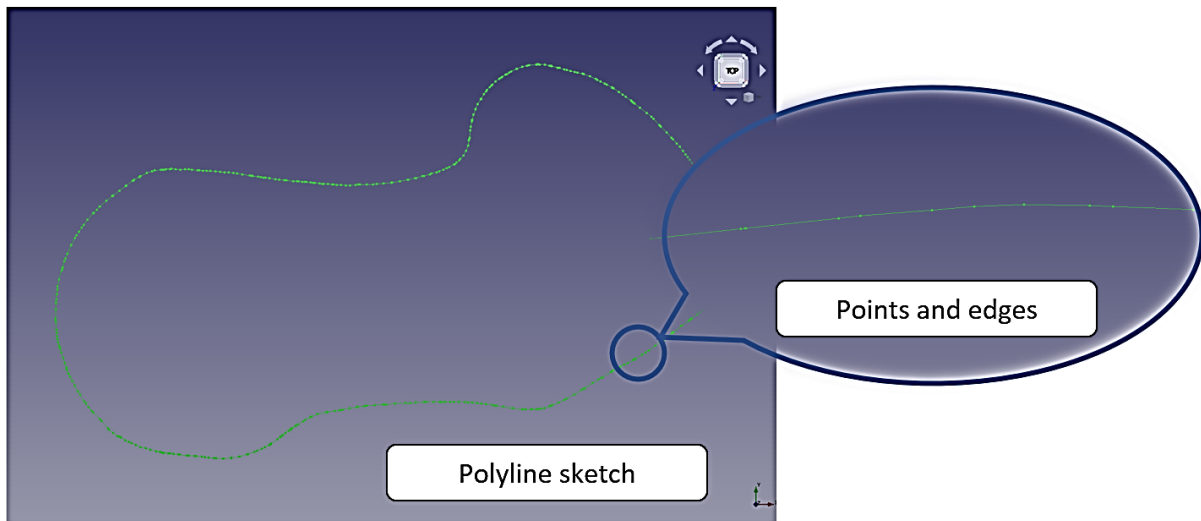


Figure 3-10 - Polyline sketch

### Step 3 – Creating sketches for lofting

The next step is to create sketches to loft between these cross-sections in an efficient manner.

- The polyline sketch can be used for lofting. However, as mentioned, this sketch is made of multiple edges and therefore requires more resources to compute the lofting. Conducting individual lofts of each section in this manner is also time-consuming. Lofts created by using the polyline are shown in Figure 3-11. In the wireframe representation, it can be seen that many surfaces have been created to complete the loft. In addition, the interpolation between surfaces is incorrect. This is probably the algorithm trying to match each edge to a corresponding edge in the following sketch during the loft. This option will be helpful in simpler shapes where there is a liberty of reducing the number of points in the curve without sacrificing geometrical accuracy (In that case, when lofting, fewer points need to be computed).

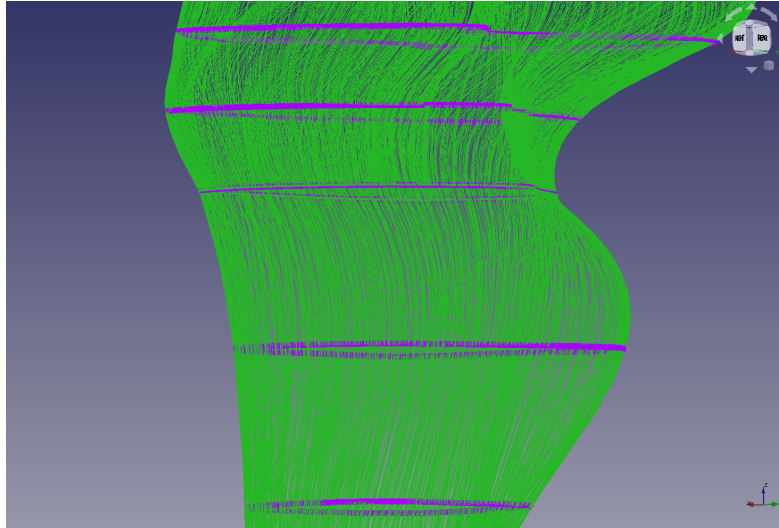


Figure 3-11 - Loft created using polyline (wireframe representation)

- A possible procedure to overcome this problem will be to convert the polyline sketch to a curved closed sketch with a single edge that will allow fewer surfaces to be interpolated when lofting. Different options such as Bezier, Cubic Bezier, and NURBS curves will be investigated to interpolate the already existing points in these curves. The drafts workbench in FreeCAD contains tools for creating the abovementioned curves.
  - **Bezier Curves** – a Bezier curve is created by using the vertices of a closed polygon as a reference [141]. The curve's degree is less than the number of control points used to create the curve. The curve only passes through the first and last points of the polygon, and the curve follows the tangent of the other sides of the polygon. The initial sketch created using the Bezier curve is shown in Figure 3-12. This was created by selecting points along with the sketch. It can be seen in the image that the curve does not match the profile of the polyline sketch. However, a closed-loop sketch was created.

Thereafter the control points of the Bezier curve were manipulated to try and fit the profile of the polyline sketch. This can be seen in Figure 3-13. Even though the representation in Figure 3-12 is closer than in Figure 3-13, it does not match the profile of the polyline

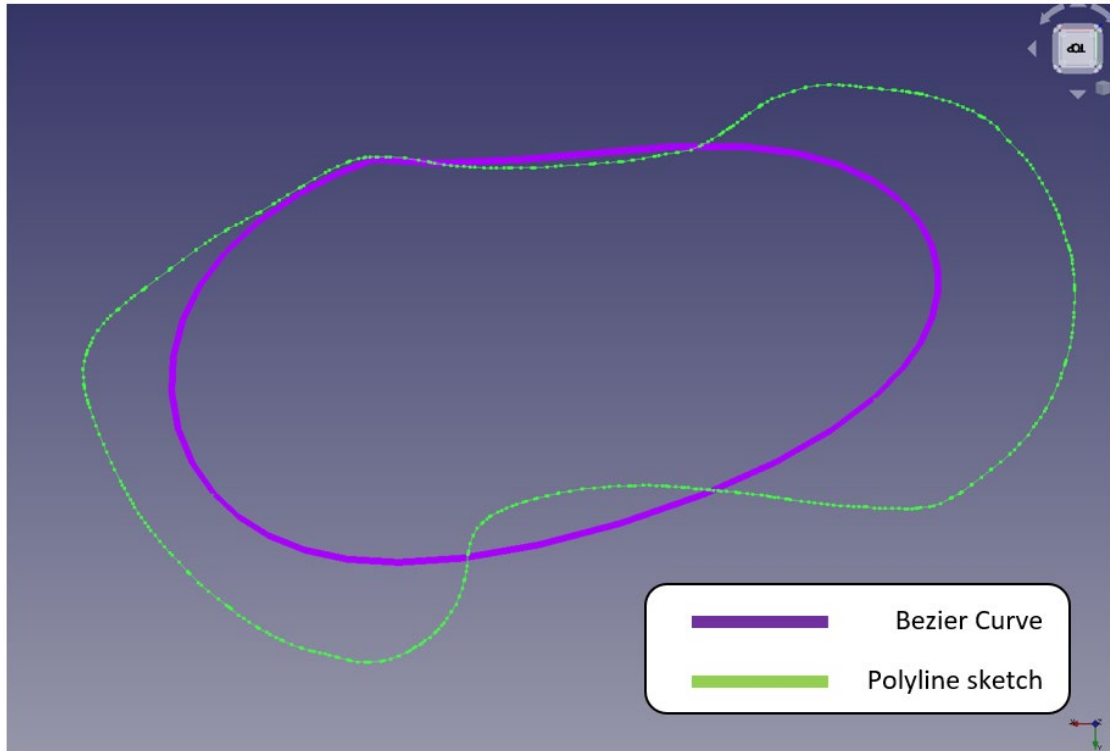


Figure 3-12 - Sketch using Bezier Curve (before adjustments)

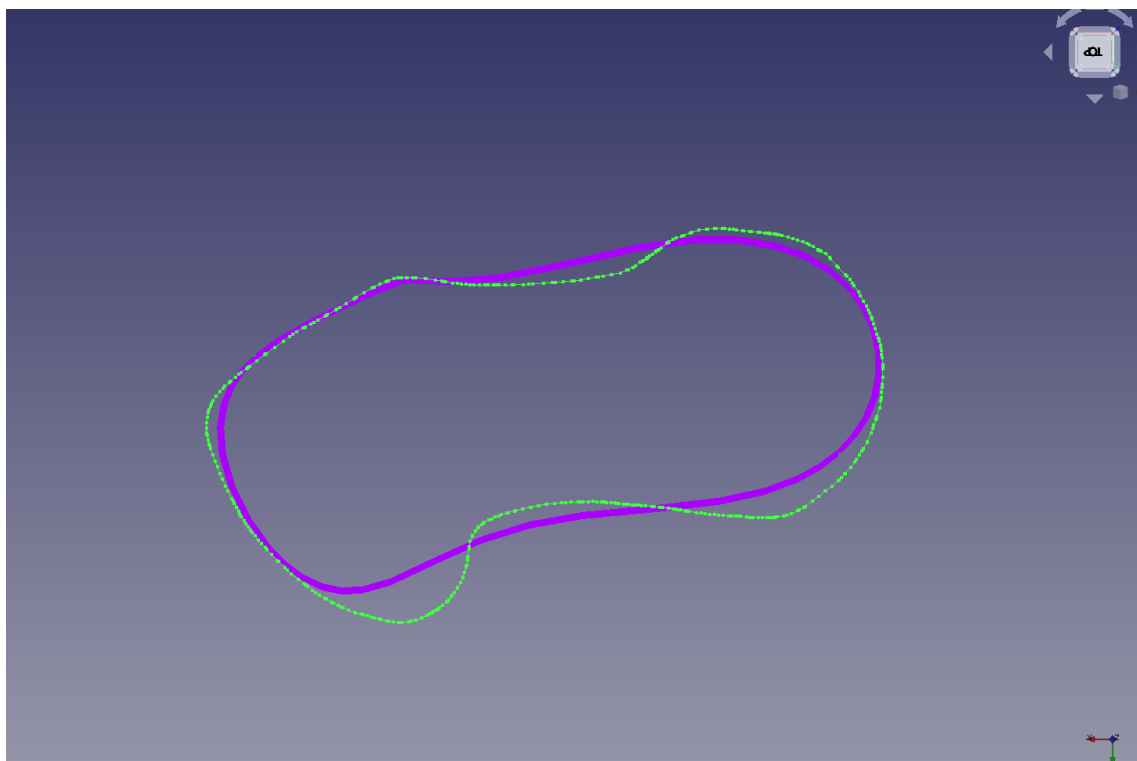


Figure 3-13 - Sketch using Bezier Curve (after adjustments)



- **Cubic Bezier curves** – are curves that are of order three and use four control points. This tool in FreeCAD can be used to make continuous splines made up of several Bezier curves of degree three. It can be seen in Figure 3-14 that the cubic Bezier curve does provide a closer representation of the sketch, but the segments create a very rough outline compared to the polyline sketch. This was created by selecting points along with the sketch.

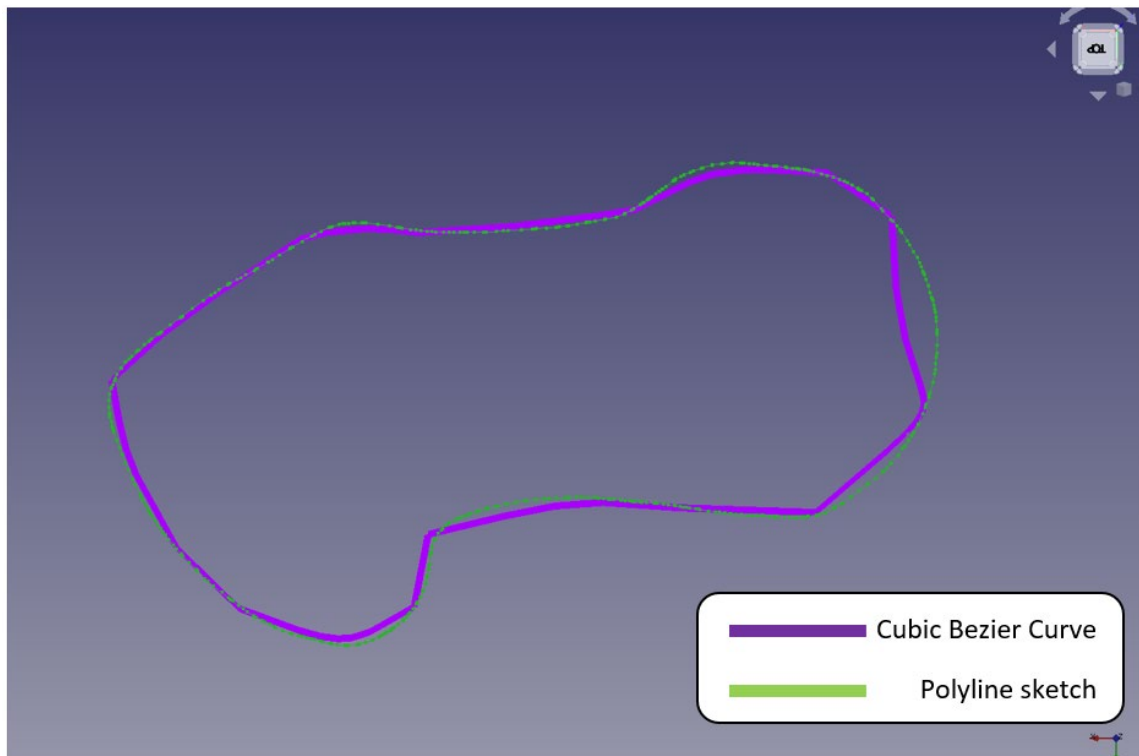


Figure 3-14 - Sketch using Cubic Bezier Curve

- **B-spline curves** – are an improvement of Bezier curves that use several Bezier curves joined end to end [141]. B-spline curves allow for local modifications, and the degree of the curve is independent of the number of control points. It can be seen in Figure 3-15 that the cubic B-spline curve provides a good representation of the sketch, and the segments create a good outline and match the polyline sketch. This was created by selecting points along with the sketch.



Figure 3-15 - Sketch using B-spline curve

- The abovementioned process is a manual procedure to create sketches. An efficient alternative will be to create the curves automatically using the points on the polyline sketch. That is to interpolate between the points using the points on the polyline sketch. The curves workbench in FreeCAD provide tools to interpolate between points. The options available are to interpolate between points using B-Spline curves, approximate points with a NURBS curve, or join all edges using B-Spline curves
  - **NURBS curve** – A *non-uniform rational B-spline* curve is similar to a non-uniform B-spline curve but makes use of additional parameters in the blending function. A NURBS curve allows for more versatile modification of a curve than B-spline curves. In addition, NURBS curves can represent conic curves exactly, while B-splines only provide an approximation [141].

The tool provided in FreeCAD, however, creates an approximate NURBS curve using the points. This tool may not be completely useful as it requires adjustments such as closing the loop and changing the maximum degree of the curve to create a smooth closed loop without oscillations. The original curve and the adjustments made thereafter are shown in Figure 3-16.

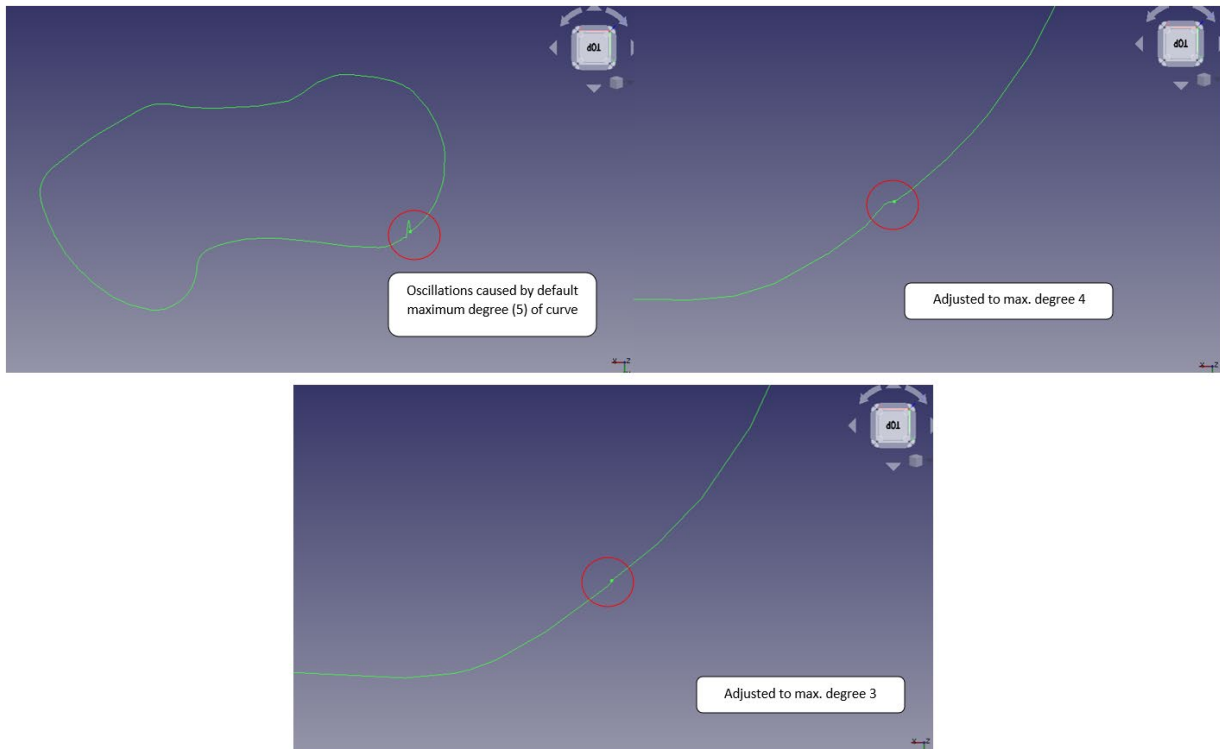


Figure 3-16 - Sketch created using NURBS Curve

- **Interpolate using B-splines / Join using B-splines** – These two functions differ in just two aspects. The interpolation function does not create a closed loop. It requires an additional step of setting the parameter “periodic” to “true” to create a closed-loop sketch. The join tool does not create a smooth curve. Besides that, the tools can be used to create a single closed-loop sketch using all the points from the polyline sketch.

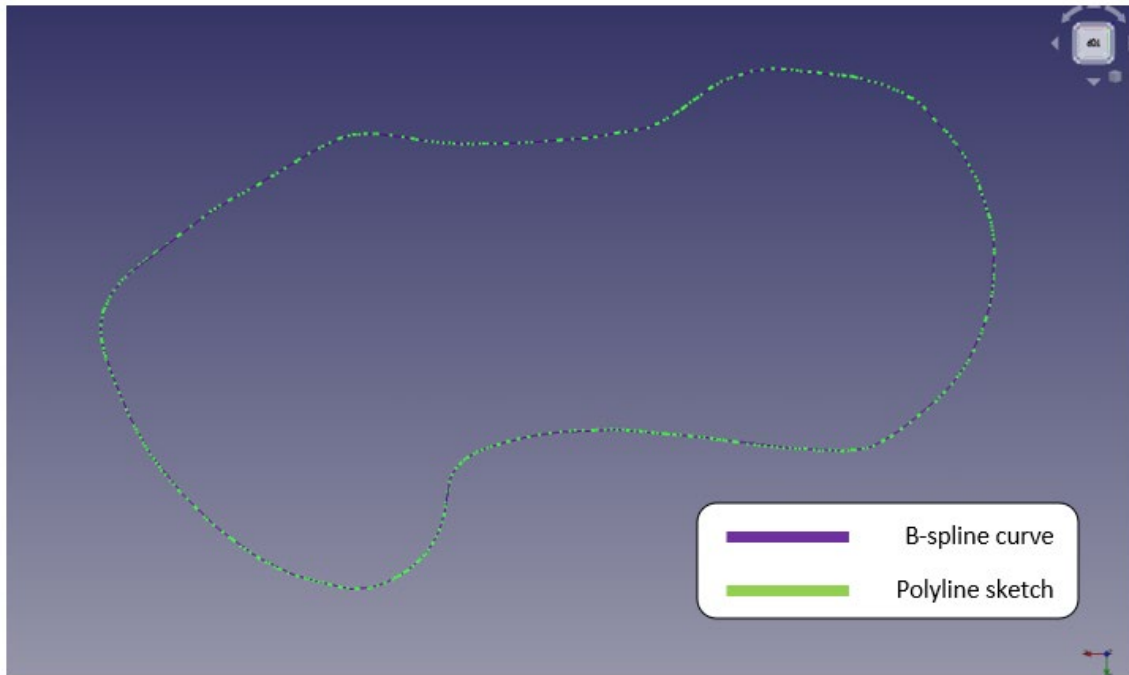


Figure 3-17 - Sketch created by joining points using B-Spline Curves

Once these three steps have been followed, it is possible to create a solid model of the femur. It might be convenient, however, to split the mesh during the modelling process, as the entire femur model need not be sectioned in the same plane.

The femur mesh model was split into three regions (Figure 3-18 a). This can be achieved by the trim mesh tool that creates a polygon to split a mesh model. Thereafter steps one to three, as mentioned above, was implemented. Each mesh section was sectioned and converted to a closed-loop sketch using the interpolate using points function (Figure 3-18 b). Once enough interpolation curves were obtained, each section was then lofted to create a solid model (Figure 3-18 c)). The entire process can be seen in Figure 3-18.

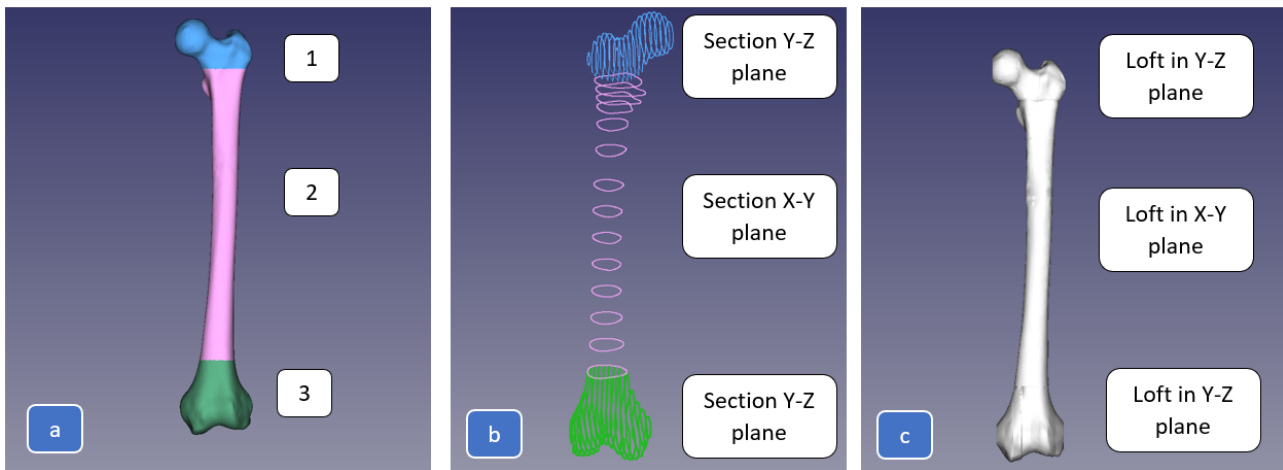


Figure 3-18 - Split mesh model of the femur

The loft function in FreeCAD makes use of B-spline surfaces between the sketches. The interpolation is dependent on the number of sketches. For less than ten sketches, the maximum degree is one less than the number of sketches, while for more than ten sketches, the interpolation is of degree three. Due to this, several solid lofts were created using these profiles and thereafter merged using the union tool in FreeCAD.

A more robust approach will be to conduct Boolean functions to combine each loft. This is a simple process in FreeCAD. The first step is to change the solid feature from “false” to “true” in the data tab. Each loft can be combined using the Boolean function “union” in the part workbench.

## **CHAPTER 4: MEDICAL IMAGING, 3D PRINTING, AND REVERSE ENGINEERING: COMPATIBILITY STUDY OF HUMAN FEMUR BONE**

This chapter describes *in detail* the methods, processes and resources utilised in this thesis for 3D printing and RE purposes. In particular, the methodology implemented in the compatibility study of a human femur bone model created using 3D printing will be presented. Furthermore, the methodology implemented during the RE process will be presented as well.

The methodology implemented in this thesis was developed from the information gathered in Table 2-2 and Table 3-1, which describes the different resources used for accuracy assessment within AM and RE medical applications for various anatomical structures. Taking inspiration from this information, a unique approach was developed to conduct the experiment in this thesis for analysing the femur bone by making use of different non-contact scanning technologies and opensource software packages to conduct the deviation analysis.

To investigate the compatibility of medical images with 3D printing file formats, an accuracy assessment will be conducted where the quality of medical image reconstruction. The assessment will include qualitative (visual and subjective) and quantitative (numerical and objective) analyses using the RE process.

In the major medical modalities, as seen in the previous section, large volumes of data are produced in the form of medical images to visualise the internals of a patient for either diagnostic or treatment purposes. As highlighted in the various literature in the previous section, there are several applications of 3DP within the medical sector that usually start with the process of obtaining these medical images. In the case where the internals of a patient are of interest, medical images are applicable.

There are various types of medical images that can contain information in an array form, either in pixel form (2D) or voxel (3D). The major types of medical image formats are DICOM, Analyze, Nifti, Minc and NRRD. The different medical images can be separated into diagnostic images (e.g., DICOM) and images for further analysis, such as post-processing (Analyze, Nifti, Minc) [148].

The aim of this section is to demonstrate the transformation process of medical image reconstruction for 3D printing. To study the medical image transformation process, an organ will be segmented from a medical image and thereafter will be converted to STL files for 3DP purposes. After 3D printing,

the model will be used for the reverse engineering process. To achieve this, medical images from the online repository Embodi3D were downloaded for training and trial purposes. Embodi3D is an online platform that contains 3D medical models and offer 3DP and medical model creation services [2]. For the experiment, DICOM files from CT scans of human femur bone were acquired from SUS. The scans were from a 40-year-old male who weighed 80kgs.

Several software packages are available to conduct this kind of study for clinical and research purposes, both open source and commercial packages. To name a few: 3D slicer, 3DView, Image J, Invesalius 3, Mimics, The Medical Imaging Interaction Toolkit, OsiriX Lite, Seg3D and Volume Extractor 3.0 [149]. For this study, the software package 3D slicer will be used. 3D Slicer is a free, open-source software package mainly used for medical, biomedical, and related imaging research [150, 151]. For 3D printing purposes, the Fortus 450mc FDM printer was used. The material used for printing is PLA. Three different 3D scanners and technologies were used for 3D scanning for reverse engineering the printed femur. The compatibility analysis was conducted using the scanned data by determining the deviation of the scanned data from the original scanned model.

#### **4.1. Segmentation And Preparation Of Medical Image Data**

For training purposes, medical images from Embodi3D have been downloaded. The file formats of these are NRRD which is different from DICOM images in that NRRD files are anonymized and contain no sensitive patient information. In addition, NRRD files store medical scans in a single file, contrary to DICOM data sets are usually made up of hundreds of individual files.

The following operations apply to other medical image file formats such as DICOM images. The first model that was imported was a CT scan of the whole body. Importing is a simple procedure, similar to importing files into, e.g., CAD software. The commands *Add data* or *Add DICOM data* can be used to import medical images.

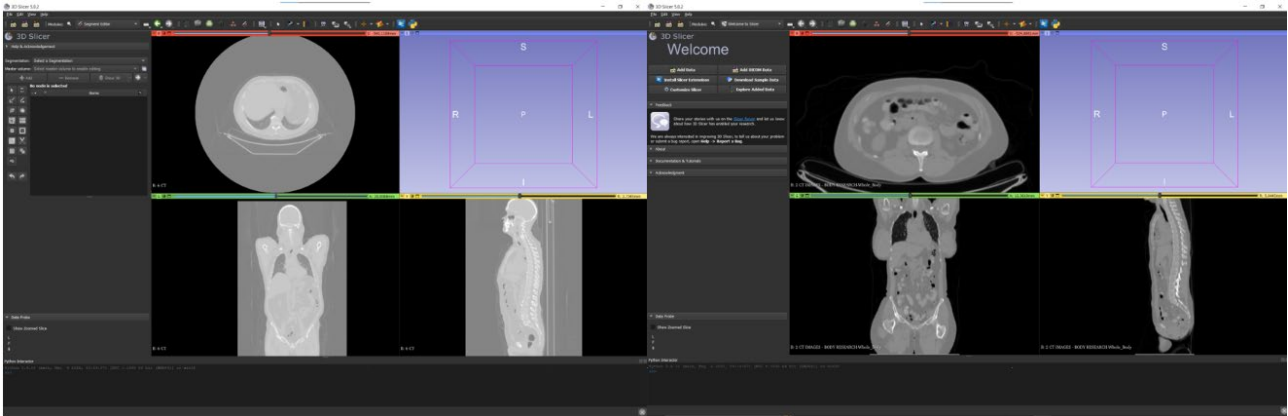


Figure 4-1 - Import medical image into 3D Slicer

The next step is to open the segmentation editor toolbox to start segmenting the medical images and extract the region of interest (ROI). The aim is to contour an ROI corresponding to, e.g., anatomical structures or tumours or lesions etc., such that the ROI can be visualised, analysed, 3D printed etc. The segmentation can be done both manually, semi-automatically and fully automatically. Manual segmentation involved iterating through each slice of a medical image and selecting the ROI. For this study, the lungs and the air will be segmented.

Several segmentation techniques can be implemented to extract a particular ROI [152–157]. Some of the most common techniques include:

- Threshold segmentation
- Region-based segmentation
- Edge-based or boundary-based segmentation
- Clustering or unsupervised segmentation
- Hybrid methods

The 3D slicer software offers several tools for segmentation based on various algorithms. In order to access these techniques, the Segmentation editor module needs to be selected and a new empty segmentation needs to be added (Figure 4-3). In this example, the left lung area within the medical image will be used as an example:

- *Paint* – for the purposes of manual segmentation, the paint tool can be used. With this option a brush tool can be used to select the ROI on each slice of the medical image. To demonstrate this process, the left lung region of a single random slice of the medical image as been



“painted” in red (Figure 4-2). The selection is automatically highlighted in the other views of the medical image (highlight in yellow).

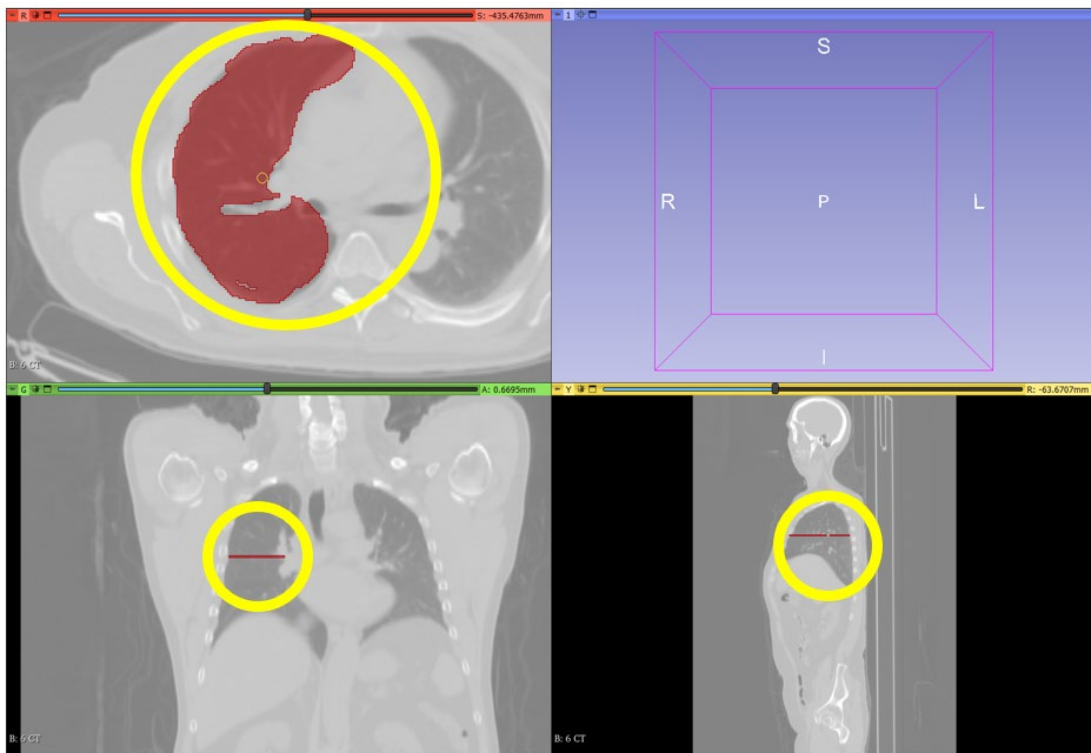


Figure 4-2 - Highlighting the lung region using the paint tool

- *Level tracing* – this method allows for selecting ROIs based on contrast changes. By hovering over the image, the tool allows for selecting an entire anatomical region. The lung area, as seen Figure 4-2, was selected again using the level tracing tool as seen in Figure 4-3. In Figure 4-3, it can also be seen how hovering over the image, the software is able to select varying contrast regions. This is achieved by the software by selecting all pixels that have the same current background pixel [158].

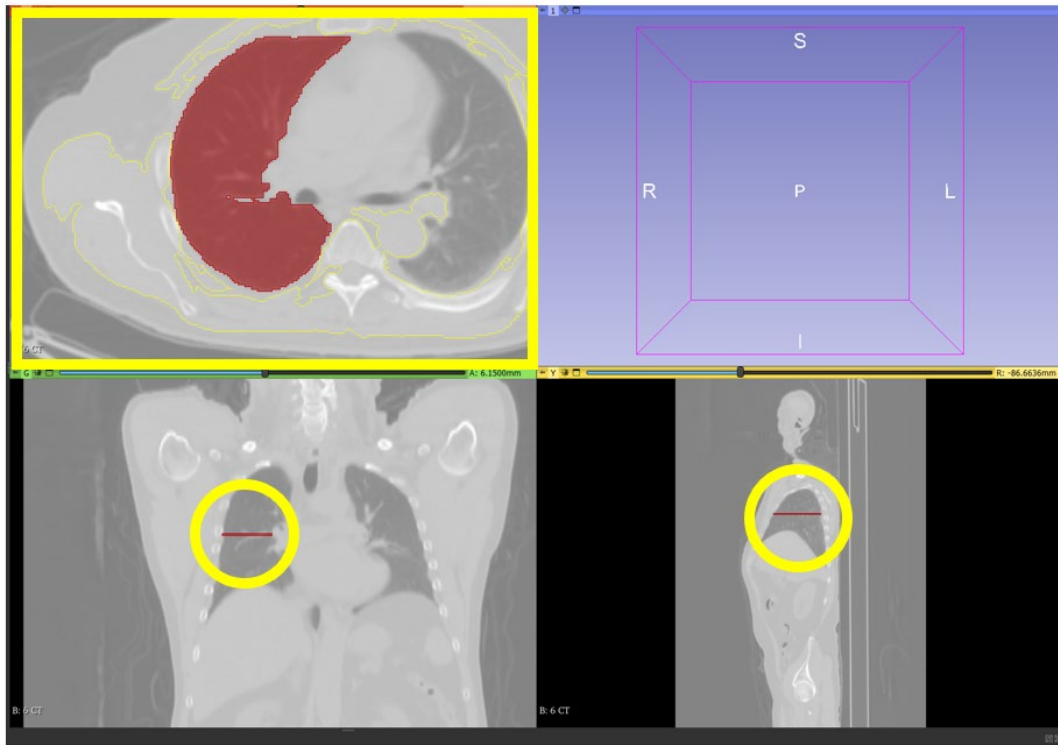


Figure 4-3 - Highlighting the lung region using the level tracing tool

- *Thresholding* – in this method, segmentation is conducted by trying to select an area of interest using a particular Hounsfield unit intensity range. CT images are a map describing the penetrability of X-rays i.e, they are a pixel map of the linear X-ray attenuation coefficient of tissue. The linear scale of the X-ray attenuation coefficient is such that the value of air equals -1024 and that of water equals 0. This scale is called the Hounsfield scale

The threshold was adjusted such that the entire lung region could be selected. This was done to some level of success, however, since the threshold corresponded to air, the entire outer region of the body was also selected (Figure 4-4). When the segmentation was initialised, a significant amount of unnecessary data was also captured. All attempts to post the process were unsuccessful as the program kept crashing.

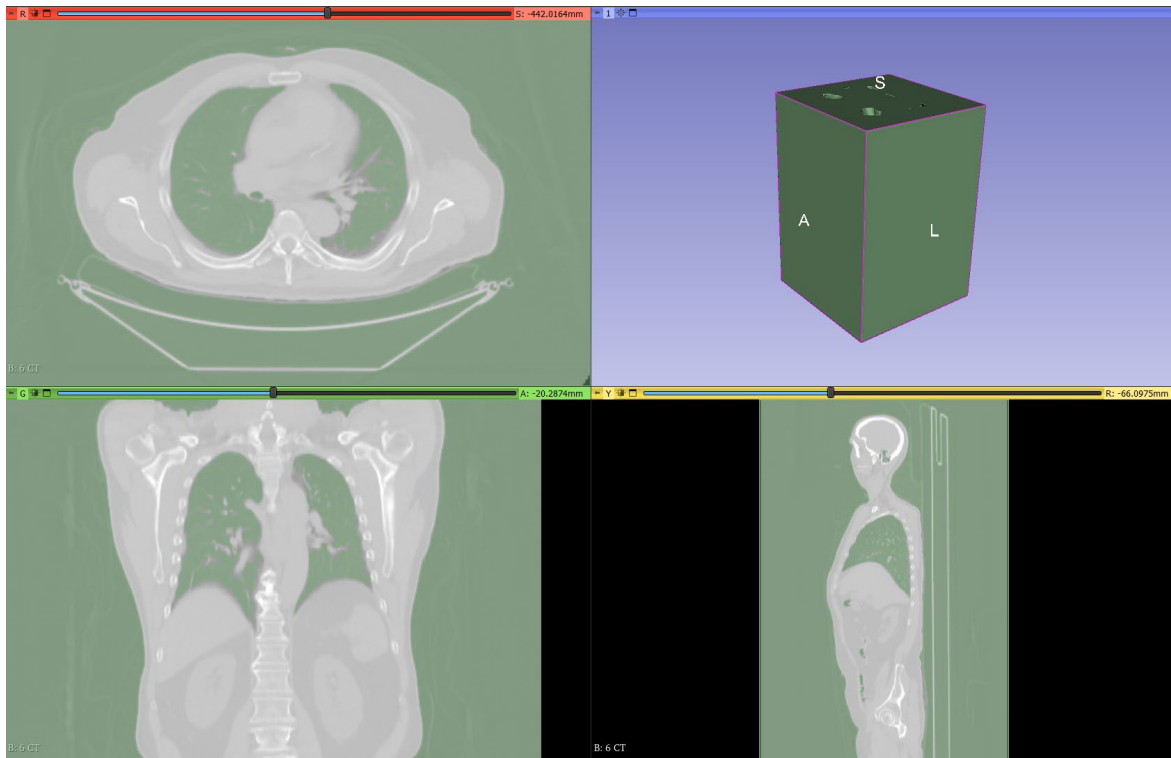


Figure 4-4 – Segmentation of the lungs using thresholding

- *Fill between slices* – when using this method, the ROI is selected in a set of slides that do not necessarily have to be consecutive. The algorithm is based on contour interpolation mentioned in [159]. The areas selected can be seen in Figure 4-5. Thereafter, the algorithm interpolates between the selected slices that include the ROIs.

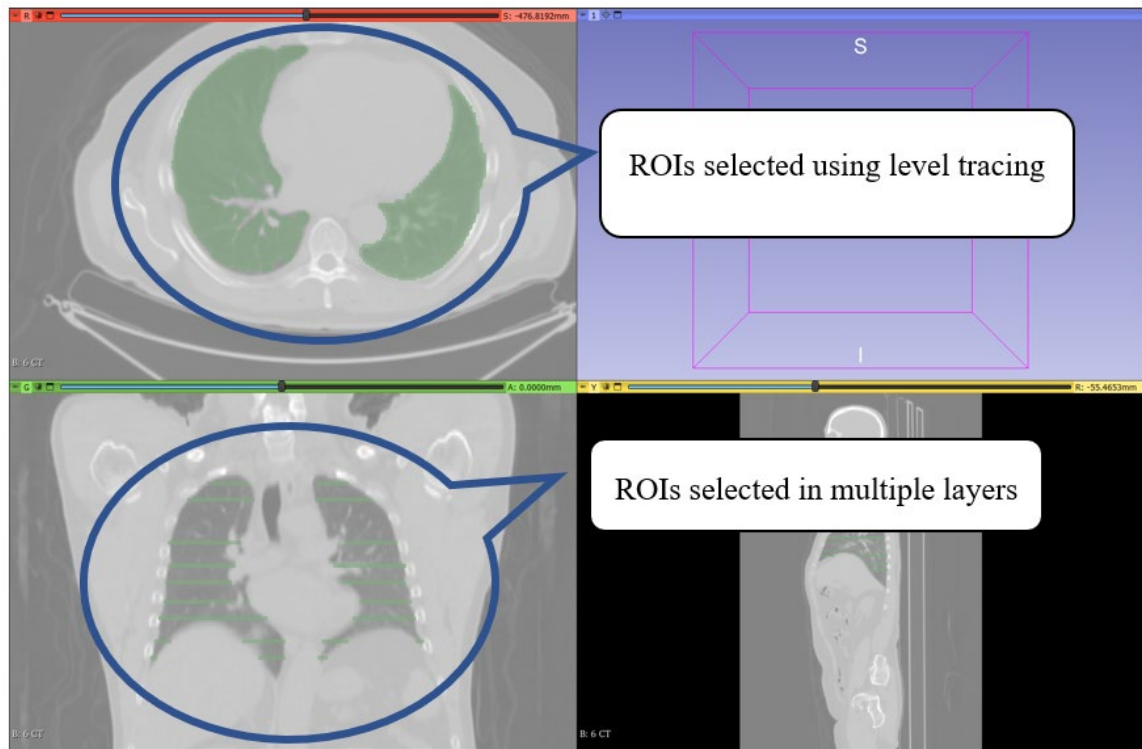


Figure 4-5 – Level tracing for filling between slices

The segmentation was initialised after the preview was generated. This can be seen in Figure 4-6. Each lung and the air pipe had to be segmented individually to achieve this segmentation

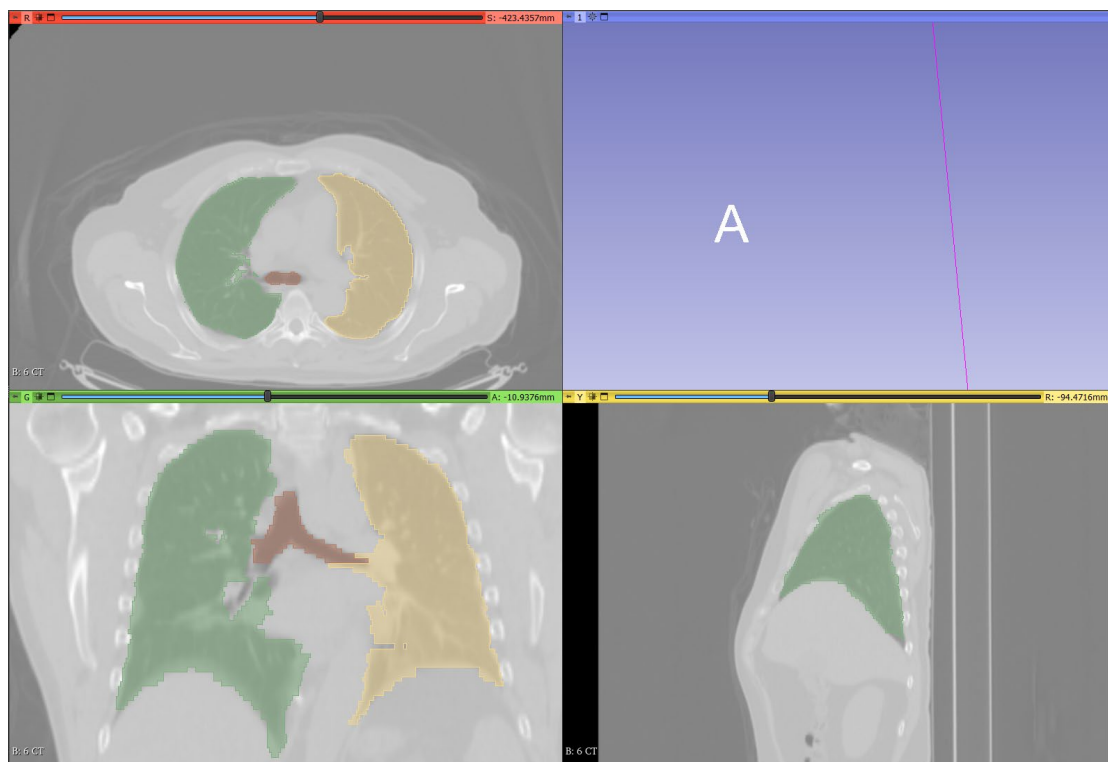


Figure 4-6 – Fill between slices segmentation

- A 3D visualisation of the segmentation can be obtained, as seen in Figure 4-7.
- Once the model was created, the Gaussian smoothing option was selected to smoothen the model (Figure 4-8).
- The model was then exported to STL format so that it can be used for mesh analysis or 3D printing

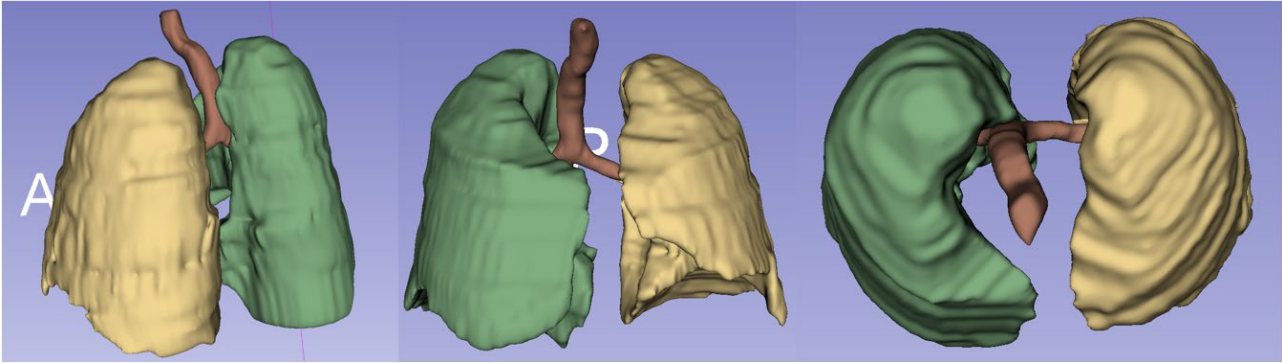


Figure 4-7 – 3D visualisation of segmentation conducted by fill between slices

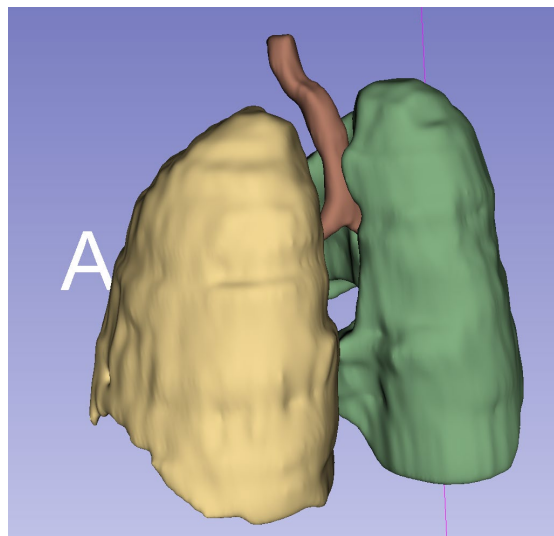


Figure 4-8 – Smoothened model of lungs (fill between slices)

- *Grown from seeds* – in the paint and level tracing method, an entire ROI had to be selected to be processed. The grow from seeds tool uses growing segments for segmentation. The algorithm detects sudden changes in the volume brightness as it grows from the “seeds” or selected segments. The paint tool is used to select at least two segments. Thereafter, based on the satisfactory previews, the segmentation is updated. The method used by the software to achieve this is based on the grow-cut algorithm described by Gao et al. [160].

To get a 3D model of the lungs and the air pipe, the steps were as follows:

- Selecting seed segments of the lung and the background (Figure 4-9)
- The software initialises the process of growing seeds and provides a preview to be checked (Figure 4-10)
- Thereafter the segmentation was applied to select the lung region (Figure 4-11)
- A 3D visualisation of the segmentation can be obtained as seen in Figure 4-12.
- Once the model was created, the Gaussian smoothing option was selected to smoothen the model.
- The model was then exported to STL format so that it could be used for mesh analysis or 3D printing.

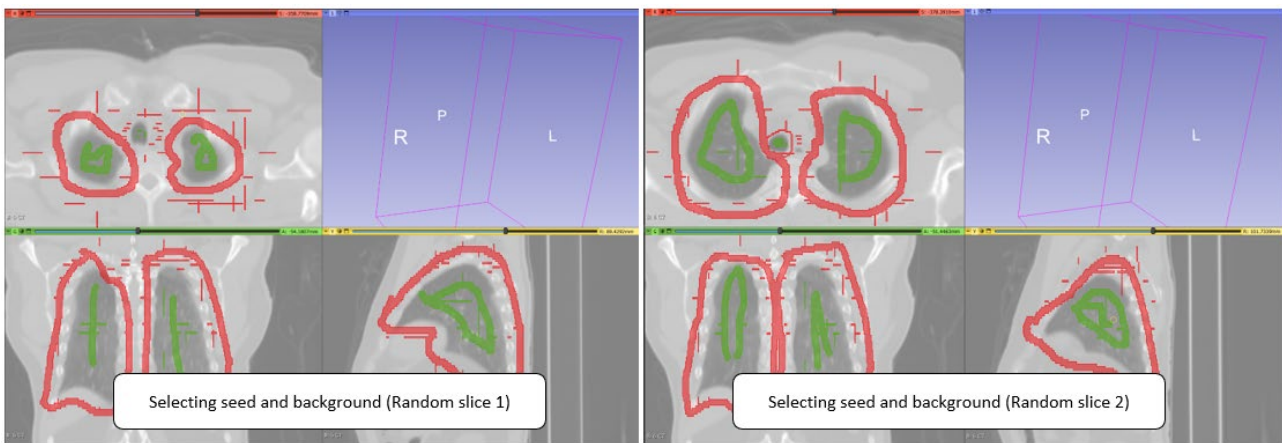


Figure 4-9 - Selecting seed and background segment

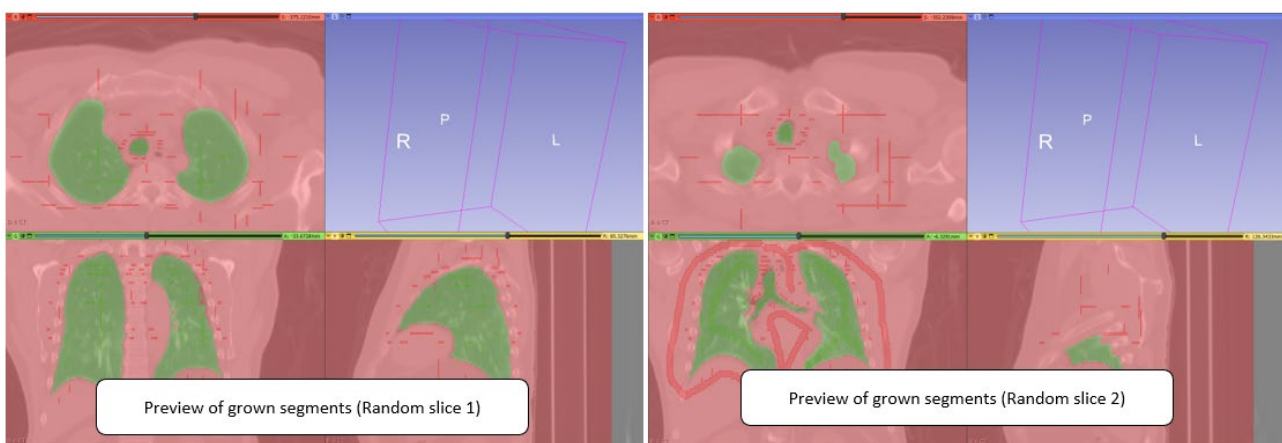


Figure 4-10 – Preview of grown segments

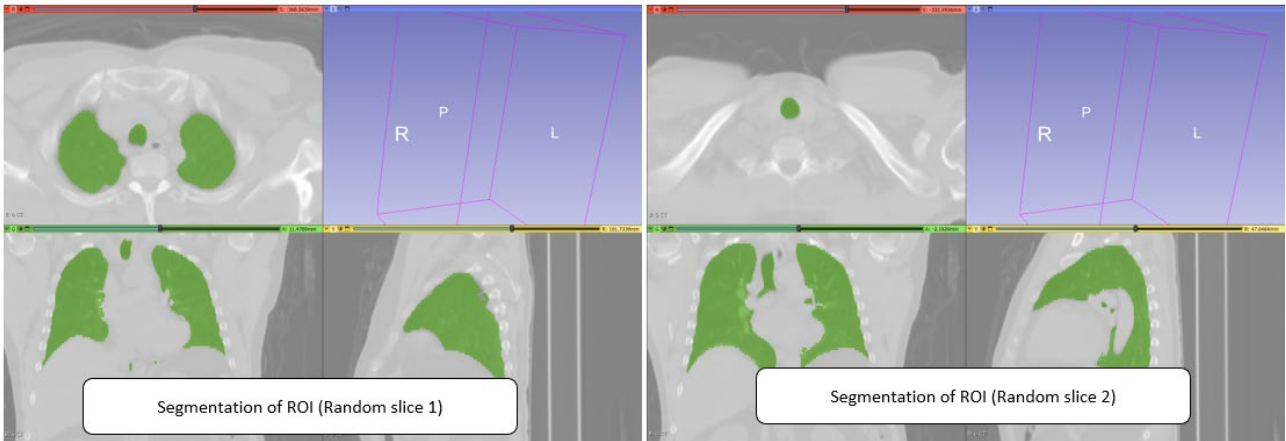


Figure 4-11 – Segmentation of the lungs

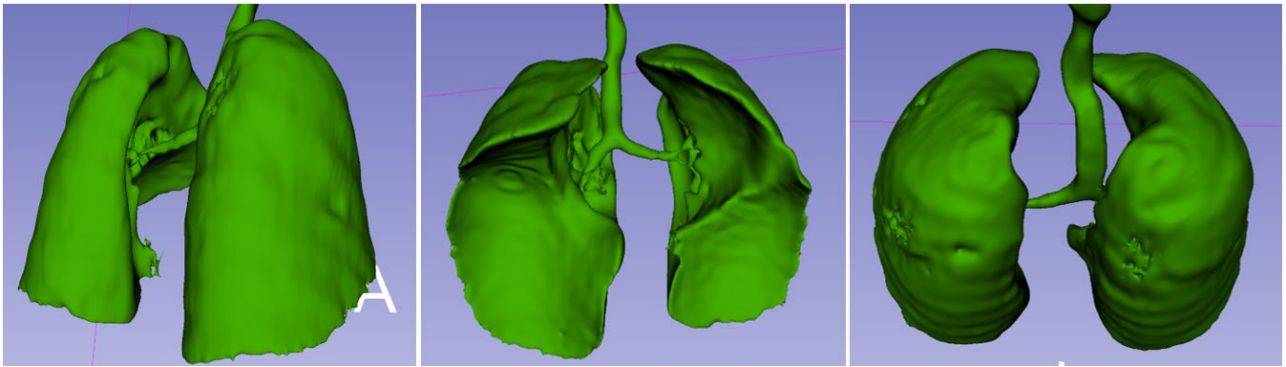


Figure 4-12 – 3D visualisation of the lungs

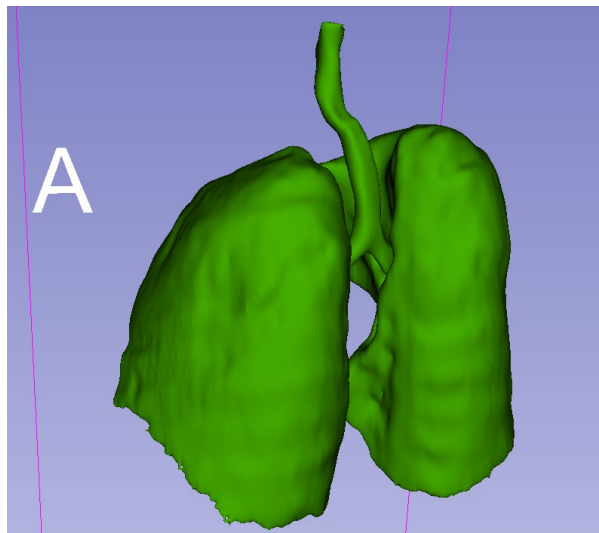


Figure 4-13 – Smoothened model of the lungs (grow from seeds)

## 4.2. Segmentation Of Femur Bone

Norway is one of the countries with the highest registered incidence of hip fractures in the world. About 60% of the hip fractures are in the femoral neck, a few in the caput, and the rest are in the trochanteric region, called trochanteric, pertrochanteric, or intertrochanteric fractures. As such, the anatomical structure used in this thesis is a human femur bone model.

DICOM files from CT scans of a human femur bone were acquired from the Stavanger universitetssjukehus (SUS). The DICOM image is from a 40-year-old male (80 Kg). CT images are a map describing the penetrability of X-rays i.e., they are a pixel map of the linear X-ray attenuation coefficient of tissue. The values are scaled so that the linear X-ray attenuation coefficient of air equals -1024 and that of water equals 0. This scale is called the Hounsfield scale. The DICOM files were then converted to image files using Mimics software.

The DICOM images were then processed in MIMICS 24.01 (Figure 4-14). The 3D model of the femur bone was created by implementing the following steps:

- *Thresholding* - This was based on Hounsfield Units (HU) so that the ROI chosen is only those pixels of the image within the defined value. For bones, the HU ranges from 200-250 to 3000 HU [87].
- The region growing process allows splitting the segmentation into the ROI and background (surround area of ROI).
- The generated region mask was used to develop a 3D model for the bone. The 3D reconstruction is based on 3D interpolation techniques that transform the 2D images into a 3D model. For this reconstruction case, grey values interpolation was used associated with the accuracy algorithm for achieving a more accurate dimensional representation of the femur.
- 3 Matic software was used to convert the 3D model to STL files for 3D printing.



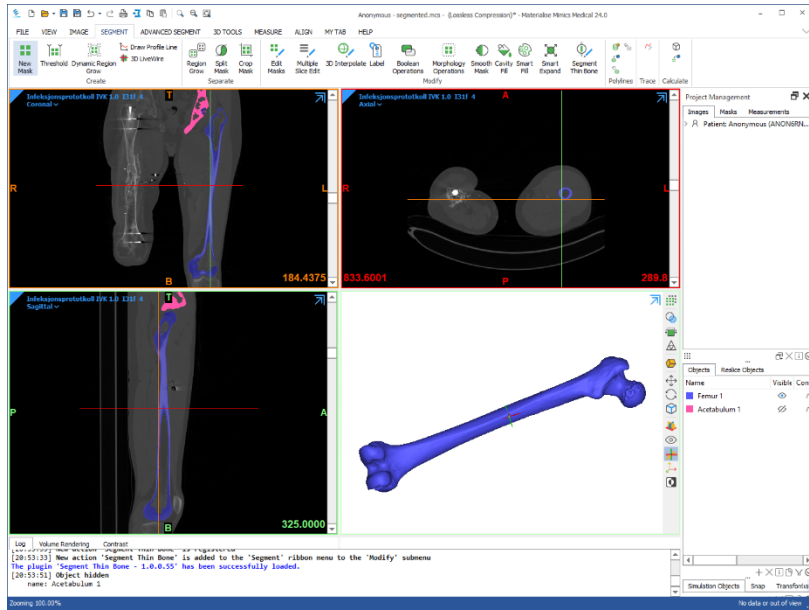


Figure 4-14 – Mimics environment (segmentation)

### 4.3. Post-processing

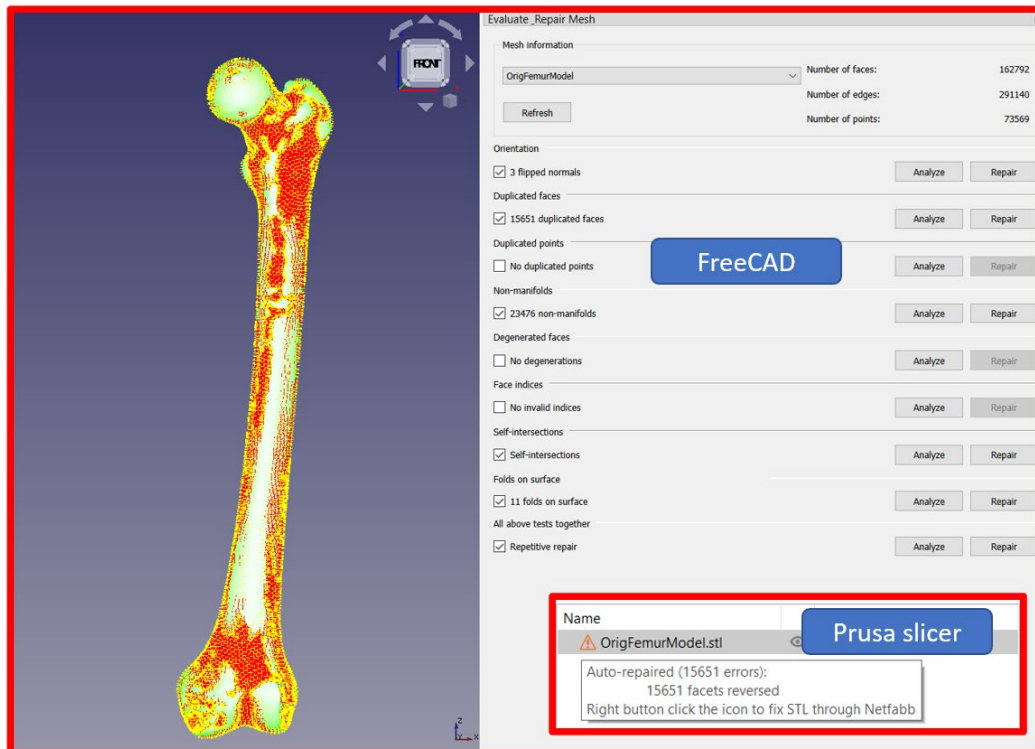


Figure 4-15 - Mesh Analysis in FreeCAD and Prusa slicer

The STL file exported from Mimics contained some errors, as shown in Figure 4-15. The model was imported into FreeCAD and the Prusa slicer to demonstrate the possible errors in the slicing software. If left unprocessed, there will be several errors in the slicing process and even incorrect slicing (as can be seen from the Prusa slicer error message). The post processing and cleaning of the mesh file was conducted in MeshLab.

#### **4.4. 3D Printing Process**

The femur model was 3D printed using the Fortus 450mc, an industrial FDM 3D printer (Figure 4-16). The STL file created from 3 Matic software was then imported into the slicing software used for this printer, Insight. Thereafter the sliced model is then imported into the control centre where the model was placed in the exact location and orientation for printing.

FDM printers are AM technology that is based on material extrusion. An extrusion tool melts filament material (polymer or metal) and traces the profile of a slice of a model. This is done in succession while either the build platform moves down, or the extruder moves up fractions of a millimetre (usually defined by the user). With regards to medical applications, FDM printers are useful in creating medical models. In one such study conducted by Christian et al. [161], 3D printed models created from SLS and consumer-grade FDM were compared, and their results showed that even consumer-grade FDM printers can produce medical models with sufficient dimensional accuracy for use in maxillofacial surgery.



Figure 4-16 - Fortus 450mc (Industrial FDM 3D printer at UiS)

The STL file was then imported into the slicing software for the Fortus 450mc. The slicing software options for the Fortus 450mc include Insight and GrabCAD. The software used in this instance was Insight.

The initial import and slicing are shown in Figure 4-17. This sliced model was generated based on the best option with minimal supports option. The printing time would be 24 hours with a large support structure. However, to minimise the material usage the model was scaled to 97% of the original size and sliced within the Insight environment as shown in Figure 4-18. The final printing time was approximately 11 hours and 15 minutes. Figure 4-19 displays the 3D printed model.

Table 4-1 - Printing Parameters for femur bone (FDM Fortus 450mc)

Printing Parameter	Value
Printing nozzle size	T16 (0,254 mm) for model T12 (0,178 mm) for support
Nozzle temperature	315°C for model 293°C for support
Bed temperature	90°C
Shell thickness	4 mm
Layer Height	0.2542
Total printing time	11,25 hours

Material used	202 cm <sup>3</sup> model 122 cm <sup>3</sup> model
Number of layers	330
Type of printing	sparse

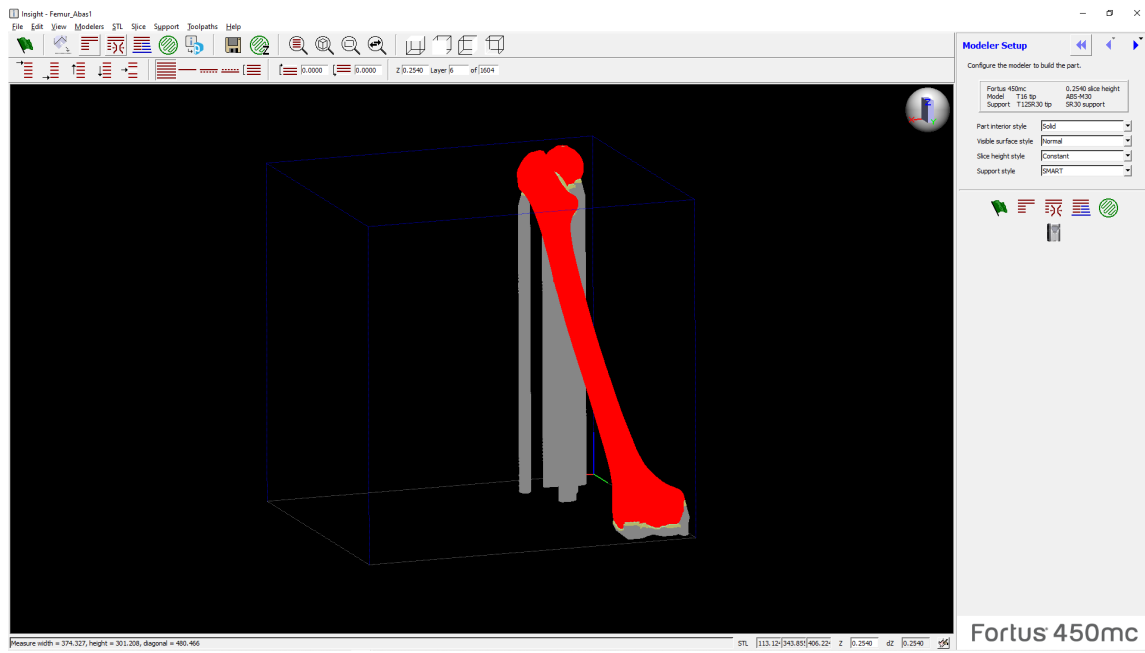


Figure 4-17 - Initial import and slicing

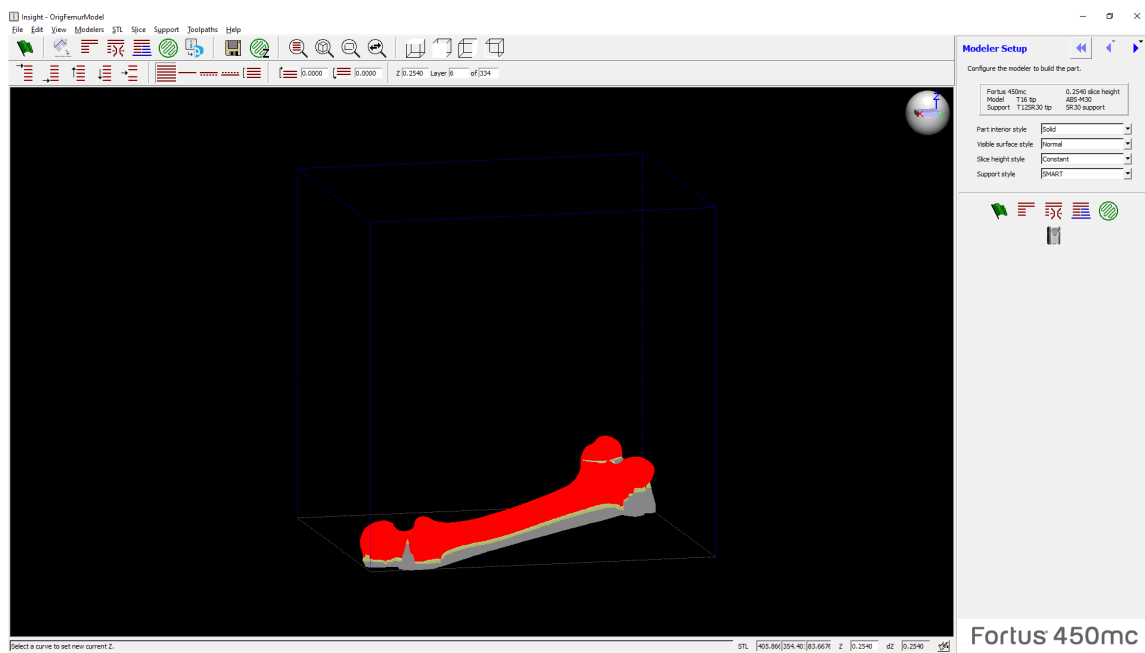


Figure 4-18 - Final import and slicing



Figure 4-19 - 3DP Model of femur

The printed part, especially with no overhanging parts, had minimal support structures printed as well. These support structures have different properties for the ease of removal upon printing of the part. The difference in properties from the main filler material could be either a completely different material or the same material as filler but with a thinner layer height and resolution. In this case it was a different material

The additional material created from supports was dissolved while the femur model remained as the final part. This was achieved by melting the 3D printed part in a solution of sodium hydroxide. In a sodium hydroxide bath of about 85 °C the excess support material dissolved away.

#### **4.5. Reverse engineering**

The femur bone that was 3D printed to a scale 97% was used as a basis for the reverse engineering process. Some of the aims of this study are as follows:

- 3D scanning with different 3D scanners
- Comparison of the different 3D scanning software environment
- Development of 3D models from the 3D scanned point clouds
- Assessing solid modelling techniques (already presented in section 3.6)

- Using 3D scanning as a dimension verification/quality control tool and conducting deviation analysis

#### 4.5.1 3D Scanning Of Femur

The first step of RE of physical objects (as outlined in Figure 3-2) is the 3D scanning of the component. The bone model that was 3D printed was then scanned using three portable non-contact 3D scanners available at the university at the time. The three scanners that were used are the Handyscan 700, Einscan HX, and the Artec EVA-M 3D scanner. The specification of each scanner is mentioned in Table 4-2. With the scanning process itself, the aim is to obtain a point cloud with a good resolution that can be further used for modelling and analysis purposes.

Table 4-2 - 3D scanner Details ( [162–164])

Scanner			
<b>Scan method</b>	Triangulation and binocular vision	Structured light	Structured light
<b>Scan Speed (pts/s)</b>	480,000	1,200,000	18,000,000
<b>Light Source</b>	7 laser crosses and an additional line	LED	Flashbulb + 12 Led array
<b>Range (m)</b>	0.3	0.3 – 1	0.4 – 1
<b>Accuracy (mm)</b>	0.03	0.05	0.1
<b>Resolution (mm)</b>	0.05	0.25 – 0.3	0.2

<b>Data processing</b>	Markers	Markers/features/ hybrid/texture	Geometry and texture based
<b>Weight (kg)</b>	0.85	0.71	0.9
<b>Accompanying software</b>	VX Elements (VX Scan, VX Model, VX Inspect)	Shining3D	Artec Studio

Prior to scanning the full femur model a test run was done with half a femur model to get acquainted with the 3D scanner and the VX software environment. To achieve this, the STL file of a femur from the online repository Embodi3D was downloaded. For practical reasons, the STL file was divided into 2 parts using FreeCAD. This was then printed on an Original Prusa i3 MK3 3D printer available for students at the university. The process has been displayed in Figure 4-20.

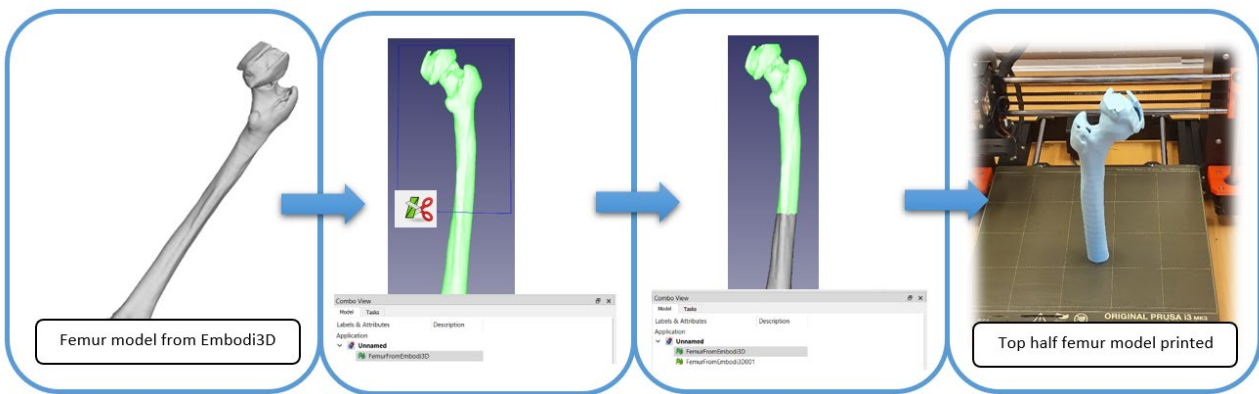


Figure 4-20 - 3D printed femur model from Embodi3D

The trial scan was conducted in the 3DP lab at UiS with the Handyscan 700. The top half of the femur was placed erect on the rotating platform. The femur was then scanned to obtain a point cloud which included the platform and the surrounding with some noise. The VX scan software module allows for post-processing of scanned data for cleaning up and refinement purposes. Using these features, the point cloud data was cleaned and thereafter meshed and converted to STL format.

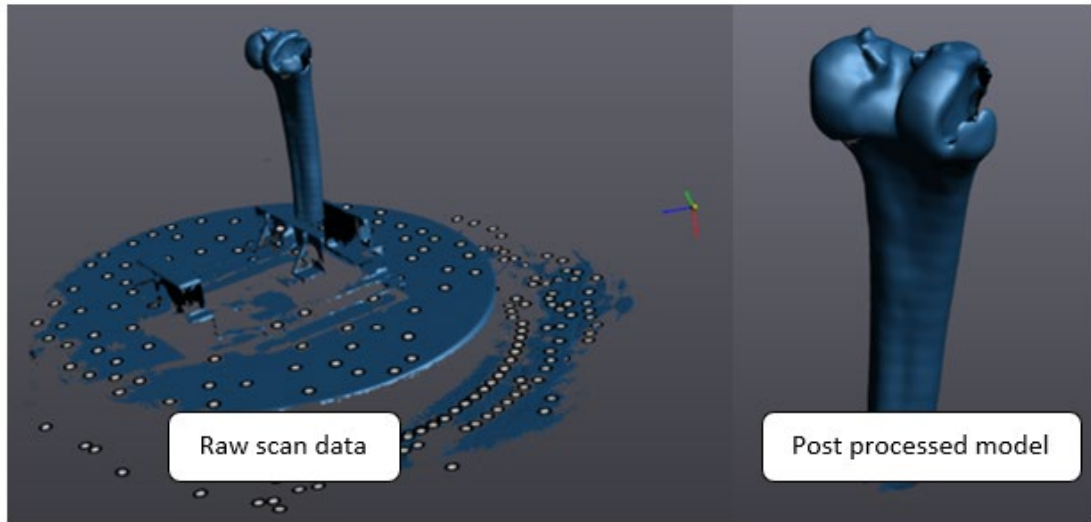


Figure 4-21 - Raw scan data vs post processed model

The steps taken to obtain the model are:

- Using the *remove background* together with *add clipping plane* and *free hand clipping*, the bulk of the background data was removed
- Thereafter the *Remove Isolated Patches* filter was applied plus *Brush selection* and *Delete Face* tools.





### Figure 4-22 - 3D printed model vs. scanned model

In Figure 4-22 views 1 and 2, it can be seen that there is good coherence between the 3DP model and the scanned model with respect to capturing features of the 3DP model. The acquisition data was significantly better when there was an angle of incidence w.r.t the reference line.

However, with views 3 and 4, it can be seen there's quite a significant deviation. With this particular model, the gaps seen in view three are not a problem as the 3DP model itself has a flat surface, and the scanned model can be refined to create that surface during postproduction.

With regards to view 3, there's a significant lack of detail and missing data in the point cloud. The problem was persistent even when position marking stickers were added to the 3DP model, while the scanner was used by someone with good experience in utilising the technology.

The problem can be attributed to the scanner's angle, as shown in Figure 4-23. The relatively small surface area of the model coupled with fewer retroreflective targets used to triangulate must have resulted in the lack of information perceived by the scanning cameras. It must be noted this issue is specific to the model being used since on models with a wider surface area, more retroreflective targets can be used, which could lead to a different outcome during the scanning process.

Overall, this trial scanning process was a success in that lessons were learned to take forward in scanning the full femur model with regards to:

- Surface preparation
- Model positioning during the scanning process
- Familiarity with the VX Scan, VX Model and VX Inspect software modules.

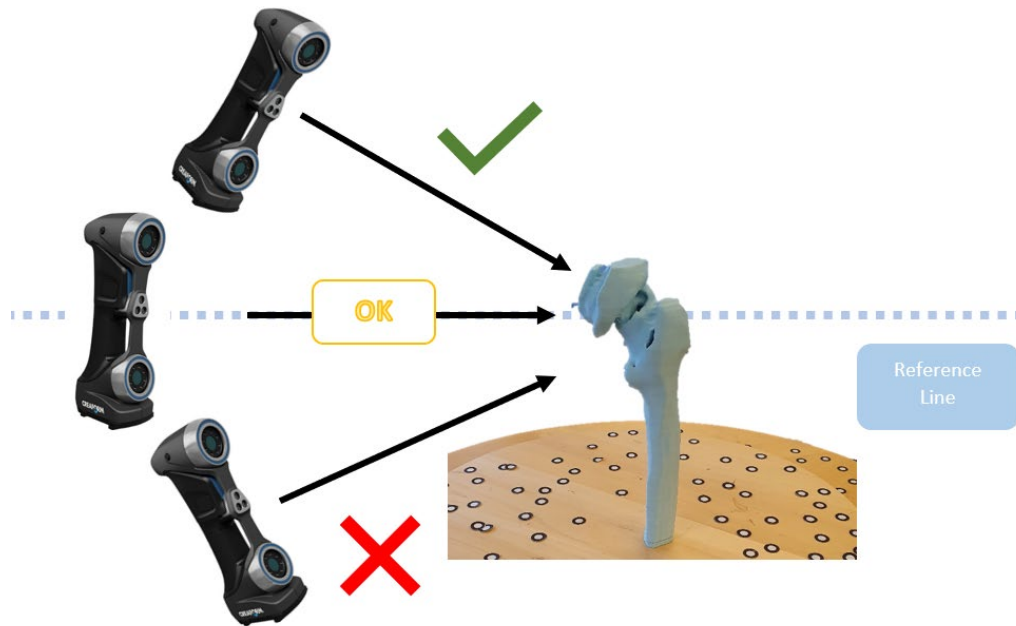


Figure 4-23 - Suitable scanning angle of a femur model for Handyscan 700

All three scanners are handheld scanners and portable, while only the Artec scanner had a portable power source. The preparation process for each scanning process was similar but differed due to the environments (physical locations) in which the scanners were used.

### *3D scanning of full femur model*

As mentioned in section 3.2, 3D scanning technologies can be either contact or non-contact. An attempt was made to scan using the CMM. The use of CMM is based on having a CAD model and thereafter scanning using physical probes by using datum points on the CAD model. Due to the femur's non-linear or organic shape, it was impossible to orient the physical model and the CAD accurately as a datum point. The way forward would be to add linear or planar extrusions to the CAD model and conduct the printing. This would eliminate the problem of needing datum or reference points. Due to time constraints, this could not be achieved. However, some distances were measured along the femur model.



Figure 4-24 - Scanning of femur using CMM

#### *Non-contact scanning*

From the lessons learnt during the trial scan, it was decided that the full 3DP femur model will be scanned twice in different orientations and thereafter combined using the post-processing tools available in VX Scan/VX Model, Shining 3D, and Artic Studio. The post-processing will also be tried in MeshLab.

## 4.5.2 Handyscan 700



Figure 4-25 - Handyscan 700

The Handyscan 700 (Figure 4-25) is a portable 3D scanner that works on triangulation and binocular vision principles. It is a lightweight scanner that is simple to use. The challenge with using this scanner is that it highly depends on the retroreflective markers for objects with a small surface area. Despite the problems faced during the trial scan, the full femur was erected on the rotating platform to try scanning but with no success, even with retroreflective markers (Figure 4-26 right). Again, this could be due to the scanning object being slender with minimal markers and surface area to triangulate.

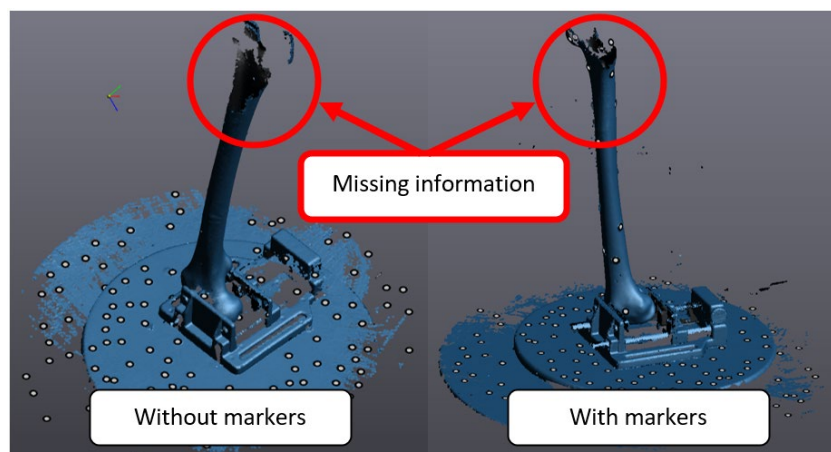


Figure 4-26 – Initial scan of the femur using Handyscan 700

To overcome this problem, the femur model was positioned such that the scanning height would be minimised and to maximise the capture of the platform and the markers on it. The preparation is displayed in Figure 4-27. The setup worked well, and the scanning took just a few minutes.

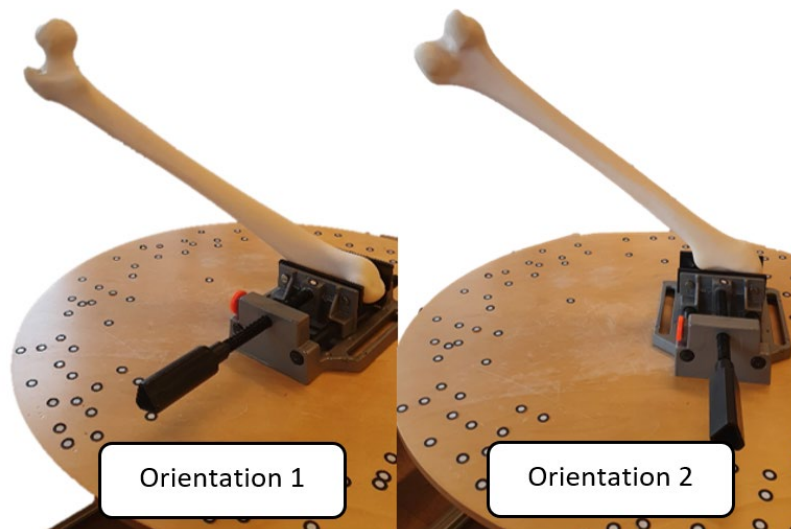



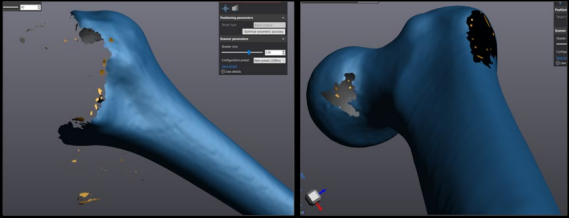
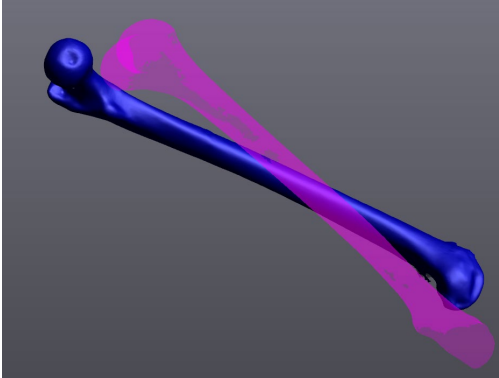
Figure 4-27 – 3DP model setup of femur for scanning (Handyscan 700)

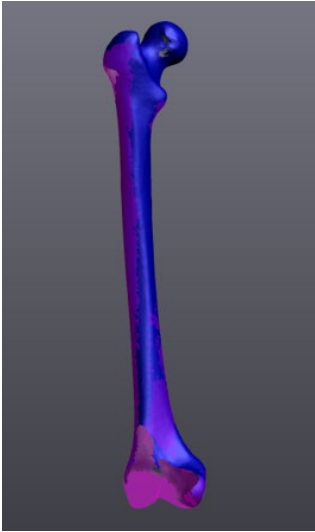
The two scans (orientation 1 and 2 in Figure 4-27) were conducted in the same project in VX Scan. Once they were scanned, the data was then cleaned, repaired and then aligned. The procedure that was followed has been outlined in Table 4-3. VX Scan provides the option of aligning and merging scans. The alignment can be based on:

- Target best fit – using a minimum of points that have to match in addition to an accepted level of tolerance to align two scans
- Surface best fit – using a maximum distance between two scans for alignment
- Global registration – for aligning and merging three or more scans.

For the alignment of the femur scans, since the mid-section for the model is common in both scans, the surface best fit option seemed optimal. This tool was then used to align the two scans and thereafter merge them to provide a single mode.

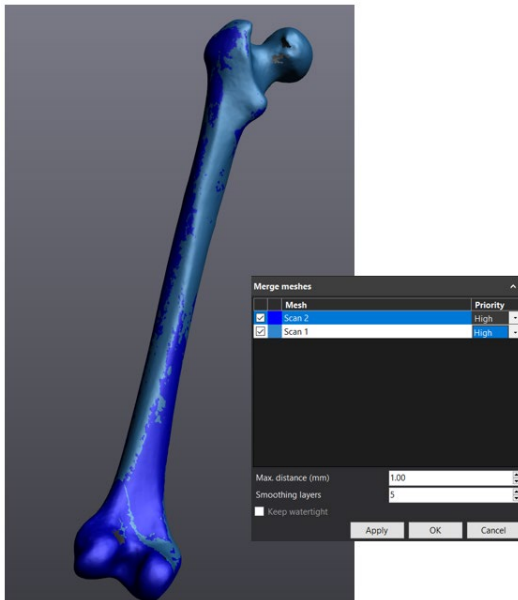
Table 4-3 - Post processing of femur scan in VX Elements

Images of the scan	Process
	<p data-bbox="772 434 1062 463"><b><u>Background Removal</u></b></p> <p data-bbox="772 519 1433 719">The raw files that are used by the VX Elements software package comes in the CSF format. The two scans contained background data and noise that needed to be removed.</p> <p data-bbox="772 775 1433 913">Using the <i>remove background</i> together with <i>add clipping plane</i> and <i>free hand clipping</i>, the bulk of the background data was removed.</p>
	<p data-bbox="772 1003 1142 1032"><b><u>Removal of isolated patches</u></b></p> <p data-bbox="772 1088 1433 1341">Once the bulk of the background data was removed, the <i>Remove Isolated Patches</i> filter was applied, plus <i>Brush selection</i> and <i>Delete Face</i> tools to remove unwanted, isolated data. (Seen in gold colour on the figure to the left)</p> <p data-bbox="772 1397 1433 1482">The file size at this point was approximately 230Mb.</p>
	<p data-bbox="772 1572 967 1601"><b><u>Pre-alignment</u></b></p> <p data-bbox="772 1657 1433 1800">In this mode, using one scan as a reference, points were chosen on the other so that the models are pre-aligned.</p>



### **Alignment**

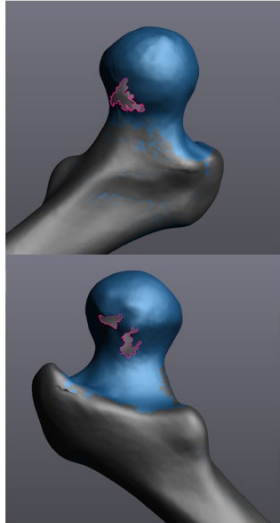
The align tool launches the alignment of the scan based on the given parameters



### **Merge**

The two scans that were aligned in VX Scan, were then taken across to the VX Model module. The scans were then merged by giving each scan high priority.

The file size at this point is approximately 463Mb.



### **Filling of holes**

Using the fix hole function in VX Elements and an appropriate curvature setting, all holes in the merged model were then fixed.



### **Conversion to CAD format**

The merged model was then converted to different CAD formats that could be used e.g., in software like MeshLab or Autodesk Inventor for further analysis or modelling. On the left is the STL model of this scan and the STL file size is approximately 5.5Mb.

---

## **4.5.3 Artec EVA-M**





Figure 4-28 – Artec EVA-M

The Artec EVA-M (Figure 4-28) is a portable 3D scanner that works that has a portable power supply and works on the principles of structured light. It is a lightweight scanner that is simple to use. There were minimal challenges when using this scanner. Together with the Artec Studio software, the scanner provides multiple options to use during scanning and for alignment when scanning, including an HD scanning mode that will use its specialised algorithms to conduct post-processing with minimal interference. The post-processing is very similar to that mentioned in Table 4-3 for the Handyscan 700, i.e., removal of the background information, removal of isolated data and patches, alignment and merging of the two scans. Figure 4-29 is a summary of the model transformation from raw scan to the final model

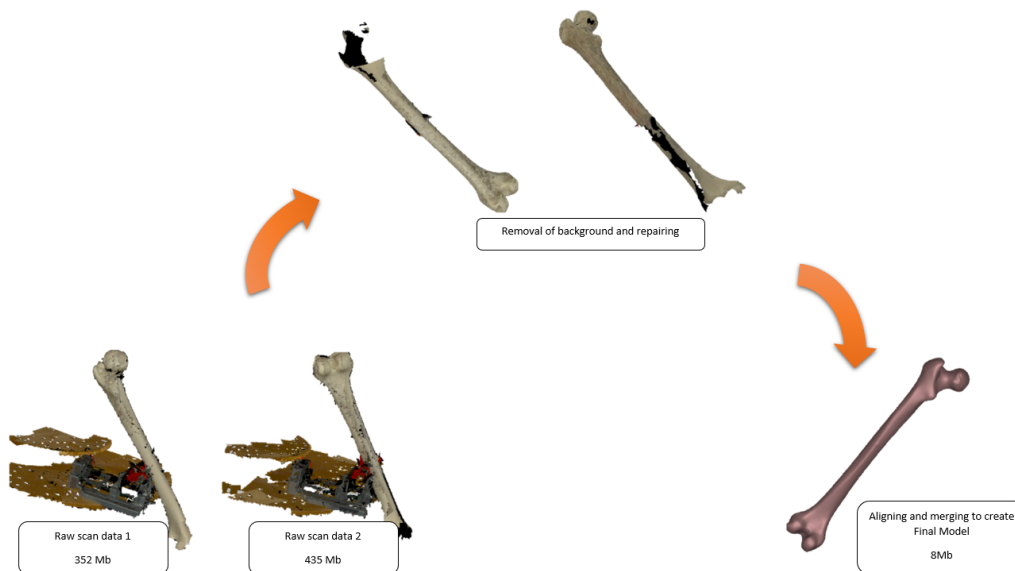


Figure 4-29 – Scanning process using Artec EVA-M

#### 4.5.4 Einscan HX



Figure 4-30 - Einscan HX

The Einscan HX (Figure 4-30) is a portable 3D scanner that works on the principles of structured light. It is a lightweight scanner that is simple to use. There were minimal challenges when using this scanner. Together with Shining3D software, the scanner provides multiple pre-setting options to use during scanning for alignment when scanning.

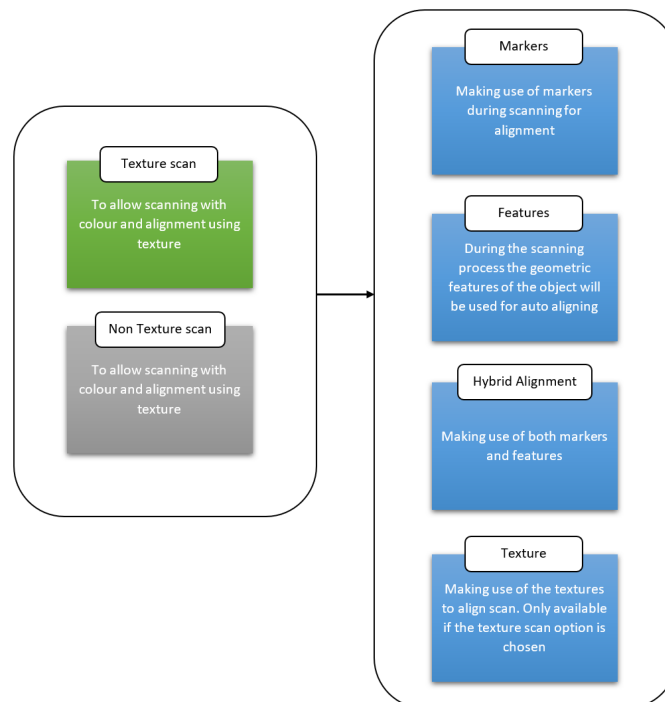


Figure 4-31 - Shining3D Pre-setting

For scanning using the Einscan HX, the femur model was placed erect on a table on a vice (Figure 4-32). Since the femur has an organic shape, the model was scanned using the non-texture scan based on features. The setup worked quite well, and the scanning process took just a few minutes.



Figure 4-32 – 3DP model setup of femur for scanning (Einscan HX)

A very similar process was followed in the Shining3D environment as mentioned in Table 4-3 when it came to the post-processing, i.e., removal of the background information, removal of isolated data and patches, alignment and merging of the two scans. The scanned file using the Shining3D software was ASC format and about 3Mb. The final alignment can be seen in Figure 4-33.

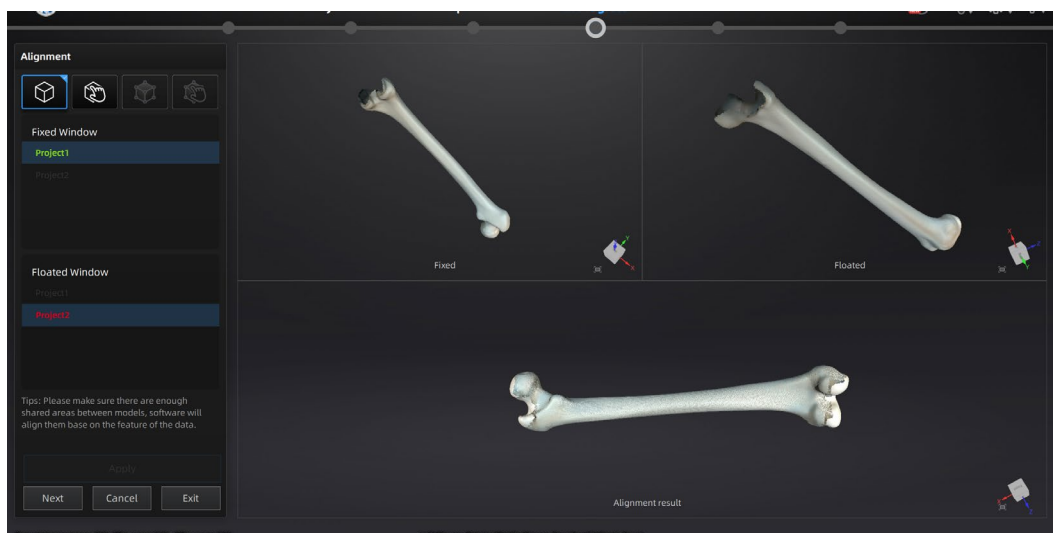


Figure 4-33 - Alignment of femur scans in Shining3D

## 4.6. Post-processing using MeshLab

MeshLab is open-source software available for editing 3D triangular mesh files [165]. The software is based on an open-source C++ mesh processing library, The Visualization and Computer Graphics Library (VCG), for manipulation, processing, and displaying triangle and tetrahedral meshes.

The raw data from each of the scanning entities produce quite large files that require significant computational power for handling and manipulation. For e.g., in VX elements, the file size of the raw scans is roughly 230Mb, while in the Artec Studio is about 800Mb. A possible alternative will be to conduct the post-processing, i.e., course segmentation (i.e., removal of background data and isolated patches) and conduct alignment and post-processing of the mesh in open-source software like MeshLab that require fewer resources.

### Proposed steps for merging scans in MeshLab

All three software provided the option to convert their original files, i.e., in CSF, ASC, and SPROJ file formats, to STL once scanned data was obtained. In order to demonstrate the post-processing in MeshLab, the two scans obtained from the Handyscan 700 will be used for post-processing and merging the two scans.

### Step 1 – Convert to STL and import into MeshLab

- Export each scan as a mesh in VXscan to STL file format
- Import the STL files into the initial scans into MeshLab one at a time

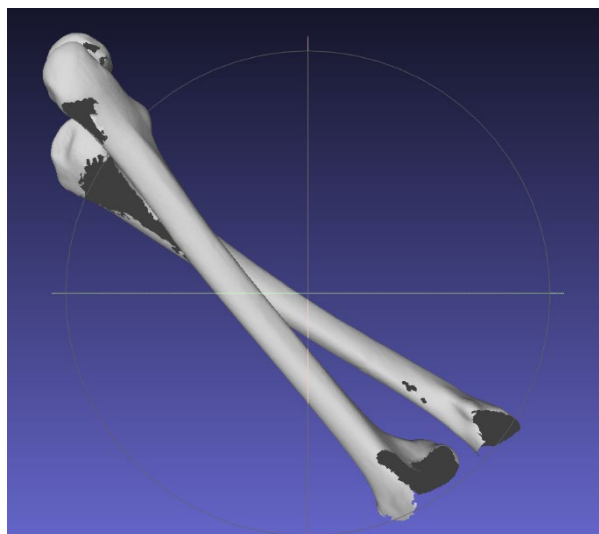


Figure 4-34 - Imported scans in MeshLab

The imported files do not lie in the same plane and have different global and local coordinate systems. Each scan file has a completely different set of global and local coordinate systems, as seen in Figure 4-34. In order to merge the two scans, they have to be aligned in position. One of the best-known algorithms to align point clouds/meshes is the iterated closest point (ICP) algorithm [166]. The algorithm compares a reference model and the model of interest and tries to minimise the Euclidian distance between them. Mathematically, the mean squared distance between two point clouds is minimised using a transformation matrix that includes rotation and translation components [167].

### **Step 2 – Align meshes**

- The MeshLab align tool is based on the ICP algorithm and can be used to align the two scans.
- Open the Align dialogue box. Freeze one of the scans to use as the reference model. In this case, the scan with more vertices was glued. An asterisk should appear once
- Next, select the second scan in the dialogue box and choose *point based gluing*.
- This is a pre-aligning step where at least four mutual points are selected on each scan model to bring them close to each other before implementing the aligning algorithm.
- The point base glueing can be done using point rendering for more accurate pre-alignment.
- The points chosen for this particular case are shown in Figure 4-35, and the pre-alignment is shown in Figure 4-36.
- Once the pre-alignment is complete, the processing for alignment can begin. The aligned models are shown in Figure 4-36, together with the error bound. As a confirmation of the transformation, a comparison of the transformation matrices of scan one and scan two can be seen in Figure 4-37.
- It is desirable to save the model information as a transformation. Therefore, do not fix the alignment of the transformed model matrix as an identity matrix. That is, do not use the freeze matrix option under filters.

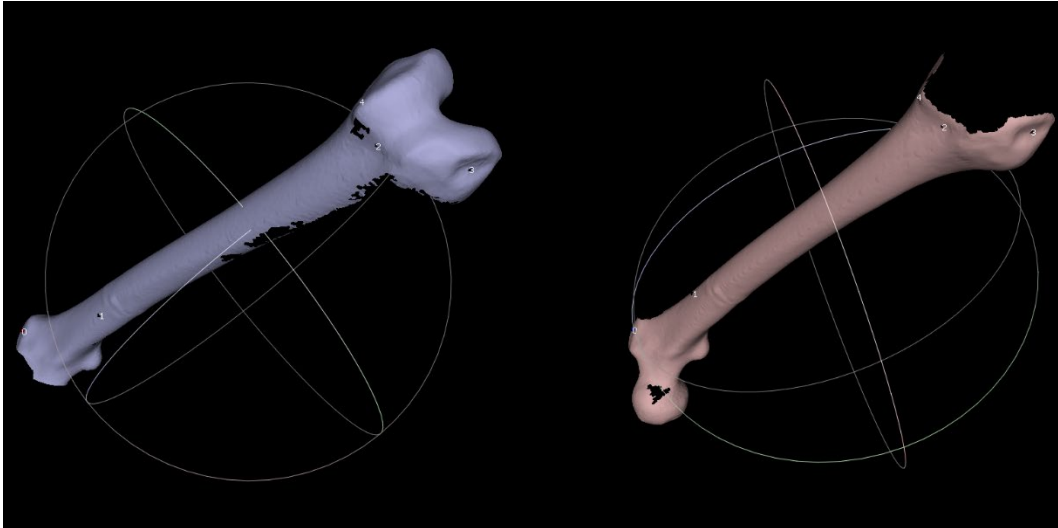


Figure 4-35 - Points chosen for pre-alignment

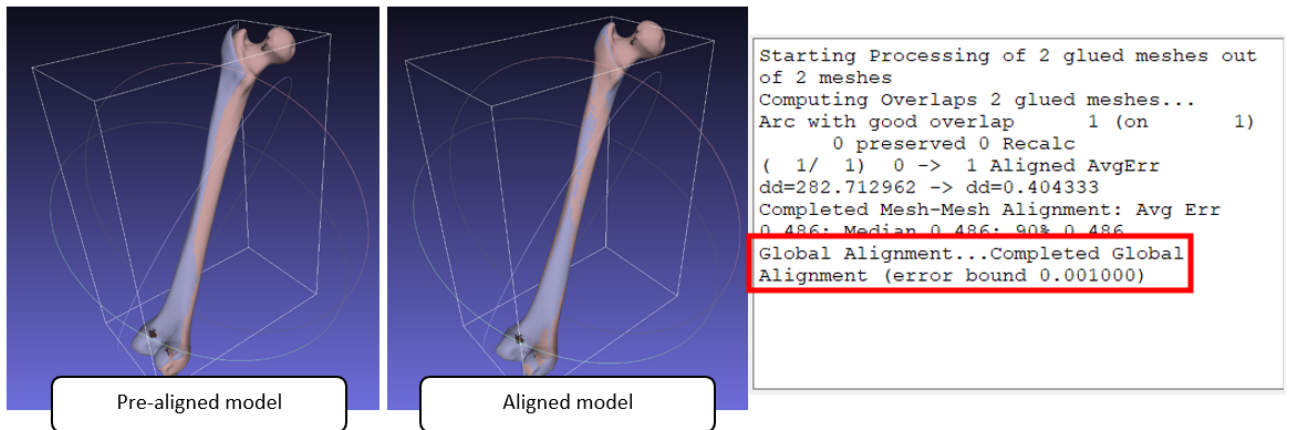


Figure 4-36 - Completed Global Alignment

Current Mesh: Scan 1	1.00	-0.00	0.00	-0.00
Vertices: 46,748 (92,420)	0.00	1.00	0.00	-0.00
Faces: 92,314 (181,812)	-0.00	-0.00	1.00	-0.00
Selection: v: 0 f: 0	0.00	0.00	0.00	1.00
Current Mesh: Scan 2	-0.01	0.91	0.41	-626.83
Vertices: 45,672 (92,420)	0.93	-0.15	0.35	373.31
Faces: 89,498 (181,812)	0.38	0.39	-0.84	675.87
Selection: v: 0 f: 0	0.00	0.00	0.00	1.00

Figure 4-37 - Transformation matrices (reference vs. transformed)

### Step 3 – Merge meshes

- Now that the meshes are aligned, they can merge using the flatten visible layers command to merge the two meshes. This function is desirable in this circumstance as it allows for the merging of scans by taking into consideration the transformation matrix used for alignment.

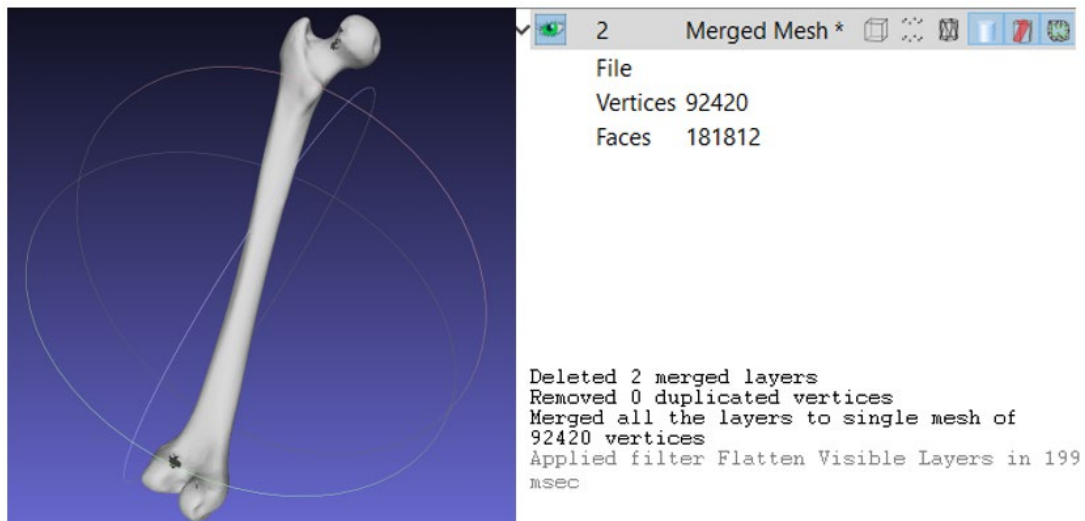


Figure 4-38 - Merged Model

#### **Step 4 – Repair and fix (watertight model)**

- Once the model is merged, some evaluations and repairs that could be done. Some of the most common operations include: *Removal of duplicate faces, removal of isolated patches, removal of non-manifolds and removal of self-intersections*
- As can it been seen in Figure 4-38 the merged model is not completely watertight and contains holes that need to be covered.
- There are several hole-fixing algorithms [168], and the one used in MeshLab is based on the method described by Liepa [169].
- Using the close function, all holes in the model can be closed up by using a maximum threshold value to be considered for closing.
- However, as can be seen in Figure 4-39, the hole closing was not smooth. Therefore, it is recommended to use the close hole function for “small” holes, i.e., holes that fulfil the default threshold or are smaller.
- Another drawback is that the model may not be entirely watertight. In order to create a watertight model using this function, several iterations have to be conducted using different thresholds.

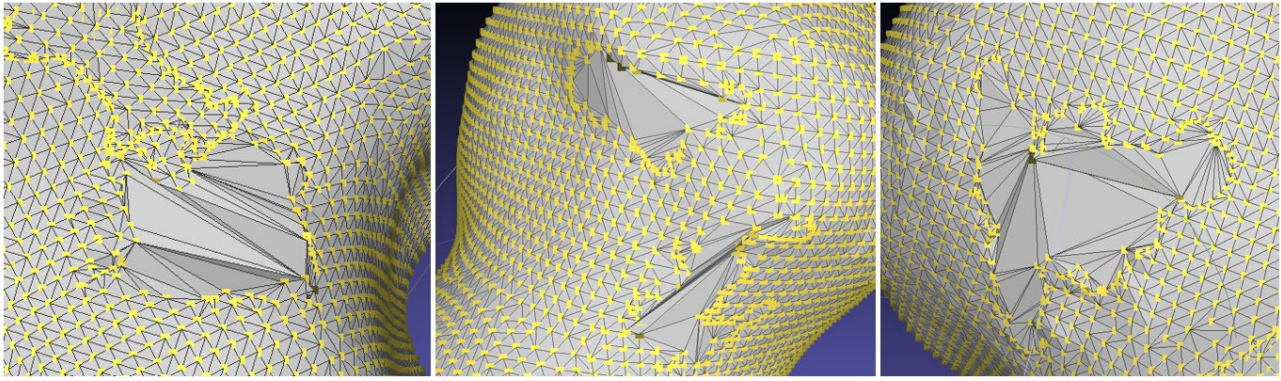


Figure 4-39 - Holes fixed using close hole function in MeshLab

- In addition to fixing holes, therefore, requires further functions that need to be implemented such as decimation of the affected areas and smoothing. Again, the model may not be entirely watertight since holes that satisfy the maximum threshold will be rectified.
- An alternative will be to use a function that will make the entire model watertight. The *screened poisson surface reconstruction* function in MeshLab (based on the algorithm presented by Kazhdan et al. [170]) does exactly that. Using this model, a watertight model can be created that fixes all holes much smoother than the fix hole function.
- A major drawback of this surface reconstruction is that the initial mesh will be very rough. However, this problem can be overcome using an appropriate remeshing tool and smoothing
- E.g. for this case the *Isotropic Explicit Remeshing* tool (based on [171]) and the *HC Laplacian Smoothing tool* (based on [172]) were used. The difference in applying these filters can be seen in Figure 4-40.



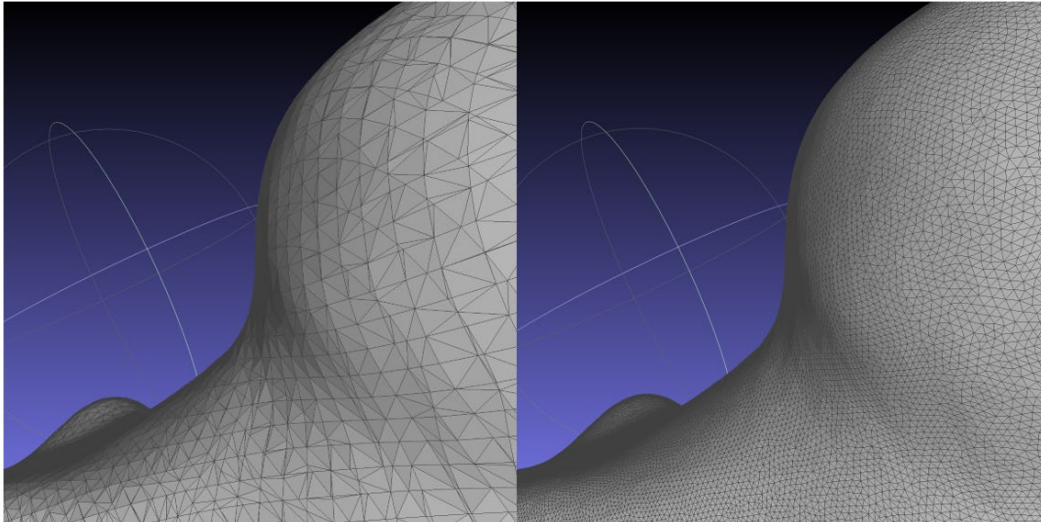


Figure 4-40 - Before and applying remeshing filter to Poisson Reconstructed model

## 4.7. Deviation Analysis

The analysis was conducted individually for each scan as it was not possible to align all three STL models with the original femur model. Nevertheless, each model was imported into the VX Inspect and MeshLab environments together with the original femur model as the reference file.

### *VX Inspect*

Once the 3D models were developed and converted to STL files, they were imported into VX Inspect. VX Inspect is a dimensional inspection software module of VX Elements. It can be used to perform inspections for the purposes of quality control and assurance [173]. The aim is to compare the models created by the three different scanning processes and determine the extent of deviations of the model from the original STL model and determine the model accuracy of the different scanned models by comparing them with the initial STL file. The scanned model from each scanner was then aligned with the reference model using the surface best fit option.

The colour map is a very useful tool to visualise the deviations of the models from the reference model. For the scanned models presented here, the tolerance has been set between -0.5mm to 0.5mm. The colour map displays the deviations based on this tolerance. Several values from different views and cross-sections were taken during the analysis. VX inspect provides the option of exporting the information analysed in the software in the form of a report.

## ***MeshLab***

The deviation analysis can also be conducted in MeshLab as well. The first step is to conduct the aligning process as described in section 4.6. Once they are aligned different filters can be added to the model to determine the deviation.

One option is the filter *Distance from reference mesh*, where both the model's negative and positive and negative distances can be determined with respect to a reference model. This filter adds the distance as a vertex quality. Meaning, in each data point would have the associated deviation distance as an additional value stored together with the vertex data. This data can be exported from MeshLab as a non-binary PLY file. This measure was used to assess the models created by each scanner.

Another option is to use the *Hausdorff distance* filter. This filter determines the Hausdorff distance between two data sets which is an absolute value. In this case, it is the distance between the original femur model and the scanned models. The algorithm used in MeshLab can be seen on their GitHub page [174]. The algorithm is based on the Hausdorff distance calculation mentioned by Shonkwiler [175]. This measure will be used to determine the deviation of the 3D printed model from the original CAD model as the filter calculates the absolute distances between the reference and target mesh. The mathematical expression of the Hausdorff distance is given below:

$$h(A, B) = \max_{a \in A} \left\{ \min_{b \in B} \{d(a, b)\} \right\}$$

## CHAPTER 5: RESULTS AND DISCUSSION

In this chapter the results obtained from the solid modelling process and the comparative deviation analysis will be presented and discussed. The qualitative and quantitative results will be presented and analysed for the deviation analysis.

### 5.1. Solid Modelling Results

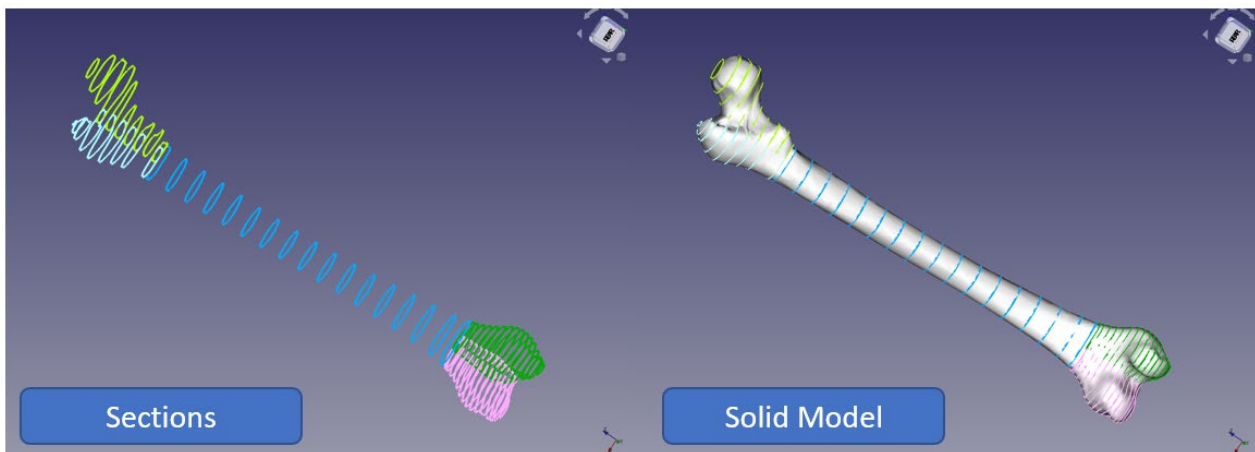


Figure 5-1 - Final Solid Model of the femur

The aim of this section is to compare the solid model created using the method described in section 3.6 and the solid model created by Autodesk Inventor using the automatic conversion function. Using the method described in section 3.6, a solid model of the femur was created using the STL file from the Handyscan 700. The initial model created did not capture most of the geometry. Therefore, the femur model was split into even smaller sections, as seen in Figure 5-1 left. This made it possible to capture the features of the femur much easier.

The Handyscan model was chosen for solid modelling purposes because it was the only model that was able to be converted directly to solid using CAD software Autodesk Inventor. This was required to use as a reference to compare the final model created using the methods proposed in section 3.6. The other scanned model files were too large in size to be converted by Autodesk Inventor

The distance from the reference mesh filter was used on the solid model; this can be seen in Figure 5-2. When comparing the designed model vs. the reference STL file, there are a few deviations. But there not significant.

To determine the properties of the solid model, the FreeCAD model was converted to .STEP file and imported into Autodesk Inventor. To compare the properties of the solid models, both the converted and the designed models were given Titanium material properties. The results can be seen in Figure 5-3, Figure 5-4, and in Table 5-1.

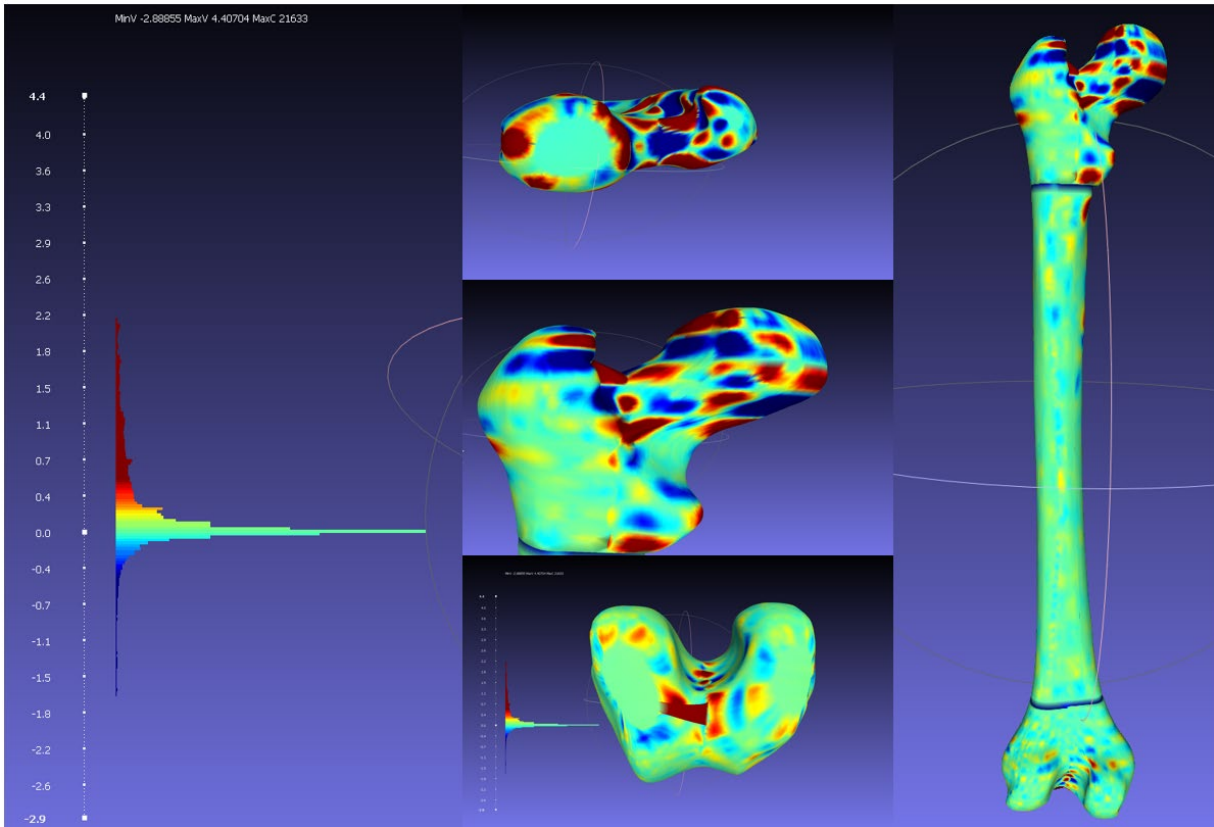


Figure 5-2 - Final solid model vs. reference model

Table 5-1 - FreeCAD vs. Autodesk Model

	<b>FreeCAD Model</b>	<b>Autodesk Model</b>
Weight	2.564 kg	2.566 kg
Volume	568485.596 mm <sup>3</sup>	568861.768 mm <sup>3</sup>
Area	66471.137 mm <sup>2</sup>	66088.332 mm <sup>2</sup>

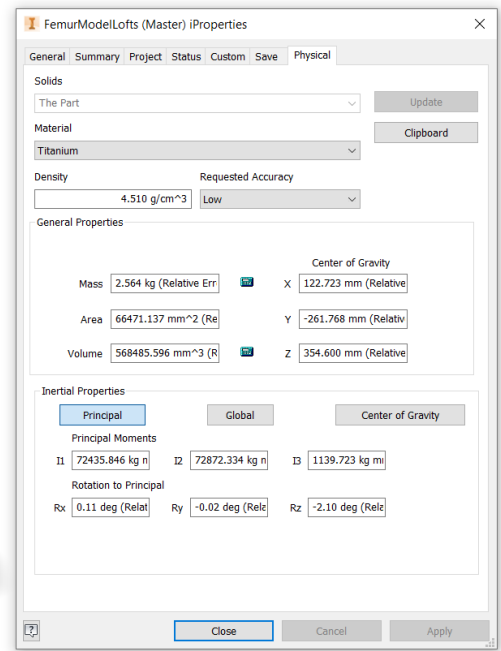


Figure 5-3 - Solid model using FreeCAD

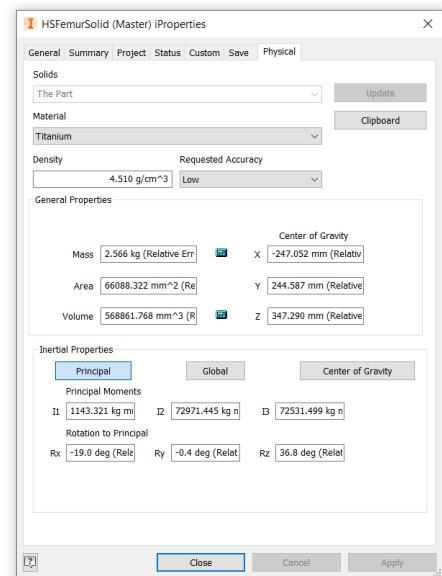


Figure 5-4 - Handyscan 700 model converted directly to solid in Autodesk Inventor

The results show that the proposed method for obtaining a solid femur model is useful since it has similar properties to the directly converted model. This type of model is essential, e.g., in FEA analysis. Therefore the proposed method can be a viable option to use open source software to create solid models with an organic shape using a reference STL file.

## 5.2. Qualitative analysis

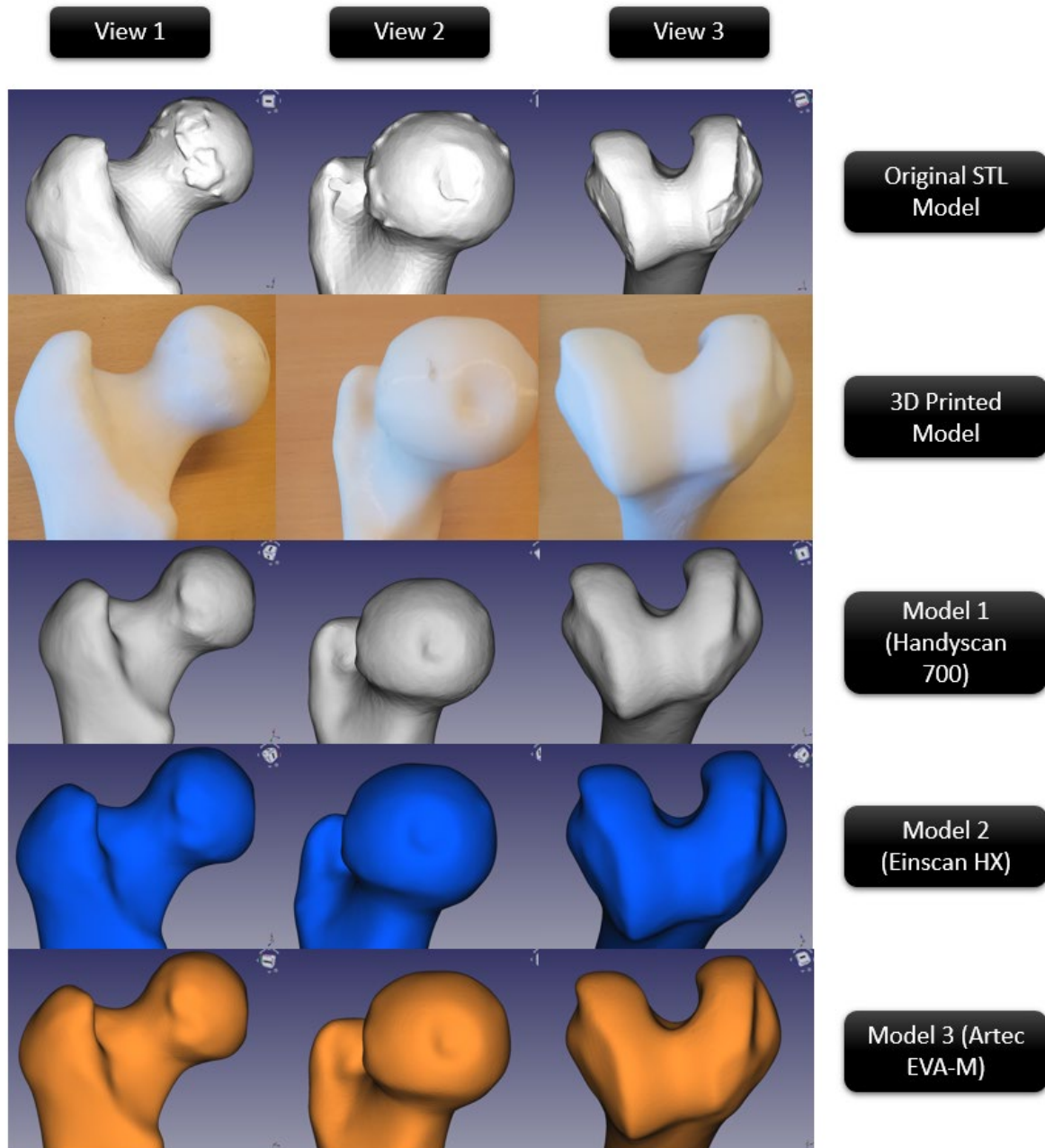


Figure 5-5 - Feature-based comparison of the original CAD model, 3D printed model, and CAD models obtained from the different scanning processes

Based on the visual inspection and comparison shown in Figure 5-5, some deductions can be made:

- The most distinct difference between the 3D printed model and the original CAD model is that all sharp edges have been smoothed. This is probably caused by the resolution of the 3D printer, which was unable to accurately print the curvature.
- All small protrusive features have been smoothed during the 3D printing process. This can be seen in views 2 and 3. This is probably caused by slicing. As highlighted in section 2.2.2, the slicing process interpolates points obtained while sectioning a CAD model. If the resolution of points taken was too high, i.e., wider than the features, then this information is lost due to the smoothing effect of the interpolation.
- All scanners have captured the distinctive features of the 3D printed model, as can be seen in views 1,2 and 3

### ***Contact scanning results***

Despite being unable to take a complete scan of the femur using the CMM, some distances were measured along the femur model. These are presented in Figure 5-6. The average deviation determined from these results is about 0.93 mm. The limitation with these results is that the measurements taken were highly subjective, i.e., without proper constraints to a reference point.

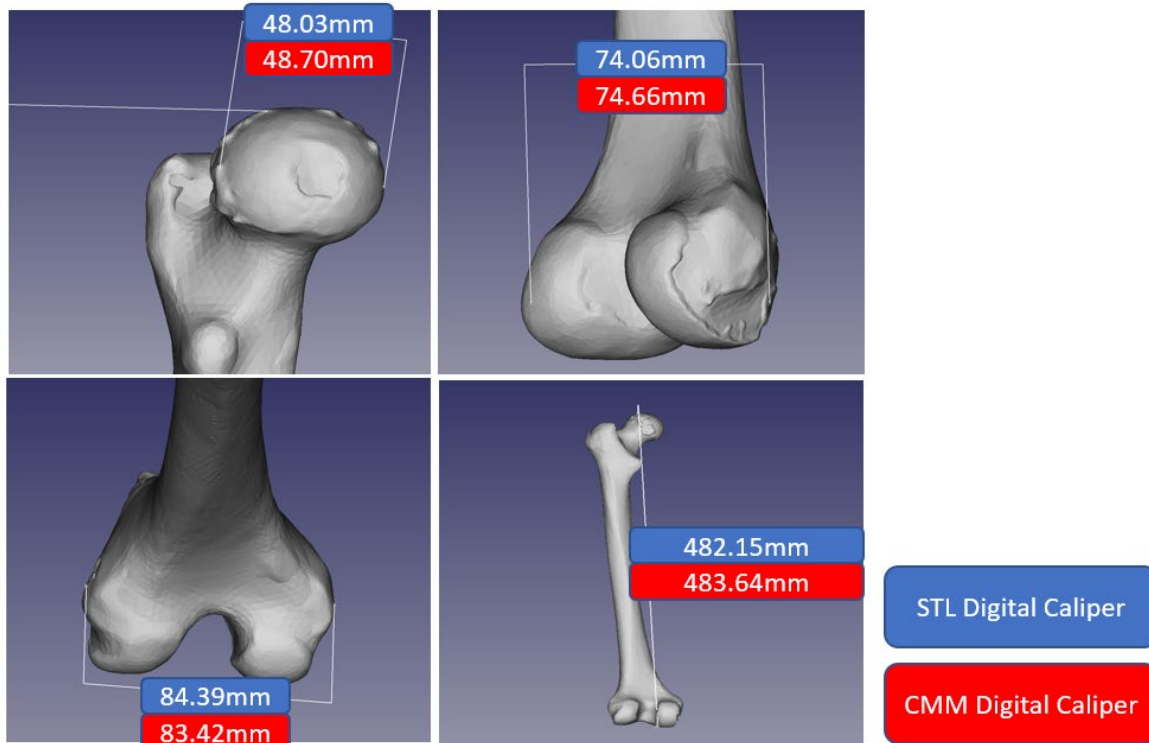


Figure 5-6 - CMM measurement vs. STL CAD Model digital measurement

### 5.3. Quantitative Analysis

The result from each scanning process is a point cloud. The point cloud was then processed within the different software entities associated with each scanner. Once the post-processing was complete, the final models were converted to STL format (and others). The comparison of the file size of each model obtained from different scanners is shown in Figure 5-7.

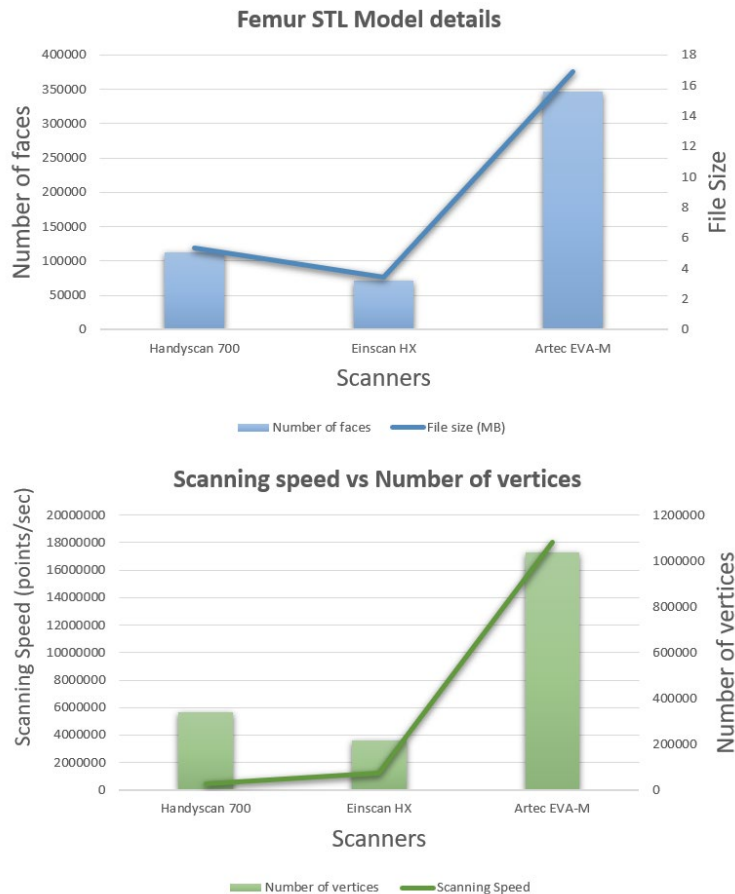


Figure 5-7 - Femur STL model details (top) Scanning points vs. no. of vertices comparison(bottom)

From the data presented in Figure 5-7, it can be seen that there is a direct correlation between the number of faces and the file size. The STL file created from the Artec EVA-M has significantly more vertices. This can be attributed to the very high-speed scanning of about 18 million points per second.

#### ***Deviation Analysis Results***

In the VX Inspect environment, once the models were aligned, the colour map tool was used to determine the deviations between the reference model and the scanned model. This was conducted for each model. The software provides statistical data that was obtained from the deviation analysis



tool and has been summarised and displayed in Figure 5-8. In the MeshLab environment, once the models were aligned, the *Distance from the reference mesh* filter was applied. The results obtained are displayed in Figure 5-8.

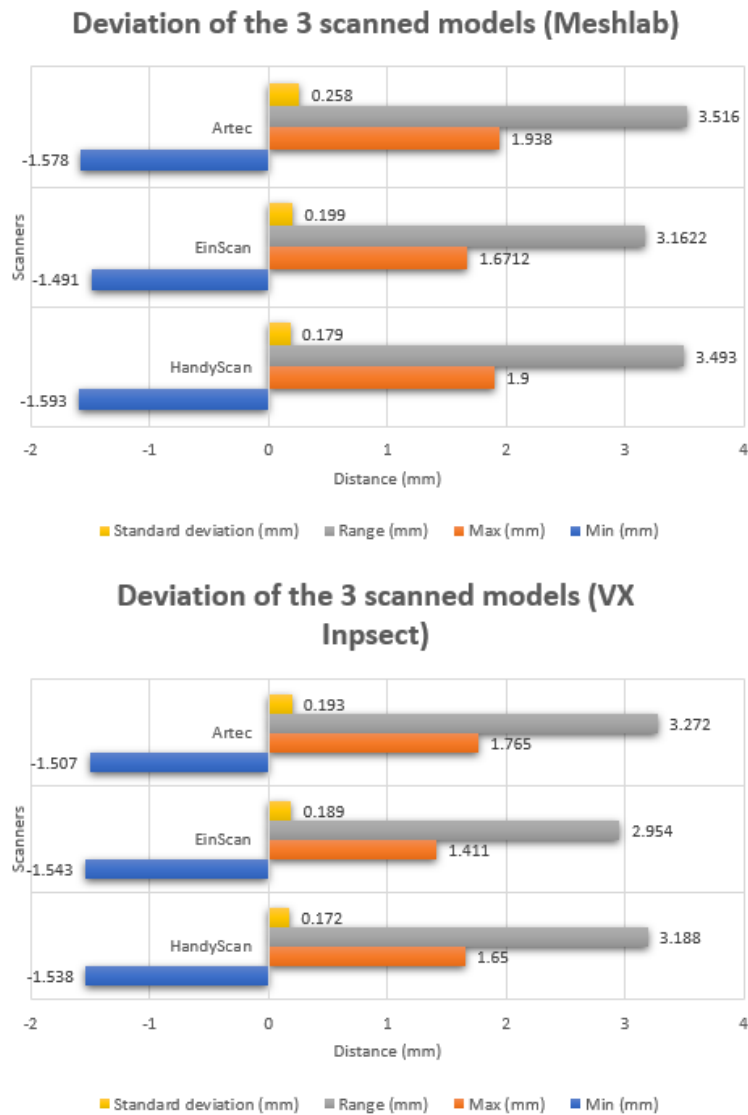


Figure 5-8 – Maximum, minimum, and the range of deviation of the scanned models

On average, the range of deviation is approximately  $3.34\text{mm}$ , while the average minimum deviations and maximum deviations are approximately  $-1.54\text{mm}$  and  $1.72\text{mm}$ , respectively. The maximum and minimum values could be found in approximately the same region on the 3DP model. This has been highlighted in Figure 5-9 a). These deviations are possibly due to the scanning processes. The region highlighted is affected by the shadows of the femur features in the two planes, as shown in Figure 5-9 b) and c). The area consists of a curved intrusion feature in the original STL file. Due to

the shadows, not many points have been captured in that region during scanning. When the points are then interpolated, the original curvature is lost, thus standing out as a large deviation.

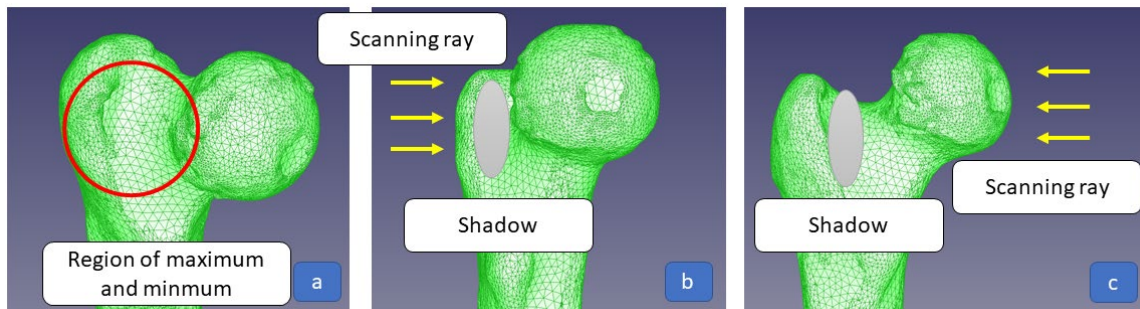


Figure 5-9 - Region of maximum and minimum deviation

## 5.4. VX Inspect results

The data extracted from VX Inspect w.r.t to the deviations of each model from the original mesh file is presented in Figure 5-10, Figure 5-11, Figure 5-12, and Figure 5-13. The histograms provide a good comparison of the performance of each scanner since the local deviation values are compared. This is a closer look at the various regions of the femur itself. The histograms represent the deviations in mm at different points on the various snapshots for the models created from each scanner. These diagrams can be analysed in terms of the different scanning technologies used and the orientation of the part that was scanned in.

The reading obtained at each point is a local value. These were obtained using the *toggle map* function available in VX inspect that allows viewing of the colour map and deviations in the viewing mode. The snapshots taken were not taken accurately aligned in the same plane. Due to the organic shape of the model, it was very difficult to find reference planes equal to all models. However, the snapshots were taken in views that were almost equal and provided a good comparison of the deviations in different regions from each model. The reports extracted during the analysis have been presented in Appendix A, Appendix B, and Appendix C. The corresponding colour map for each snapshot from Figure 5-10 to Figure 5-13 can be found in Appendix A, Appendix B, and Appendix C.

In the discussion to follow, the Artec EVA-M, Einscan HX, and Handyscan 700 will be referred to as scanners 1, 2, and 3, respectively.

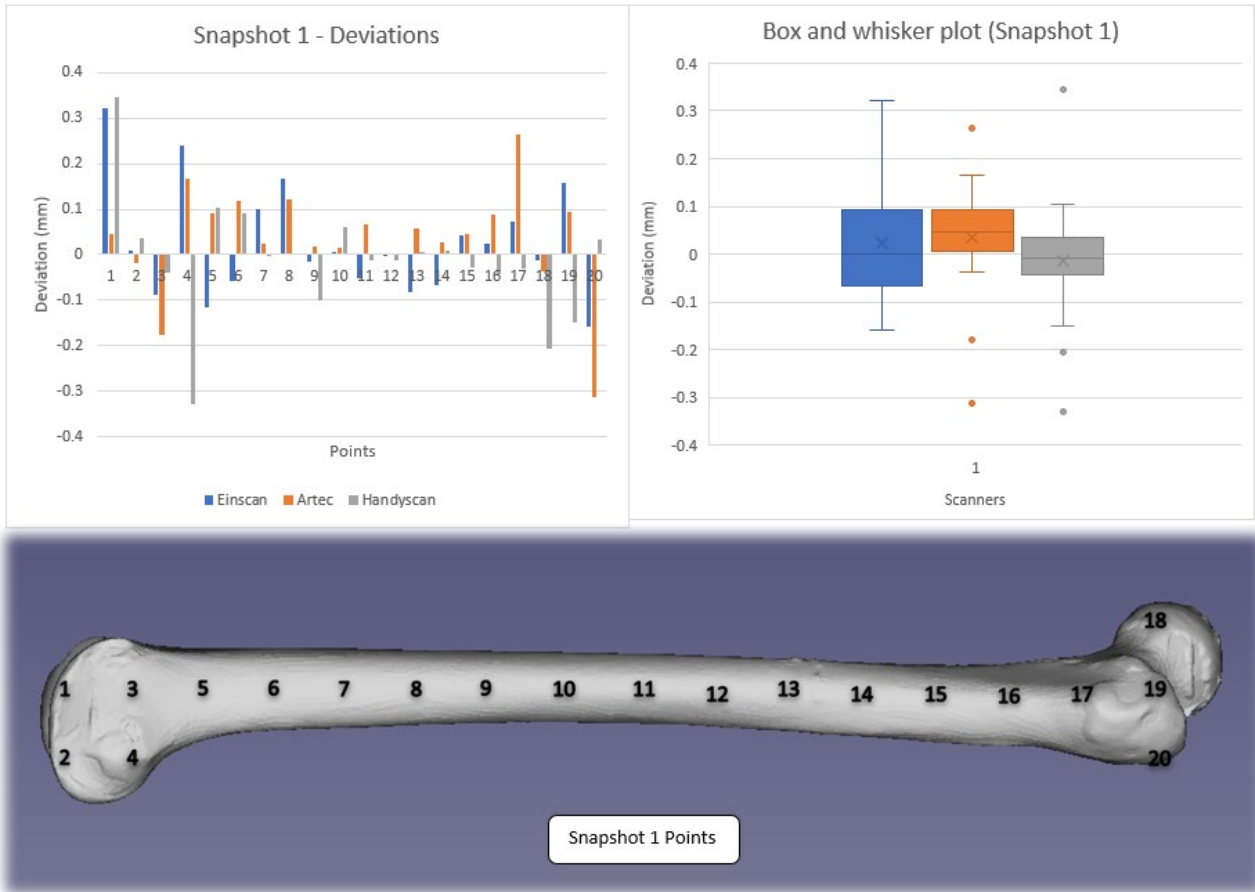


Figure 5-10 – Deviations (left) and Box & Whisker plot (right) for Snapshot 1

In Figure 5-10, the deviations along the longitudinal section can be seen. The histogram on the left shows that the deviation increases with increasing curvature. The observation is based on the lower deviations in the midsection of the model in comparison to the deviations towards the outer sections of the model.

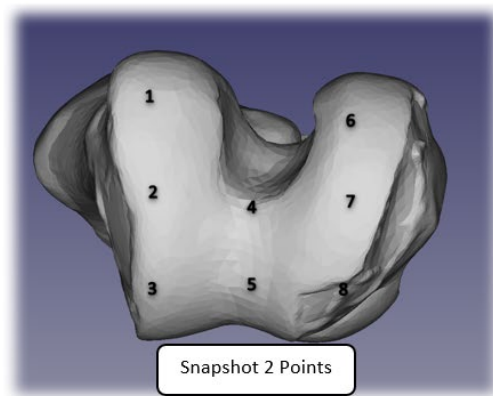
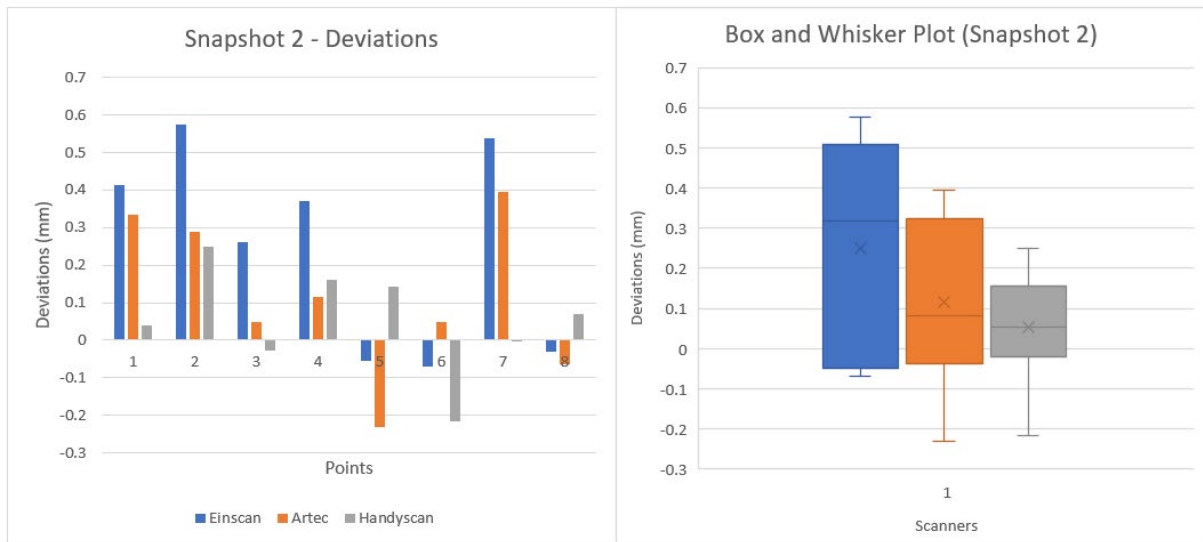


Figure 5-11 - Deviations (left) and Box & Whisker plot (right) for Snapshot 2

In Figure 5-11, the deviations are consistent to some degree between each scanner as most of the deviation values are positive. The differences seen for points 5 and 8 can be attributed to the scanning orientation of the different scanners. For scanners 1 and 2, the model was placed vertically erect for scanning, while for scanner 3, the orientation was angled. Hence the similarity in deviation for scanners 1 and 2 in comparison to scanner 3. Scanner 3 performed best in this view based on both the histogram results (lower values of deviation) and the box and whisker plot (smaller interquartile range). This can be attributed to the scanning orientation and the lower resolution of scanner 3.

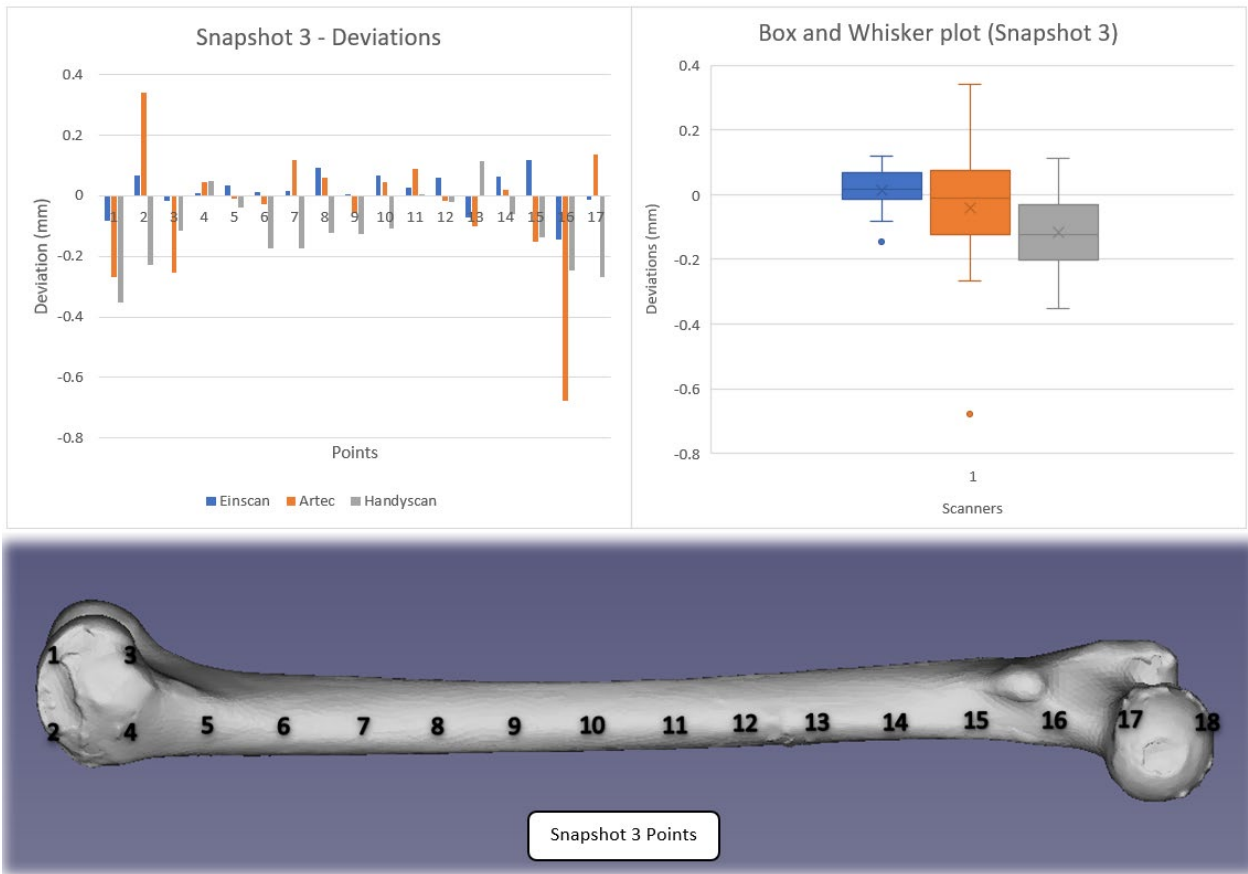


Figure 5-12 - Deviations (left) and Box & Whisker plot (right) for Snapshot 3

A similar observation, as seen in Figure 5-10, can be made in Figure 5-12 regarding the deviations along the longitudinal section. The histogram on the left shows that the deviation increases with increasing curvature. The observation is based on the lower deviations in the midsection of the model in comparison to the deviations towards the outer sections of the model. However, the performance of the scanners can be observed to be different when comparing the results in Figure 5-10 and Figure 5-12. Scanners 1 and 2 have produced better results than scanner 3.

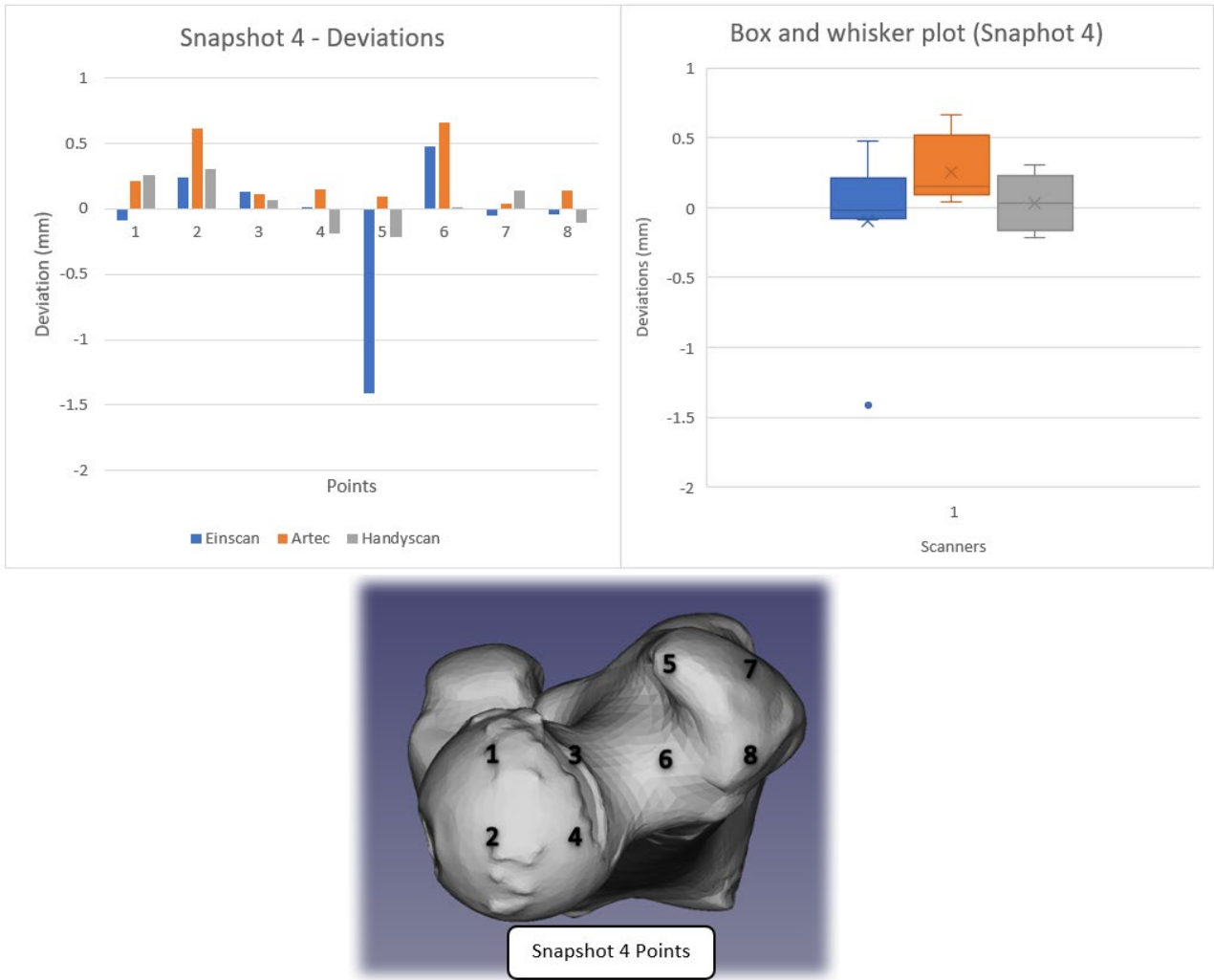


Figure 5-13 - Deviations (left) and Box & Whisker plot (right) for Snapshot 4

In Figure 5-13, the deviations are consistent across all three scanners besides the outlier in point 5. It must be noted that the maximum and minimum values of deviation for all three scanners were found in the regions of points 5 and 6, as mentioned at the beginning of this section. Scanners 2 and 3 produced better results in this section of the femur model in comparison to scanner 1.

## 5.5. MeshLab Results

In the MeshLab environment, once the models were aligned, the *Distance from reference mesh* filter was applied. The data extracted from MeshLab was then imported into Matlab to create the box and whisker plots seen in Figure 5-14. This is a good representation of the deviation results as the extreme values of deviation are considered as outliers to the general set of data. Since there are both positive and negative values, it is not practical to analyse the mean value of the data; therefore, the root mean

square (RMS) value will be compared. This analysis shows the range of where the majority of the deviations lie. The reference model used for this analysis is the original STL CAD file. Therefore, these results also include deviations caused by the 3D printing process as well. However, this analysis provides a good overview of the range of deviation caused by the scanning process since the outliers are not considered in the data.

The box and whisker plots are shown in Figure 5-14 display the deviation results of each scanner. All plots are relatively symmetric, meaning that the distribution of results is a normal distribution. Since the distribution is normal, the range of deviation will be considered from the maximum and minimum of the box plot. In summary, the range of deviation is:

- Einscan HX : -0.315mm to 0.409mm; RMS = 0.206 mm; Range = 0.724mm
- Artec EVA-M : -0.36mm to 0.371mm; RMS = 0.26 mm; Range = 0.731mm
- Handyscan 700 : -0.449mm to 0.385mm; RMS = 0.181 mm; Range = 0.834 mm

It can be seen that the two structured light-based scanners have a very similar range of deviations, while the Handyscan 700 deviations were about 0.1mm more. On average, the RMS value for the scanning deviation is about 0.22mm, and the average range of deviations from the scanners ranges from -0.375 mm to 0.388 mm, i.e., about 0.763mm.

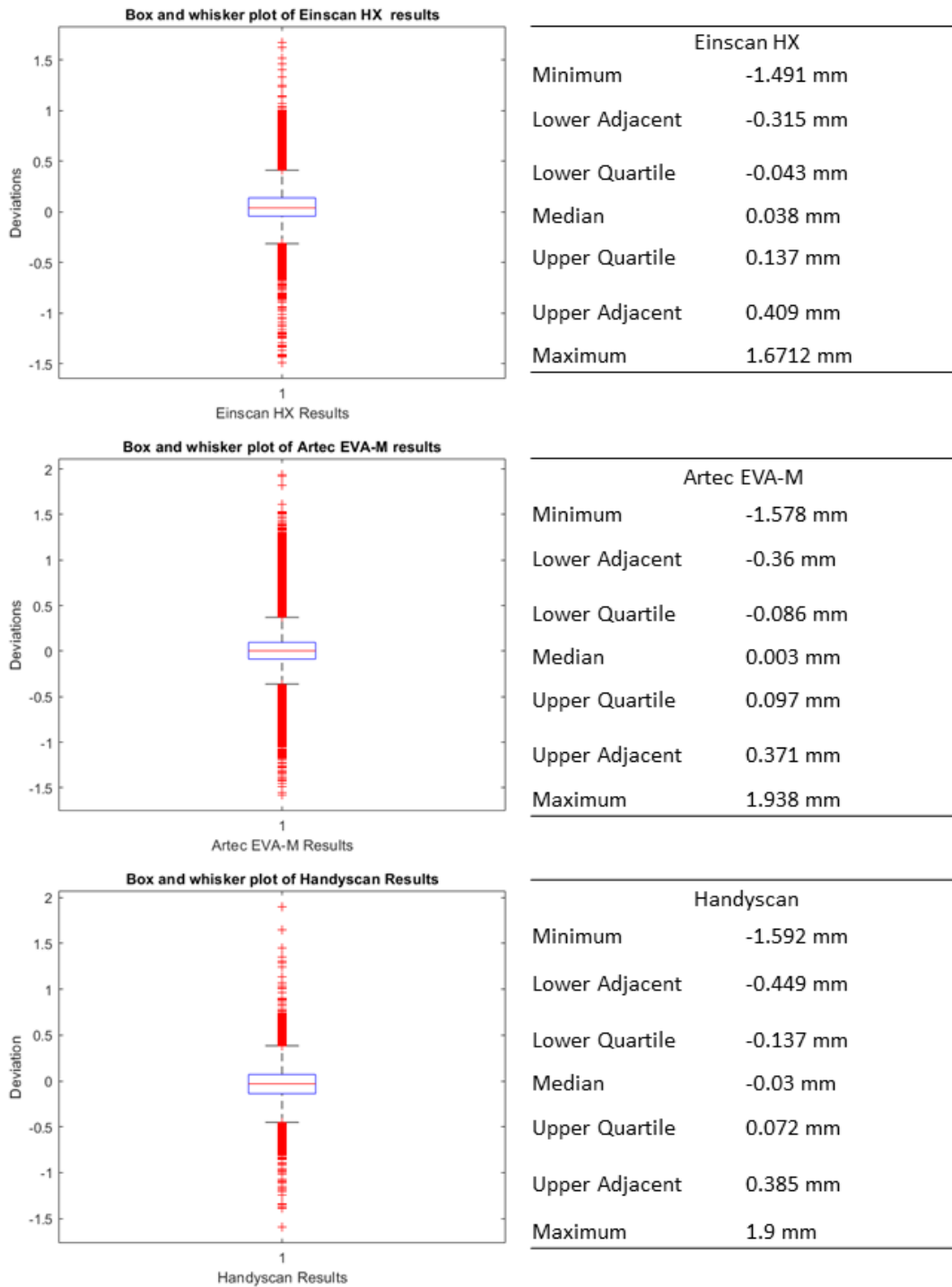


Figure 5-14 - Box and whisker plots of deviation data from each scanner

### ***Hausdorff distance***

In the MeshLab environment, once the models were aligned, the *Hausdorff distance* filter was applied. The data extracted from MeshLab was then imported into Matlab to create the box and



whisker plots seen in Figure 5-15. All median values are approximately 0.1mm. In summary, the interquartile ranges are:

- Einscan HX : 0.045mm to 0.205 mm ; mean = 0.151 mm
- Artec EVA-M : 0.041 mm to 0.213 mm ; mean = 0.174 mm
- Handyscan 700 : 0.051 mm to 0.212 mm ; mean = 0.154 mm

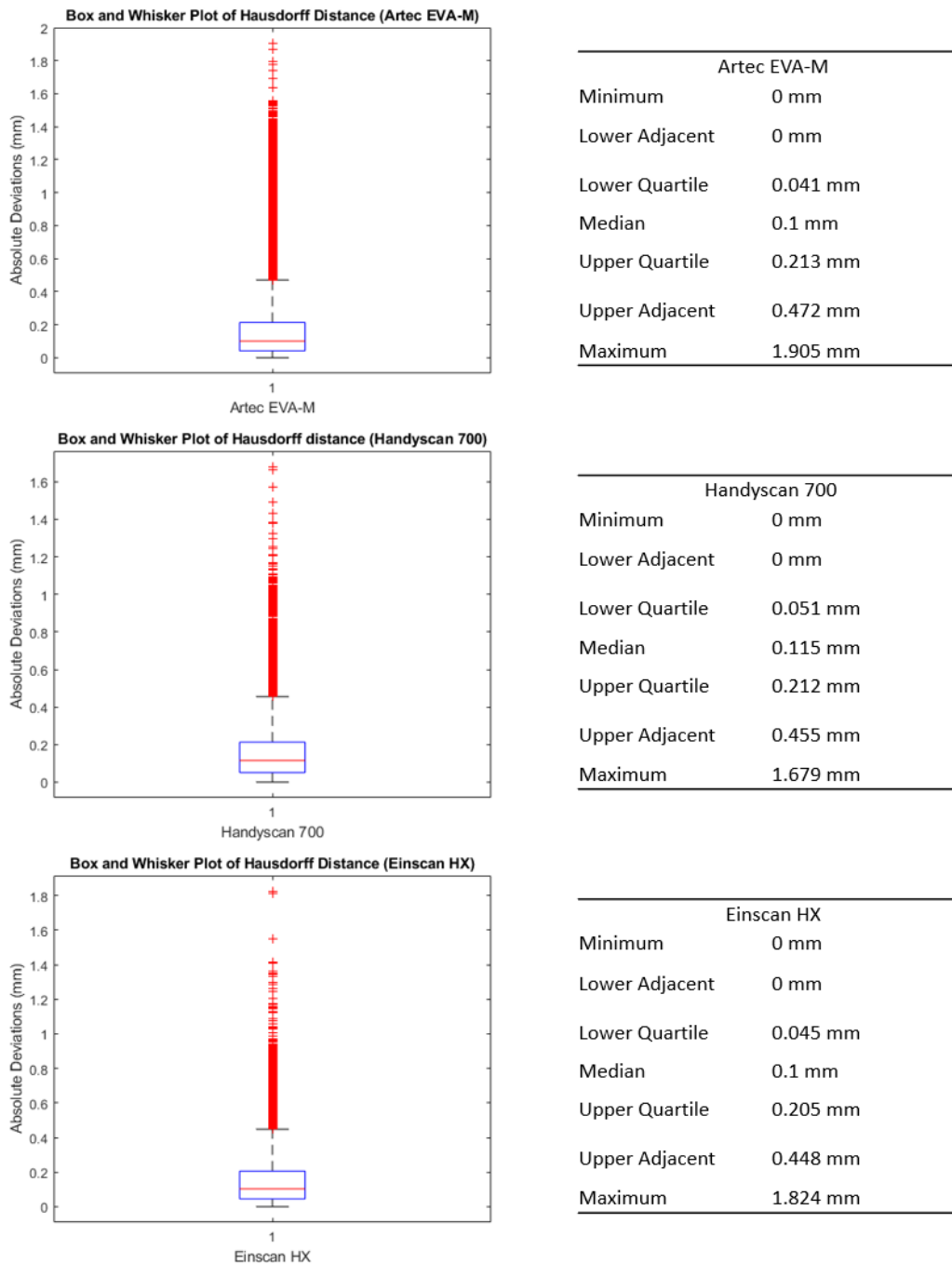


Figure 5-15 - Box and Whisker plots of Hausdorff distances

The maximum and minimum value range are:

- Einscan HX : 0.448 mm ; mean = 0.151 mm
- Artec EVA-M : 0.472 mm; mean = 0.174 mm
- Handyscan 700 : 0.455 mm ; mean = 0.154 mm

On average, the deviation of the 3D printed model from the original STL can be said to be around 0.46mm. In an interlaboratory study conducted by Soodmand et al. [87] on the reconstruction of femur models, it is mentioned that medical model reconstruction should be within the range of 1mm. Based on this consideration, the results show that the 3D printed model from medical image reconstruction is within acceptable levels of tolerance.

## **CHAPTER 6: CONCLUSION**

A literature study was conducted to determine the recent applications of AM within the medical field. The study found that there has been quite a significant amount of research regarding AM and 3DP applications in the medical sector, especially within tissue engineering and medical implants. In addition, the study showed a high focus in research globally on tissue engineering and medical implants. Countries such as China, the USA, Germany, the UK, and Italy have a higher number of publications in this regard. The literature study also showed the variety of AM technologies and the various materials that have been implemented in different medical applications. Another observation from the literature study is the popularity of opensource software for clinical studies.

Similarly, a literature study was conducted to determine the recent applications of RE within the medical field. The most common uses of RE within the medical field were found to be for solid modelling, 3D printing, virtual surgery planning, quality control and generative design. The process of RE has both direct and indirect applications in the medical industry and is an excellent support technology for medical applications as it provides viable alternate methods for digital model creation for various purposes.

A medical image was segmented, reconstructed to a 3D model, and successfully 3D printed using an industrial FDM printer. Medical image transformation has been demonstrated in this process. The printed model was successfully reverse-engineered for comparative deviation analysis and solid modelling purposes. The advantage, convenience and efficiency of non-contact scanning were

realised when conducting the experimental work for this thesis. The use of non-contact scanning is highly efficient for RE.

The proposed solid modelling process using opensource software FreeCAD proved to be very useful as the results from this process matched the results from a directly converted STL file. Based on this method, the solid modelling of an anatomical structure (femur) was successfully conducted using the process of RE.

The comparative deviation analysis was completed where a 3D printed model's deviations were successfully analysed using the RE and 3D scanning process. The results show that the scanners' range of deviations was found to be approximately -0.375 mm to 0.388 mm (range of about 0.763mm) with an average RMS of about 0.22 mm. The results showed that the mean deviation of the 3D printed model (based on 3D scanning) has an average range of about 0.46mm, with an average mean value of about 0.16 mm.

In conclusion, all the aims and objectives of this thesis, i.e., a literature study on medical applications of AM and RE, the conversion process of medical image data for 3D printing purposes and the case study on RE of an anatomical structure for compatibility analysis have been conducted successfully.

### ***Future Works***

The methodology presented in this thesis is a robust and efficient one for comparative deviation analysis through RE. Each step in the process of medical image reconstruction and comparative deviation analysis through RE can be isolated and studied further. Possible future works based on this thesis are as follows:

- Using the presented methodology to conduct deviation analysis on multiple samples using different AM technologies to create a broad data set. Thereafter integrate the data with Artificial Intelligence / Machine Learning algorithms to predict the deviation of the 3D printed model based on the AM technology utilised or other factors such as material, slicing height, etc.
- Since medical image data are already in 2D slices, algorithms can be researched to move directly from pixel map data in 2D medical image slices to GCODE instead of 3D model reconstruction first. A possible avenue is to make use of geometric curves such as B-splines to trace the segmented area during segmentation and convert the resulting profiles to GCODE. Thereafter the presented deviation analysis through RE can be used to determine the deviations.

- Another possible area of research is to implement mathematic algorithms to improve the slicing process, similar to the methods presented by Manmadhachary et al. [59]. That is to smoothen the sliced profile by adding more points to interpolate between, and the presented deviation analysis through RE can be used to determine the deviations.

## CHAPTER 7: References

- [1] Norwegian Institute of Public Health, *Hip fractures in Norway: Predictors, incidence and survival. Norwegian Epidemiologic Osteoporosis Studies (NOREPOS)*. [Online]. Available: <https://www.fhi.no/en/cristin-projects/ongoing/hip-fractures-in-norway-predictors-incidence-and-survival.-norwegian-epidem/> (accessed: Jun. 20 2022.015Z).
- [2] embodi3D.com, *About Us*. [Online]. Available: <https://www.embodi3d.com/about-us/> (accessed: Jun. 2 2022.929Z).
- [3] *ISO/ASTM 52900(en), Additive manufacturing — General principles — Terminology*. [Online]. Available: <https://www.iso.org/obp/ui/> (accessed: Jun. 20 2022.439Z).
- [4] W. Gao *et al.*, “The status, challenges, and future of additive manufacturing in engineering,” *Computer-Aided Design*, vol. 69, no. 2, pp. 65–89, 2015, doi: 10.1016/j.cad.2015.04.001.
- [5] I. Gibson, D. Rosen, and B. Stucker, *Additive Manufacturing Technologies*. New York, NY: Springer New York, 2015.
- [6] J. D. Hiller and H. Lipson, “STL 2.0: A Proposal for a Universal Multi-Material Additive Manufacturing File Format,” 2009.
- [7] O. Diegel, A. Nordin, and D. Motte, *A practical guide to design for additive manufacturing*. Singapore: Springer, op. 2020.
- [8] GitHub, *Releases · prusa3d/PrusaSlicer*. [Online]. Available: <https://github.com/prusa3d/PrusaSlicer> (accessed: Jun. 13 2022.438Z).
- [9] GitHub, *Slic3r/TriangleMesh.hpp at master · slic3r/Slic3r*. [Online]. Available: <https://github.com/slic3r/Slic3r> (accessed: Jun. 13 2022.688Z).
- [10] GitHub, *PrusaSlicer/TriangleMeshSlicer.hpp at master · prusa3d/PrusaSlicer*. [Online]. Available: <https://github.com/prusa3d/PrusaSlicer/blob/master/src/lib slic3r/TriangleMeshSlicer.cpp> (accessed: Jun. 13 2022.349Z).

- [11] *libslic3r: Slic3r::TriangleMeshSlicer< A > Class Template Reference*. [Online]. Available: [https://manual.slic3r.org/libslic3r-doc/class\\_slic3r\\_1\\_1\\_triangle\\_mesh\\_slicer.html](https://manual.slic3r.org/libslic3r-doc/class_slic3r_1_1_triangle_mesh_slicer.html) (accessed: Jun. 13 2022.551Z).
- [12] V. Mohanavel, K. S. Ashraff Ali, K. Ranganathan, J. Allen Jeffrey, M. M. Ravikumar, and S. Rajkumar, "The roles and applications of additive manufacturing in the aerospace and automobile sector," *Materials Today: Proceedings*, vol. 47, no. 6, pp. 405–409, 2021, doi: 10.1016/j.matpr.2021.04.596.
- [13] J. Janeková, S. Pelle, D. Onofrejová, and M. Pekarčíková, "THE 3D PRINTING IMPLEMENTATION IN MANUFACTURING OF AUTOMOBILE COMPONENTS," *AT*, vol. 5, no. 1, pp. 17–21, 2019, doi: 10.22306/atec.v5i1.49.
- [14] A. Pajonk, A. Prieto, U. Blum, and U. Knaack, "Multi-material additive manufacturing in architecture and construction: A review," *Journal of Building Engineering*, vol. 45, no. 2002, p. 103603, 2022, doi: 10.1016/j.jobbe.2021.103603.
- [15] J. d. Boer, W. Lambrechts, and H. Krikke, "Additive manufacturing in military and humanitarian missions: Advantages and challenges in the spare parts supply chain," *Journal of Cleaner Production*, vol. 257, no. 3, p. 120301, 2020, doi: 10.1016/j.jclepro.2020.120301.
- [16] A. Le-Bail, B. C. Maniglia, and P. Le-Bail, "Recent advances and future perspective in additive manufacturing of foods based on 3D printing," *Current Opinion in Food Science*, vol. 35, no. 5, pp. 54–64, 2020, doi: 10.1016/j.cofs.2020.01.009.
- [17] A. H. Espera, J. R. C. Dizon, Q. Chen, and R. C. Advincula, "3D-printing and advanced manufacturing for electronics," *Prog Addit Manuf*, vol. 4, no. 3, pp. 245–267, 2019, doi: 10.1007/s40964-019-00077-7.
- [18] O. Abdulhameed, A. Al-Ahmari, W. Ameen, and S. H. Mian, "Additive manufacturing: Challenges, trends, and applications," *Advances in Mechanical Engineering*, vol. 11, no. 2, 168781401882288, 2019, doi: 10.1177/1687814018822880.
- [19] A. Jandyal, I. Chaturvedi, I. Wazir, A. Raina, and M. I. Ul Haq, "3D printing – A review of processes, materials and applications in industry 4.0," *Sustainable Operations and Computers*, vol. 3, no. 43, pp. 33–42, 2022, doi: 10.1016/j.susoc.2021.09.004.

- [20] M. Salmi, "Design and Applications of Additive Manufacturing and 3D Printing," *Designs*, vol. 6, no. 1, p. 6, 2022, doi: 10.3390/designs6010006.
- [21] M. S. Thompson, "Current status and future roles of additives in 3D printing—A perspective," *Vinyl Additive Technology*, vol. 28, no. 1, pp. 3–16, 2022, doi: 10.1002/vnl.21887.
- [22] D. Nestic, B. M. Schaefer, Y. Sun, N. Saulacic, and I. Sailer, "3D Printing Approach in Dentistry: The Future for Personalized Oral Soft Tissue Regeneration," *Journal of clinical medicine*, vol. 9, no. 7, 2020, doi: 10.3390/jcm9072238.
- [23] A. Squelch, "3D printing and medical imaging," *Journal of medical radiation sciences*, vol. 65, no. 3, pp. 171–172, 2018, doi: 10.1002/jmrs.300.
- [24] L. Lin, Y. Fang, Y. Liao, G. Chen, C. Gao, and P. Zhu, "3D Printing and Digital Processing Techniques in Dentistry: A Review of Literature," *Adv. Eng. Mater.*, vol. 21, no. 6, p. 1801013, 2019, doi: 10.1002/adem.201801013.
- [25] S. Pillai *et al.*, "Dental 3D-Printing: Transferring Art from the Laboratories to the Clinics," *Polymers*, vol. 13, no. 1, 2021, doi: 10.3390/polym13010157.
- [26] M. Revilla-León, M. Sadeghpour, and M. Özcan, "An update on applications of 3D printing technologies used for processing polymers used in implant dentistry," *Odontology*, vol. 108, no. 3, pp. 331–338, 2020, doi: 10.1007/s10266-019-00441-7.
- [27] R. Galante, C. G. Figueiredo-Pina, and A. P. Serro, "Additive manufacturing of ceramics for dental applications: A review," *Dental materials : official publication of the Academy of Dental Materials*, vol. 35, no. 6, pp. 825–846, 2019, doi: 10.1016/j.dental.2019.02.026.
- [28] A. Haleem, M. Javaid, R. H. Khan, and R. Suman, "3D printing applications in bone tissue engineering," *Journal of clinical orthopaedics and trauma*, vol. 11, Suppl 1, S118-S124, 2020, doi: 10.1016/j.jcot.2019.12.002.
- [29] K. Jacyszyn, E. Kemp, T. Laursen, and F. Rasmussen, "Investigations of the excretion of gamma-glutamyl-transpeptidase into the urine," *International urology and nephrology*, vol. 7, no. 3, pp. 205–214, 1975, doi: 10.1007/BF02082676.

- [30] M. Javaid and A. Haleem, "3D printed tissue and organ using additive manufacturing: An overview," *Clinical Epidemiology and Global Health*, vol. 8, no. 2, pp. 586–594, 2020, doi: 10.1016/j.cegh.2019.12.008.
- [31] Y. Y. C. Choong *et al.*, "The global rise of 3D printing during the COVID-19 pandemic," *Nat Rev Mater*, vol. 5, no. 9, pp. 637–639, 2020, doi: 10.1038/s41578-020-00234-3.
- [32] T. Kermavnar, A. Shannon, K. J. O'Sullivan, C. McCarthy, C. P. Dunne, and L. W. O'Sullivan, "Three-Dimensional Printing of Medical Devices Used Directly to Treat Patients: A Systematic Review," *3D Printing and Additive Manufacturing*, vol. 8, no. 6, pp. 366–408, 2021, doi: 10.1089/3dp.2020.0324.
- [33] Z. Wang and Y. Yang, "Application of 3D Printing in Implantable Medical Devices," *BioMed research international*, vol. 2021, p. 6653967, 2021, doi: 10.1155/2021/6653967.
- [34] C. Culmone, G. Smit, and P. Breedveld, "Additive manufacturing of medical instruments: A state-of-the-art review," *Additive Manufacturing*, vol. 27, pp. 461–473, 2019, doi: 10.1016/j.addma.2019.03.015.
- [35] V. Baskaran, G. Štrkalj, M. Štrkalj, and A. Di Ieva, "Current Applications and Future Perspectives of the Use of 3D Printing in Anatomical Training and Neurosurgery," *Frontiers in neuroanatomy*, vol. 10, p. 69, 2016, doi: 10.3389/fnana.2016.00069.
- [36] J. V. Chen, A. B. C. Dang, and A. Dang, "Comparing cost and print time estimates for six commercially-available 3D printers obtained through slicing software for clinically relevant anatomical models," *3D printing in medicine*, vol. 7, no. 1, p. 1, 2021, doi: 10.1186/s41205-020-00091-4.
- [37] M. L. Smith and J. F. X. Jones, "Dual-extrusion 3D printing of anatomical models for education," *Anatomical sciences education*, vol. 11, no. 1, pp. 65–72, 2018, doi: 10.1002/ase.1730.
- [38] G. Chen, Y. Xu, P. Chi Lip Kwok, and L. Kang, "Pharmaceutical Applications of 3D Printing," *Additive Manufacturing*, vol. 34, no. 176, p. 101209, 2020, doi: 10.1016/j.addma.2020.101209.



- [39] W. Jamróz, J. Szafraniec, M. Kurek, and R. Jachowicz, “3D Printing in Pharmaceutical and Medical Applications - Recent Achievements and Challenges,” *Pharmaceutical research*, vol. 35, no. 9, p. 176, 2018, doi: 10.1007/s11095-018-2454-x.
- [40] E. Mathew, G. Pitzanti, E. Larrañeta, and D. A. Lamprou, “3D Printing of Pharmaceuticals and Drug Delivery Devices,” *Pharmaceutics*, vol. 12, no. 3, 2020, doi: 10.3390/pharmaceutics12030266.
- [41] R. Kumar, M. Kumar, and J. S. Chohan, “The role of additive manufacturing for biomedical applications: A critical review,” *Journal of Manufacturing Processes*, vol. 64, no. 5, pp. 828–850, 2021, doi: 10.1016/j.jmapro.2021.02.022.
- [42] C. Li, D. Pisignano, Y. Zhao, and J. Xue, “Advances in Medical Applications of Additive Manufacturing,” *Engineering*, vol. 6, no. 11, pp. 1222–1231, 2020, doi: 10.1016/j.eng.2020.02.018.
- [43] M. Salmi, “Additive Manufacturing Processes in Medical Applications,” *Materials (Basel, Switzerland)*, vol. 14, no. 1, 2021, doi: 10.3390/ma14010191.
- [44] A. Ahmed, A. Azam, M. M. Aslam Bhutta, F. A. Khan, R. Aslam, and Z. Tahir, “Discovering the technology evolution pathways for 3D printing (3DP) using bibliometric investigation and emerging applications of 3DP during COVID-19,” *Cleaner Environmental Systems*, vol. 3, p. 100042, 2021, doi: 10.1016/j.cesys.2021.100042.
- [45] E. Huotilainen *et al.*, “Inaccuracies in additive manufactured medical skull models caused by the DICOM to STL conversion process,” *Journal of cranio-maxillo-facial surgery : official publication of the European Association for Cranio-Maxillo-Facial Surgery*, vol. 42, no. 5, e259-65, 2014, doi: 10.1016/j.jcms.2013.10.001.
- [46] M. Ramola, V. Yadav, and R. Jain, “On the adoption of additive manufacturing in healthcare: a literature review,” *JMTM*, vol. 30, no. 1, pp. 48–69, 2019, doi: 10.1108/JMTM-03-2018-0094.
- [47] A. Marro, T. Bandukwala, and W. Mak, “Three-Dimensional Printing and Medical Imaging: A Review of the Methods and Applications,” *Current problems in diagnostic radiology*, vol. 45, no. 1, pp. 2–9, 2016, doi: 10.1067/j.cpradiol.2015.07.009.

- [48] B. A. Di-Donato *et al.*, “Three-Dimensional Digitalized and Printed Tongue Models of the Cow, Dog, Pig, and Horse for Undergraduate Veterinary Educationh,” *Int. J. Morphol.*, vol. 39, no. 2, pp. 436–440, 2021, doi: 10.4067/S0717-95022021000200436.
- [49] B. Chaudhary, U. Anand, V. Kumari, P. Agrawal, P. Kumar, and R. Priyadarshi, “Feasibility and adaptation of three-dimensional model for surgical planning and training: A pilot study,” *Natl J Clin Anat*, vol. 10, no. 4, p. 220, 2021, doi: 10.4103/2277-4025.329493.
- [50] T. V. Saliba and R. S. M. d. Barros, “Development and validation of a 3D laryngeal model in surgical skills training,” *Brazilian journal of otorhinolaryngology*, 2021, doi: 10.1016/j.bjorl.2021.09.010.
- [51] C. Salewski *et al.*, “The impact of 3D printed models on spatial orientation in echocardiography teaching,” *BMC medical education*, vol. 22, no. 1, p. 180, 2022, doi: 10.1186/s12909-022-03242-9.
- [52] L. R. Kanyane, A. P. I. Popoola, S. Pityana, and M. Tlotleng, “Synthesis of Ti-Al-xNb Ternary Alloys via Laser-Engineered Net Shaping for Biomedical Application: Densification, Electrochemical and Mechanical Properties Studies,” *Materials (Basel, Switzerland)*, vol. 15, no. 2, 2022, doi: 10.3390/ma15020544.
- [53] A. Thurzo, W. Urbanová, B. Novák, I. Waczulíková, and I. Varga, “Utilization of a 3D Printed Orthodontic Distalizer for Tooth-Borne Hybrid Treatment in Class II Unilateral Malocclusions,” *Materials (Basel, Switzerland)*, vol. 15, no. 5, 2022, doi: 10.3390/ma15051740.
- [54] J.-S. Kwon *et al.*, “Durable Oral Biofilm Resistance of 3D-Printed Dental Base Polymers Containing Zwitterionic Materials,” *International journal of molecular sciences*, vol. 22, no. 1, 2021, doi: 10.3390/ijms22010417.
- [55] J. Schweiger, J.-F. Güth, D. Edelhoff, K. Seidel, and T. Graf, “Application of 3D-printed colored 3D-models for the fabrication of full ceramic restorations: A technical report,” *Journal of esthetic and restorative dentistry : official publication of the American Academy of Esthetic Dentistry ... [et al.]*, vol. 34, no. 1, pp. 235–243, 2022, doi: 10.1111/jerd.12873.
- [56] A. Unkovskiy, F. Huettig, P. Kraemer-Fernandez, and S. Spintzyk, “Multi-Material 3D Printing of a Customized Sports Mouth Guard: Proof-of-Concept Clinical Case,” *International*

*journal of environmental research and public health*, vol. 18, no. 23, 2021, doi: 10.3390/ijerph182312762.

- [57] J. Lüchtenborg *et al.*, “Implementation of Fused Filament Fabrication in Dentistry,” *Applied Sciences*, vol. 11, no. 14, p. 6444, 2021, doi: 10.3390/app11146444.
- [58] S. Arutyunov *et al.*, “Microbial Adhesion to Dental Polymers for Conventional, Computer-Aided Subtractive and Additive Manufacturing: A Comparative In Vitro Study,” *Journal of functional biomaterials*, vol. 13, no. 2, 2022, doi: 10.3390/jfb13020042.
- [59] M. A., R. K. Y., and K. L., “Improve the accuracy, surface smoothing and material adaption in STL file for RP medical models,” *Journal of Manufacturing Processes*, vol. 21, pp. 46–55, 2016, doi: 10.1016/j.jmapro.2015.11.006.
- [60] Y. Tian *et al.*, “A Review of 3D Printing in Dentistry: Technologies, Affecting Factors, and Applications,” *Scanning*, vol. 2021, p. 9950131, 2021, doi: 10.1155/2021/9950131.
- [61] D. Chamo, B. Msallem, N. Sharma, S. Aghlmandi, C. Kunz, and F. M. Thieringer, “Accuracy Assessment of Molded, Patient-Specific Polymethylmethacrylate Craniofacial Implants Compared to Their 3D Printed Originals,” *Journal of clinical medicine*, vol. 9, no. 3, 2020, doi: 10.3390/jcm9030832.
- [62] J. S. Akmal *et al.*, “Cumulative Inaccuracies in Implementation of Additive Manufacturing Through Medical Imaging, 3D Thresholding, and 3D Modeling: A Case Study for an End-Use Implant,” *Applied Sciences*, vol. 10, no. 8, p. 2968, 2020, doi: 10.3390/app10082968.
- [63] J. M. Pinto *et al.*, “Sensitivity analysis of geometric errors in additive manufacturing medical models,” *Medical engineering & physics*, vol. 37, no. 3, pp. 328–334, 2015, doi: 10.1016/j.medengphy.2015.01.009.
- [64] M. Salmi, K.-S. Paloheimo, J. Tuomi, J. Wolff, and A. Mäkitie, “Accuracy of medical models made by additive manufacturing (rapid manufacturing),” *Journal of cranio-maxillo-facial surgery : official publication of the European Association for Cranio-Maxillo-Facial Surgery*, vol. 41, no. 7, pp. 603–609, 2013, doi: 10.1016/j.jcms.2012.11.041.
- [65] M. van Eijnatten, J. Koivisto, K. Karhu, T. Forouzanfar, and J. Wolff, “The impact of manual threshold selection in medical additive manufacturing,” *International journal of computer*

*assisted radiology and surgery*, vol. 12, no. 4, pp. 607–615, 2017, doi: 10.1007/s11548-016-1490-4.

- [66] Christian Petropolis, Md, Daniel Kozan, and Leif Sigurdson, and Md Msc Mba Frsc, “Accuracy of medical models made by consumer-grade fused deposition modelling printers,”
- [67] E. George, P. Liacouras, F. J. Rybicki, and D. Mitsouras, “Measuring and Establishing the Accuracy and Reproducibility of 3D Printed Medical Models,” *Radiographics : a review publication of the Radiological Society of North America, Inc*, vol. 37, no. 5, pp. 1424–1450, 2017, doi: 10.1148/rg.2017160165.
- [68] Andrea Sallent *et al.*, “Feasibility of 3D-printed models of the proximal femur to real bone: a cadaveric study,”
- [69] J. Witowski *et al.*, “Investigating accuracy of 3D printed liver models with computed tomography,” *Quantitative imaging in medicine and surgery*, vol. 9, no. 1, pp. 43–52, 2019, doi: 10.21037/qims.2018.09.16.
- [70] “A systematic evaluation of medical 3D printing accuracy of multi-pathological anatomical models for surgical planning manufactured in elastic and rigid material using desktop inverted vat photopolymerization,”
- [71] C. Michiels, E. Jambon, and J. C. Bernhard, “Measurement of the Accuracy of 3D-Printed Medical Models to Be Used for Robot-Assisted Partial Nephrectomy,” *AJR. American journal of roentgenology*, vol. 213, no. 3, pp. 626–631, 2019, doi: 10.2214/AJR.18.21048.
- [72] W. Wang, “Reverse Engineering: Technology of Reinvention,”
- [73] V. Raja and K. J. Fernandes, *Reverse engineering: An industrial perspective*. London: Springer, 2008.
- [74] F. Buonamici, M. Carfagni, R. Furferi, L. Governi, A. Lapini, and Y. Volpe, “Reverse engineering of mechanical parts: A template-based approach,” *Journal of Computational Design and Engineering*, vol. 5, no. 2, pp. 145–159, 2018, doi: 10.1016/j.jcde.2017.11.009.
- [75] Z. Geng and B. Bidanda, “Review of reverse engineering systems – current state of the art,” *Virtual and Physical Prototyping*, vol. 12, no. 2, pp. 161–172, 2017, doi: 10.1080/17452759.2017.1302787.

- [76] H. M., J. Kraft, and H. A., “Software Reverse Engineering in the Domain of Complex Embedded Systems,” in *Reverse Engineering - Recent Advances and Applications*, A.C. Telea, Ed.: InTech, 2012.
- [77] J. Creissac, J. Saraiva, C. Silva, and J. Carlos, “GUIsurfer: A Reverse Engineering Framework for User Interface Software,” in *Reverse Engineering - Recent Advances and Applications*, A.C. Telea, Ed.: InTech, 2012.
- [78] L. Favre, “MDA-Based Reverse Engineering,” in *Reverse Engineering - Recent Advances and Applications*, A.C. Telea, Ed.: InTech, 2012.
- [79] R. Akkiraju, T. Mitra, and U. Thulasiram, “Reverse Engineering Platform Independent Models from Business Software Applications,” in *Reverse Engineering - Recent Advances and Applications*, A.C. Telea, Ed.: InTech, 2012.
- [80] C. Li and C. Che, “Reverse Engineering the Peer to Peer Streaming Media System,” in *Reverse Engineering - Recent Advances and Applications*, A.C. Telea, Ed.: InTech, 2012.
- [81] R. H. Helle and H. G. Lemu, “A case study on use of 3D scanning for reverse engineering and quality control,” *Materials Today: Proceedings*, vol. 45, no. 5, pp. 5255–5262, 2021, doi: 10.1016/j.matpr.2021.01.828.
- [82] A. Bhatti, N. A. Syed, and P. John, “Reverse Engineering and Its Applications,” in *Omics Technologies and Bio-Engineering*: Elsevier, 2018, pp. 95–110.
- [83] Z. M. Bi and L. Wang, “Advances in 3D data acquisition and processing for industrial applications,” *Robotics and Computer-Integrated Manufacturing*, vol. 26, no. 5, pp. 403–413, 2010, doi: 10.1016/j.rcim.2010.03.003.
- [84] E. Taneva, B. Kusnoto, and C. A. Evans, “3D Scanning, Imaging, and Printing in Orthodontics,” in *Issues in Contemporary Orthodontics*, F. Bourzgui, Ed.: InTech, 2015.
- [85] S. Sehrawat *et al.*, “Study of 3D scanning technologies and scanners in orthodontics,” *Materials Today: Proceedings*, vol. 56, no. 4, pp. 186–193, 2022, doi: 10.1016/j.matpr.2022.01.064.
- [86] M. Giordano, P. Ausiello, and M. Martorelli, “Accuracy evaluation of surgical guides in implant dentistry by non-contact reverse engineering techniques,” *Dental materials : official*

*publication of the Academy of Dental Materials*, vol. 28, no. 9, e178-85, 2012, doi: 10.1016/j.dental.2012.06.006.

- [87] E. Soodmand *et al.*, “Interlaboratory comparison of femur surface reconstruction from CT data compared to reference optical 3D scan,” *Biomedical engineering online*, vol. 17, no. 1, p. 29, 2018, doi: 10.1186/s12938-018-0461-0.
- [88] A. Maier, *Medical Imaging Systems: An Introductory Guide*. Cham: Springer International Publishing AG, 2018. [Online]. Available: <https://ebookcentral.proquest.com/lib/kxp/detail.action?docID=6315606>
- [89] C. G. Miller, J. Krasnow, and L. H. Schwartz, Eds., *Medical imaging in clinical trials*. London, New York: Springer, 2014.
- [90] G. G. R. Schramek, D. Stoevesandt, A. Reising, J. T. Kielstein, M. Hiss, and H. Kielstein, “Imaging in anatomy: a comparison of imaging techniques in embalmed human cadavers,” *BMC medical education*, vol. 13, p. 143, 2013, doi: 10.1186/1472-6920-13-143.
- [91] A. Elangovan and T. Jeyaseelan, “Medical imaging modalities: A survey,” in *2016 International Conference on Emerging Trends in Engineering, Technology and Science (ICETETS)*, Pudukkottai, India, Feb. 2016 - Feb. 2016, pp. 1–4.
- [92] Y. W. Adugna, A. D. Akessa, and H. G. Lemu, “Overview study on challenges of additive manufacturing for a healthcare application,” *IOP Conf. Ser.: Mater. Sci. Eng.*, vol. 1201, no. 1, p. 12041, 2021, doi: 10.1088/1757-899X/1201/1/012041.
- [93] A. Haleem and M. Javaid, “3D scanning applications in medical field: A literature-based review,” *Clinical Epidemiology and Global Health*, vol. 7, no. 2, pp. 199–210, 2019, doi: 10.1016/j.cegh.2018.05.006.
- [94] M. Edl, M. Mizerák, and J. Trojan, “3D LASER SCANNERS: HISTORY AND APPLICATIONS,” *AS*, vol. 4, no. 4, pp. 1–5, 2018, doi: 10.22306/asim.v4i4.54.
- [95] S. Lin and X. Shi, “Research on Application of Reverse Engineering and 3D Printing Technology in Object Recognition,” *IOP Conf. Ser.: Earth Environ. Sci.*, vol. 781, no. 2, p. 22073, 2021, doi: 10.1088/1755-1315/781/2/022073.

- [96] M. Iturrate, R. Minguez, G. Pradies, and E. Solaberrieta, "Obtaining reliable intraoral digital scans for an implant-supported complete-arch prosthesis: A dental technique," *The Journal of prosthetic dentistry*, vol. 121, no. 2, pp. 237–241, 2019, doi: 10.1016/j.prosdent.2018.03.008.
- [97] P. Balamurugan and N. Selvakumar, "Development of patient specific dental implant using 3D printing," *J Ambient Intell Human Comput*, vol. 12, no. 3, pp. 3549–3558, 2021, doi: 10.1007/s12652-020-02758-6.
- [98] V. Raspudic and M. Marusic, "Redesign of Impression Trays using Reverse Engineering and Finite Element Analysis," in *DAAAM Proceedings, Proceedings of the 32nd International DAAAM Symposium 2021*, B. Katalinic, Ed.: DAAAM International Vienna, 2021, pp. 333–338.
- [99] M. Iturrate, R. Minguez, N. Toledo, H. Eguiraun, I. de Prado, and E. Solaberrieta, "A Virtual Kinematic Design of Dental Restorations Using Reverse Engineering," in *Lecture Notes in Mechanical Engineering, Advances on Mechanics, Design Engineering and Manufacturing II*, F. Cavas-Martínez, B. Eynard, F. J. Fernández Cañavate, D. G. Fernández-Pacheco, P. Morer, and V. Nigrelli, Eds., Cham: Springer International Publishing, 2019, pp. 165–173.
- [100] L. Fiorillo, M. Ciccì, C. D'Amico, R. Mauceri, G. Oteri, and G. Cervino, "Finite Element Method and Von Mises Investigation on Bone Response to Dynamic Stress with a Novel Conical Dental Implant Connection," *BioMed research international*, vol. 2020, p. 2976067, 2020, doi: 10.1155/2020/2976067.
- [101] F. Zhang, K.-J. Suh, and K.-M. Lee, "Validity of Intraoral Scans Compared with Plaster Models: An In-Vivo Comparison of Dental Measurements and 3D Surface Analysis," *PloS one*, vol. 11, no. 6, e0157713, 2016, doi: 10.1371/journal.pone.0157713.
- [102] E. Solaberrieta, R. Minguez, L. Barrenetxea, E. Sierra, and O. Etxaniz, "Computer-aided dental prostheses construction using reverse engineering," *Computer methods in biomechanics and biomedical engineering*, vol. 17, no. 12, pp. 1335–1346, 2014, doi: 10.1080/10255842.2012.745859.
- [103] J. Chen, Z. Zhang, X. Chen, C. Zhang, G. Zhang, and Z. Xu, "Design and manufacture of customized dental implants by using reverse engineering and selective laser melting

technology,” *The Journal of prosthetic dentistry*, vol. 112, no. 5, 1088-95.e1, 2014, doi: 10.1016/j.prosdent.2014.04.026.

- [104] R. Zhang, S. Li, and Y. Liu, “Assessing the accuracy of fabricated implant surgical guides by reconstructing the implant position based on cone beam computed tomography images: A dental technique,” *The Journal of prosthetic dentistry*, 2021, doi: 10.1016/j.prosdent.2021.05.005.
- [105] M. Martorelli, P. Ausiello, and R. Morrone, “A new method to assess the accuracy of a Cone Beam Computed Tomography scanner by using a non-contact reverse engineering technique,” *Journal of dentistry*, vol. 42, no. 4, pp. 460–465, 2014, doi: 10.1016/j.jdent.2013.12.018.
- [106] Q. Zhou, Z. Wang, J. Chen, J. Song, L. Chen, and Y. Lu, “Development and evaluation of a digital dental modeling method based on grating projection and reverse engineering software,” *The Journal of prosthetic dentistry*, vol. 115, no. 1, pp. 42–46, 2016, doi: 10.1016/j.prosdent.2015.06.016.
- [107] Y. Liu, H. Ye, S. Wang, L. Zhang, and Y. Zhou, “An open protocol for evaluating the accuracy of guided implant surgery by using digital casts,” *The Journal of prosthetic dentistry*, vol. 126, no. 6, pp. 731–734, 2021, doi: 10.1016/j.prosdent.2020.05.039.
- [108] A. L. Carneiro Pereira, R. F. Carvalho Porto de Freitas, M. de Fátima Trindade Pinto Campos, A. C. Soares Paiva Tôrres, A. K. Bezerra de Medeiros, and A. da Fonte Porto Carreiro, “Trueness of a device for intraoral scanning to capture the angle and distance between implants in edentulous mandibular arches,” *The Journal of prosthetic dentistry*, 2021, doi: 10.1016/j.prosdent.2021.02.039.
- [109] M. Martorelli, S. Maietta, A. Gloria, R. de Santis, E. Pei, and A. Lanzotti, “Design and Analysis of 3D Customized Models of a Human Mandible,” *Procedia CIRP*, vol. 49, pp. 199–202, 2016, doi: 10.1016/j.procir.2015.11.016.
- [110] X. Ding, J. Li, X. Zhang, and X. Yan, “Effects of 3 different residual root treatments after post-and-core restoration: An in vitro fracture resistance experiment and finite element analysis,” *The Journal of prosthetic dentistry*, vol. 124, no. 4, 485.e1-485.e10, 2020, doi: 10.1016/j.prosdent.2020.03.008.



- [111] M. M. Penteadó *et al.*, “Fatigue survival of endodontically treated teeth restored with different fiber-reinforced composite resin post strategies versus universal 2-piece fiber post system: An in vitro study,” *The Journal of prosthetic dentistry*, 2021, doi: 10.1016/j.prosdent.2021.05.020.
- [112] N. Ilie, “Microstructural dependence of mechanical properties and their relationship in modern resin-based composite materials,” *Journal of dentistry*, vol. 114, p. 103829, 2021, doi: 10.1016/j.jdent.2021.103829.
- [113] O.-B. J. Antonio, A.-L. Xabier, G.-O. Xabier, I.-M. Mikel, M.-A. Iñaki, and S.-M. Eneko, “Digitization of the Mechanical Articulator: Virtual Articulator,” in *Lecture Notes in Mechanical Engineering, Advances in Design Engineering*, F. Cavas-Martínez, F. Sanz-Adan, P. Morer Camo, R. Lostado Lorza, and J. Santamaría Peña, Eds., Cham: Springer International Publishing, 2020, pp. 212–218.
- [114] E. Solaberrieta, R. Mínguez, L. Barrenetxea, J. R. Otegi, and A. Szentpétery, “Comparison of the accuracy of a 3-dimensional virtual method and the conventional method for transferring the maxillary cast to a virtual articulator,” *The Journal of prosthetic dentistry*, vol. 113, no. 3, pp. 191–197, 2015, doi: 10.1016/j.prosdent.2014.04.029.
- [115] M. O. Al-Barqawi, B. Church, M. Thevamaran, D. J. Thoma, and A. Rahman, “Design and Validation of Additively Manufactured Metallic Cellular Scaffold Structures for Bone Tissue Engineering,” *Materials*, vol. 15, no. 9, p. 3310, 2022, doi: 10.3390/ma15093310.
- [116] P. Wang, Y. Sun, X. Shi, H. Shen, H. Ning, and H. Liu, “3D printing of tissue engineering scaffolds: a focus on vascular regeneration,” *Bio-design and manufacturing*, vol. 4, no. 2, pp. 344–378, 2021, doi: 10.1007/s42242-020-00109-0.
- [117] S. Pina *et al.*, “Scaffolding Strategies for Tissue Engineering and Regenerative Medicine Applications,” *Materials (Basel, Switzerland)*, vol. 12, no. 11, 2019, doi: 10.3390/ma12111824.
- [118] S. Gómez, M. D. Vlad, J. López, and E. Fernández, “Design and properties of 3D scaffolds for bone tissue engineering,” *Acta biomaterialia*, vol. 42, pp. 341–350, 2016, doi: 10.1016/j.actbio.2016.06.032.

- [119] N. S. Mustafa *et al.*, “Application of Computational Method in Designing a Unit Cell of Bone Tissue Engineering Scaffold: A Review,” *Polymers*, vol. 13, no. 10, 2021, doi: 10.3390/polym13101584.
- [120] Q. Yao *et al.*, “Design, construction and mechanical testing of digital 3D anatomical data-based PCL-HA bone tissue engineering scaffold,” *Journal of materials science. Materials in medicine*, vol. 26, no. 1, p. 5360, 2015, doi: 10.1007/s10856-014-5360-8.
- [121] P. Fucile *et al.*, “Reverse Engineering and Additive Manufacturing towards the design of 3D advanced scaffolds for hard tissue regeneration,” in *2019 II Workshop on Metrology for Industry 4.0 and IoT (MetroInd4.0&IoT)*, Naples, Italy, Jun. 2019 - Jun. 2019, pp. 33–37.
- [122] Z. Wang, C. Huang, J. Wang, P. Wang, S. Bi, and C. A. Abbas, “Design and Simulation of Flow Field for Bone Tissue Engineering Scaffold Based on Triply Periodic Minimal Surface,” *Chin. J. Mech. Eng.*, vol. 32, no. 1, p. 557, 2019, doi: 10.1186/s10033-019-0329-7.
- [123] T. Asmaria *et al.*, “Biomechanical Simulation of Sugita Aneurysm Clip: Reverse Engineering Approach using Metal 3D-Printing,” *J. Phys.: Conf. Ser.*, vol. 1805, no. 1, p. 12044, 2021, doi: 10.1088/1742-6596/1805/1/012044.
- [124] S. Chakravarty, “Resource constrained innovation in a technology intensive sector: Frugal medical devices from manufacturing firms in South Africa,” *Technovation*, vol. 112, no. 2, p. 102397, 2022, doi: 10.1016/j.technovation.2021.102397.
- [125] M. Zied Chaari, R. Al-Rahimi, A. Aljaberi, M. Abdelfatah, and C. Loreno, “The Efficiency of the Reverse Engineering to Fabricate a New Respirator Technology Compatible with the COVID-19 Pandemic,” in *Advances in Science, Technology & Innovation, Emerging Technologies in Biomedical Engineering and Sustainable TeleMedicine*, J. Alja’am, S. Al-Maadeed, and O. Halabi, Eds., Cham: Springer International Publishing, 2021, pp. 113–129.
- [126] D. M. Elston, “Occupational skin disease among health care workers during the coronavirus (COVID-19) epidemic,” *Journal of the American Academy of Dermatology*, vol. 82, no. 5, pp. 1085–1086, 2020, doi: 10.1016/j.jaad.2020.03.012.
- [127] M. Irfan Ul Haq *et al.*, “3D printing for development of medical equipment amidst coronavirus (COVID-19) pandemic—review and advancements,” *Res. Biomed. Eng.*, vol. 38, no. 1, pp. 305–315, 2022, doi: 10.1007/s42600-020-00098-0.

- [128] A. Manero *et al.*, “Leveraging 3D Printing Capacity in Times of Crisis: Recommendations for COVID-19 Distributed Manufacturing for Medical Equipment Rapid Response,” *International journal of environmental research and public health*, vol. 17, no. 13, 2020, doi: 10.3390/ijerph17134634.
- [129] L. Lo Russo, L. Guida, K. Zhurakivska, G. Troiano, K. Chochlidakis, and C. Ercoli, “Intaglio surface trueness of milled and 3D-printed digital maxillary and mandibular dentures: A clinical study,” *The Journal of prosthetic dentistry*, 2021, doi: 10.1016/j.prosdent.2021.05.003.
- [130] S. Liang, F. Yuan, X. Luo, Z. Yu, and Z. Tang, “Digital evaluation of absolute marginal discrepancy: A comparison of ceramic crowns fabricated with conventional and digital techniques,” *The Journal of prosthetic dentistry*, vol. 120, no. 4, pp. 525–529, 2018, doi: 10.1016/j.prosdent.2017.10.014.
- [131] M. F. Noor, F. Hasan, S. Bhardwaj, and S. Hasan, “Reverse Engineering in Customization of Products: Review and Case Study,” in *Design Science and Innovation, Ergonomics for Improved Productivity*, M. Muzammil, A. A. Khan, and F. Hasan, Eds., Singapore: Springer Singapore, 2021, pp. 587–592.
- [132] B. Kloesel, B. Juhnke, L. Irvine, J. V. Donadio, A. Erdman, and K. Belani, “Computer-Generated Three-Dimensional Airway Models as a Decision-Support Tool for Preoperative Evaluation and Procedure-Planning in Pediatric Anesthesiology,” *Journal of medical systems*, vol. 45, no. 2, p. 21, 2021, doi: 10.1007/s10916-020-01698-0.
- [133] P. Volonghi, G. Baronio, and A. Signoroni, “3D scanning and geometry processing techniques for customised hand orthotics: an experimental assessment,” *Virtual and Physical Prototyping*, vol. 13, no. 2, pp. 105–116, 2018, doi: 10.1080/17452759.2018.1426328.
- [134] P. W. Anggoro, M. Tauviquirrahman, J. Jamari, A. P. Bayuseno, B. Bawono, and M. M. Avelina, “Computer-aided reverse engineering system in the design and production of orthotic insole shoes for patients with diabetes,” *Cogent Engineering*, vol. 5, no. 1, p. 1470916, 2018, doi: 10.1080/23311916.2018.1470916.
- [135] X. Amezua-Lasuen, M. Iturrate-Mendieta, J. A. Oriozabala-Brit, X. Garikano-Osinaga, I. Martin-Amundarain, and E. Solaberrieta-Mendez, “Best-Fit Alignment in the Digital Dental

Workflow,” in *Lecture Notes in Mechanical Engineering, Advances in Design Engineering*, F. Cavas-Martínez, F. Sanz-Adan, P. Morer Camo, R. Lostado Lorza, and J. Santamaría Peña, Eds., Cham: Springer International Publishing, 2020, pp. 202–211.

- [136] N. Šimunić, T. Jurčević Lulić, J. Groš, and T. Mihalić, “Analysis of Surface Curvature Influence on 3D Scanning Accuracy of Dental Castings,” *Interdisciplinary Description of Complex Systems*, vol. 19, no. 3, pp. 449–456, 2021, doi: 10.7906/indecs.19.3.8.
- [137] G. Budzik, P. Turek, T. Dziubek, and M. Gdula, “Elaboration of the measuring procedure facilitating precision assessment of the geometry of mandible anatomical model manufactured using additive methods,” *Measurement and Control*, vol. 53, 1-2, pp. 181–191, 2020, doi: 10.1177/0020294019881708.
- [138] P. Turek and G. Budzik, “Estimating the Accuracy of Mandible Anatomical Models Manufactured Using Material Extrusion Methods,” *Polymers*, vol. 13, no. 14, 2021, doi: 10.3390/polym13142271.
- [139] A. Nikolov, V. Cantoni, D. Dimov, A. Abate, and S. Ricciardi, “Multi-model Ear Database for Biometric Applications,” in *Studies in Computational Intelligence, Innovative Approaches and Solutions in Advanced Intelligent Systems*, S. Margenov, G. Angelova, and G. Agre, Eds., Cham: Springer International Publishing, 2016, pp. 169–187.
- [140] W. Shui *et al.*, “The production of digital and printed resources from multiple modalities using visualization and three-dimensional printing techniques,” *International journal of computer assisted radiology and surgery*, vol. 12, no. 1, pp. 13–23, 2017, doi: 10.1007/s11548-016-1461-9.
- [141] K. Lee, *Principles of CAD*. Reading, Mass.: Addison-Wesley, 1999.
- [142] S. Rani, K. Lakhwani, and S. Kumar, “Three Dimensional Wireframe Model of Medical and Complex Images Using Cellular Logic Array Processing Techniques,” in *Advances in Intelligent Systems and Computing, Proceedings of the 12th International Conference on Soft Computing and Pattern Recognition (SoCPaR 2020)*, A. Abraham *et al.*, Eds., Cham: Springer International Publishing, 2021, pp. 196–207.
- [143] S. Rani, S. Kumar, D. Ghai, and K. Prasad, “Automatic Detection of Brain Tumor from CT and MRI Images using Wireframe model and 3D Alex-Net,” in *2022 International Conference*

on *Decision Aid Sciences and Applications (DASA)*, Chiangrai, Thailand, Mar. 2022 - Mar. 2022, pp. 1132–1138.

- [144] F. Buonamici *et al.*, “Reverse Engineering Techniques for Virtual Reconstruction of Defective Skulls: an Overview of Existing Approaches,” *CAD&A*, vol. 16, no. 1, pp. 103–112, 2018, doi: 10.14733/cadaps.2019.103-112.
- [145] D. Mun and B. C. Kim, “Three-dimensional solid reconstruction of a human bone from CT images using interpolation with triangular Bézier patches,” *J Mech Sci Technol*, vol. 31, no. 8, pp. 3875–3886, 2017, doi: 10.1007/s12206-017-0732-x.
- [146] B. X. Yang, M. D. Duan, Z. Y. Zhang, and J. B. Liu, “Three-dimensional solid reconstruction of femoral CT images based on reverse engineering,” *J. Phys.: Conf. Ser.*, vol. 1345, p. 32078, 2019, doi: 10.1088/1742-6596/1345/3/032078.
- [147] *FreeCAD: Your own 3D parametric modeler*. [Online]. Available: <https://www.freecadweb.org/> (accessed: Jun. 9 2022.299Z).
- [148] M. Larobina and L. Murino, “Medical image file formats,” *Journal of digital imaging*, vol. 27, no. 2, pp. 200–206, 2014, doi: 10.1007/s10278-013-9657-9.
- [149] T. Kamio, M. Suzuki, R. Asaumi, and T. Kawai, “DICOM segmentation and STL creation for 3D printing: a process and software package comparison for osseous anatomy,” *3D printing in medicine*, vol. 6, no. 1, p. 17, 2020, doi: 10.1186/s41205-020-00069-2.
- [150] A. Fedorov *et al.*, “3D Slicer as an image computing platform for the Quantitative Imaging Network,” *Magnetic resonance imaging*, vol. 30, no. 9, pp. 1323–1341, 2012, doi: 10.1016/j.mri.2012.05.001.
- [151] 3D Slicer, *3D Slicer image computing platform*. [Online]. Available: <https://www.slicer.org/> (accessed: Jun. 7 2022.337Z).
- [152] A. Afandi, I. S. Isa, S. N. Sulaiman, N. N. M. Marzuki, and N. K. A. Karim, “Comparison of Different Image Segmentation Techniques on MRI Image,” in *Smart Innovation, Systems and Technologies, Smart Trends in Computing and Communications*, Y.-D. Zhang, J. K. Mandal, C. So-In, and N. V. Thakur, Eds., Singapore: Springer Singapore, 2020, pp. 1–9.

- [153] A. S. Dar and D. Padha, "Medical Image Segmentation A Review of Recent Techniques, Advancements and a Comprehensive Comparison," *ijcse*, vol. 7, no. 7, pp. 114–124, 2019, doi: 10.26438/ijcse/v7i7.114124.
- [154] M. ElFiqi, S. M. Ismail, and M. A. Abd El Ghany, "Comparative Study on Segmentation Techniques for Biomedical Images," in *2020 32nd International Conference on Microelectronics (ICM)*, Aqaba, Jordan, Dec. 2020 - Dec. 2020, pp. 1–5.
- [155] S. P. Rajan and L. Kavitha, "Automated Retinal Imaging System for Detecting Cardiac Abnormalities Using Cup to Disc Ratio," *Ind. Jour. of Publ. Health Res. & Develop.*, vol. 10, no. 2, p. 1019, 2019, doi: 10.5958/0976-5506.2019.00430.3.
- [156] P. Tyagi, T. Singh, R. Nayar, and S. Kumar, "Performance comparison and analysis of medical image segmentation techniques," in *2018 IEEE International Conference on Current Trends in Advanced Computing (ICCTAC)*, Bangalore, Feb. 2018 - Feb. 2018, pp. 1–6.
- [157] I. Wahlang, P. Sharma, S. M. Nasreen, A. K. Maji, and G. Saha, "A Comparative Study on Segmentation Techniques for Brain Tumor MRI," in *Lecture Notes in Networks and Systems, Information and Communication Technology for Competitive Strategies*, S. Fong, S. Akashe, and P. N. Mahalle, Eds., Singapore: Springer Singapore, 2019, pp. 665–673.
- [158] *Segment editor — 3D Slicer documentation*. [Online]. Available: [https://slicer.readthedocs.io/en/latest/user\\_guide/modules/segmenteditor.html](https://slicer.readthedocs.io/en/latest/user_guide/modules/segmenteditor.html) (accessed: Jun. 7 2022.923Z).
- [159] D. Zukić *et al.*, "ND morphological contour interpolation," *The Insight Journal*, 2016, doi: 10.54294/achtrg.
- [160] L. Zhu, I. Kolesov, Y. Gao, R. Kikinis, and A. Tannenbaum, "An Effective Interactive Medical Image Segmentation Method using Fast GrowCut," *Int Conf Med Image Comput Comput Assist Interv. Workshop on Interactive Methods.*, vol. 17, WS, 2014.
- [161] C. Petropolis, D. Kozan, and L. Sigurdson, "Accuracy of medical models made by consumer-grade fused deposition modelling printers," *Plastic surgery (Oakville, Ont.)*, vol. 23, no. 2, pp. 91–94, 2015, doi: 10.4172/plastic-surgery.1000912.

- [162] F. Gehrke, “Shining 3D EinScan HX: Specs, Price, Release & Reviews,” *All3DP*, 10/28/2019, 10/28/2019. <https://all3dp.com/1/shining3d-einscan-hx-review-3d-scanner-specs/> (accessed: Jun. 2 2022.657Z).
- [163] B. Katalinic, Ed., *Proceedings of the 32nd International DAAAM Symposium 2021: DAAAM International Vienna, 2021*. [Online]. Available: [https://www.creaform3d.com/sites/default/files/assets/brochures/files/handyscan3d\\_silver\\_series\\_brochure\\_en\\_hq\\_20210819.pdf](https://www.creaform3d.com/sites/default/files/assets/brochures/files/handyscan3d_silver_series_brochure_en_hq_20210819.pdf)
- [164] Professional 3D scanning solutions | Artec and 3D, *3D Object Scanner Artec Eva | Best Structured-light 3D Scanning Device*. [Online]. Available: [https://www.creaform3d.com/sites/default/files/assets/brochures/files/handyscan3d\\_silver\\_series\\_brochure\\_en\\_hq\\_20210819.pdf](https://www.creaform3d.com/sites/default/files/assets/brochures/files/handyscan3d_silver_series_brochure_en_hq_20210819.pdf) (accessed: Jun. 2 2022.550Z).
- [165] *MeshLab*. [Online]. Available: <https://www.meshlab.net/> (accessed: Jun. 5 2022.774Z).
- [166] Yue Wang and Justin M. Solomon, “Deep Closest Point: Learning Representations for Point Cloud Registration,”
- [167] H. Sobreira *et al.*, “Map-Matching Algorithms for Robot Self-Localization: A Comparison Between Perfect Match, Iterative Closest Point and Normal Distributions Transform,” *J Intell Robot Syst*, vol. 93, 3-4, pp. 533–546, 2019, doi: 10.1007/s10846-017-0765-5.
- [168] E. Pérez, S. Salamanca, P. Merchán, and A. Adán, “A comparison of hole-filling methods in 3D,” *International Journal of Applied Mathematics and Computer Science*, vol. 26, no. 4, pp. 885–903, 2016, doi: 10.1515/amcs-2016-0063.
- [169] P. Liepa, “Filling Holes in Meshes,” in *Eurographics Symposium on Geometry Processing*, 2003.
- [170] M. Kazhdan and H. Hoppe, “Screened poisson surface reconstruction,” *ACM Trans. Graph.*, vol. 32, no. 3, pp. 1–13, 2013, doi: 10.1145/2487228.2487237.
- [171] H. Hoppe, T. DeRose, T. Duchamp, J. McDonald, and W. Stuetzle, “Mesh optimization,” in *Proceedings of the 20th annual conference on Computer graphics and interactive techniques - SIGGRAPH '93*, Not Known, 1993, pp. 19–26.

- [172] J. Vollmer, R. Mencl, and H. Muller, “Improved Laplacian Smoothing of Noisy Surface Meshes,” *Computer Graphics Forum*, vol. 18, no. 3, pp. 131–138, 1999, doi: 10.1111/1467-8659.00334.
- [173] Creaform, *VXinspect: dimensional inspection software module*. [Online]. Available: <https://www.creaform3d.com/en/metrology-solutions/vxinspect-dimensional-inspection-software-module> (accessed: May 30 2022.888Z).
- [174] GitHub, *GitHub - cnr-isti-vclab/meshlab: The open source mesh processing system*. [Online]. Available: <https://github.com/cnr-isti-vclab/meshlab/blob/main/src/external/libigl-2.3.0/include/igl/hausdorff.h> (accessed: Jun. 18 2022.865Z).
- [175] R. Shonkwiler, “Computing the Hausdorff set distance in linear time for any  $L_p$  point distance,” *Information Processing Letters*, vol. 38, no. 4, pp. 201–207, 1991, doi: 10.1016/0020-0190(91)90101-M.



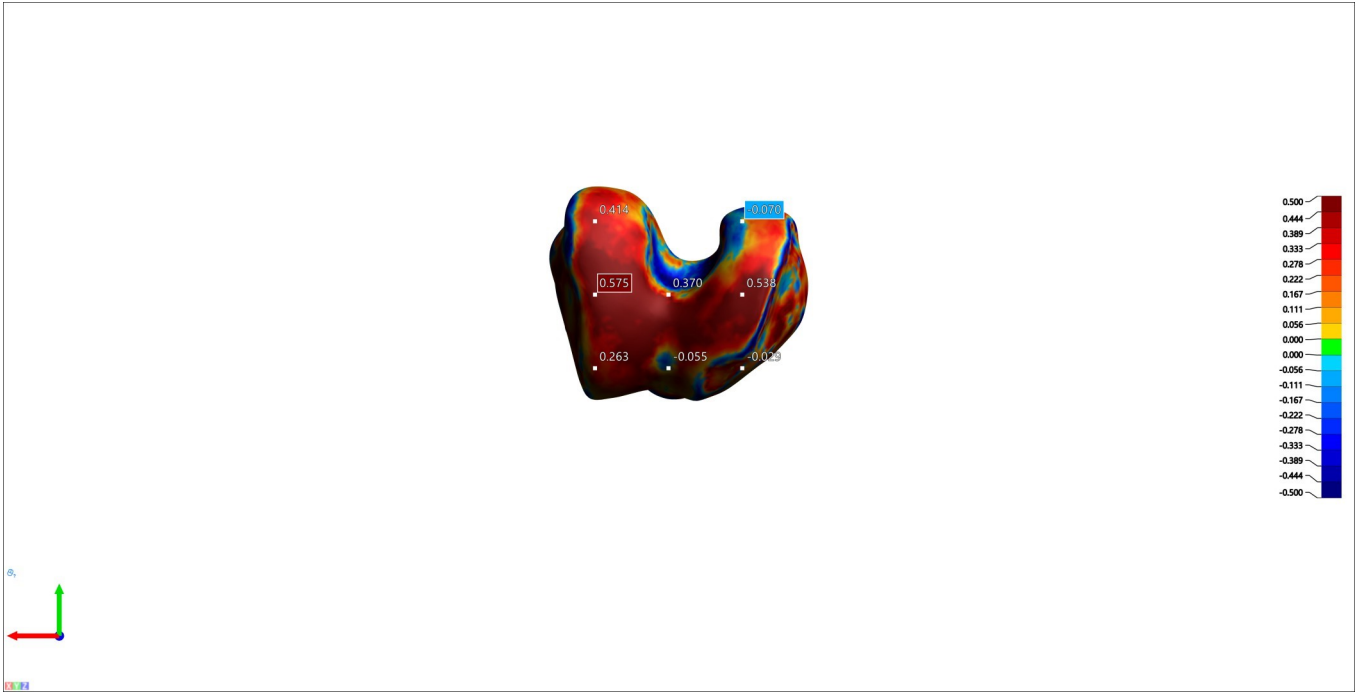
# APPENDIX A

## Einscan femur models

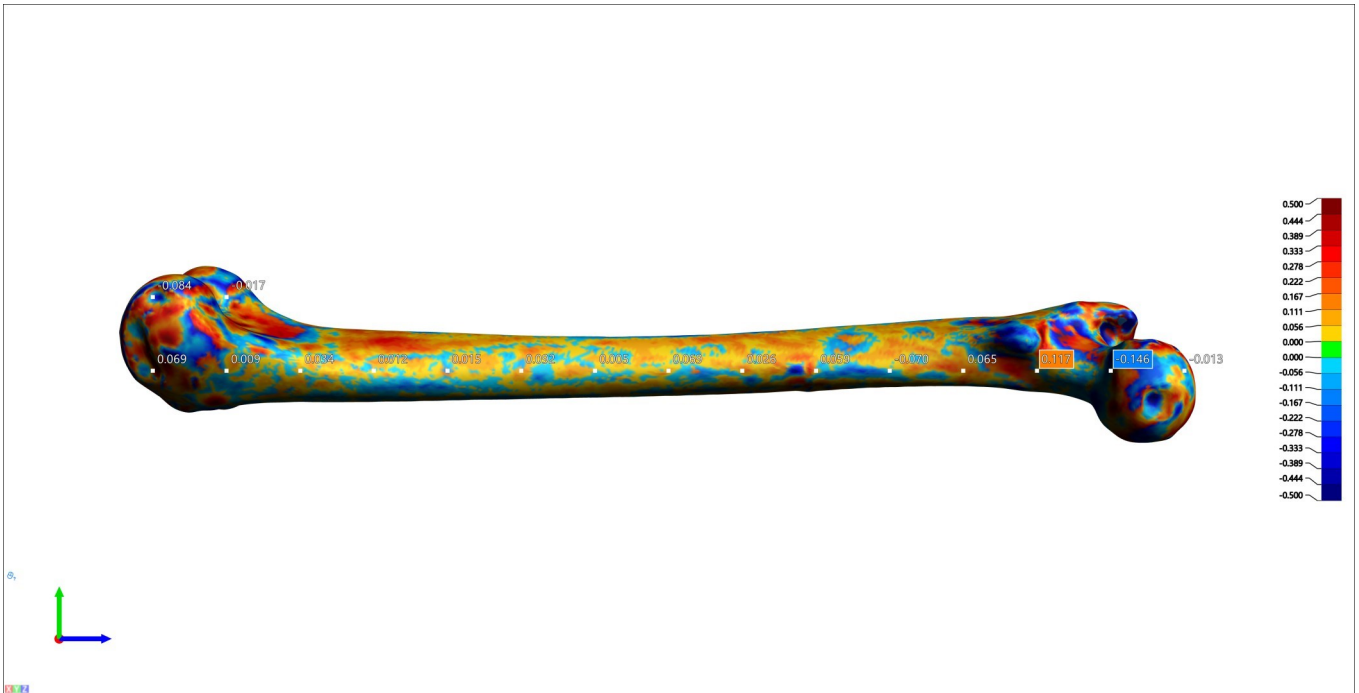
### Snapshot 1



### Snapshot 2



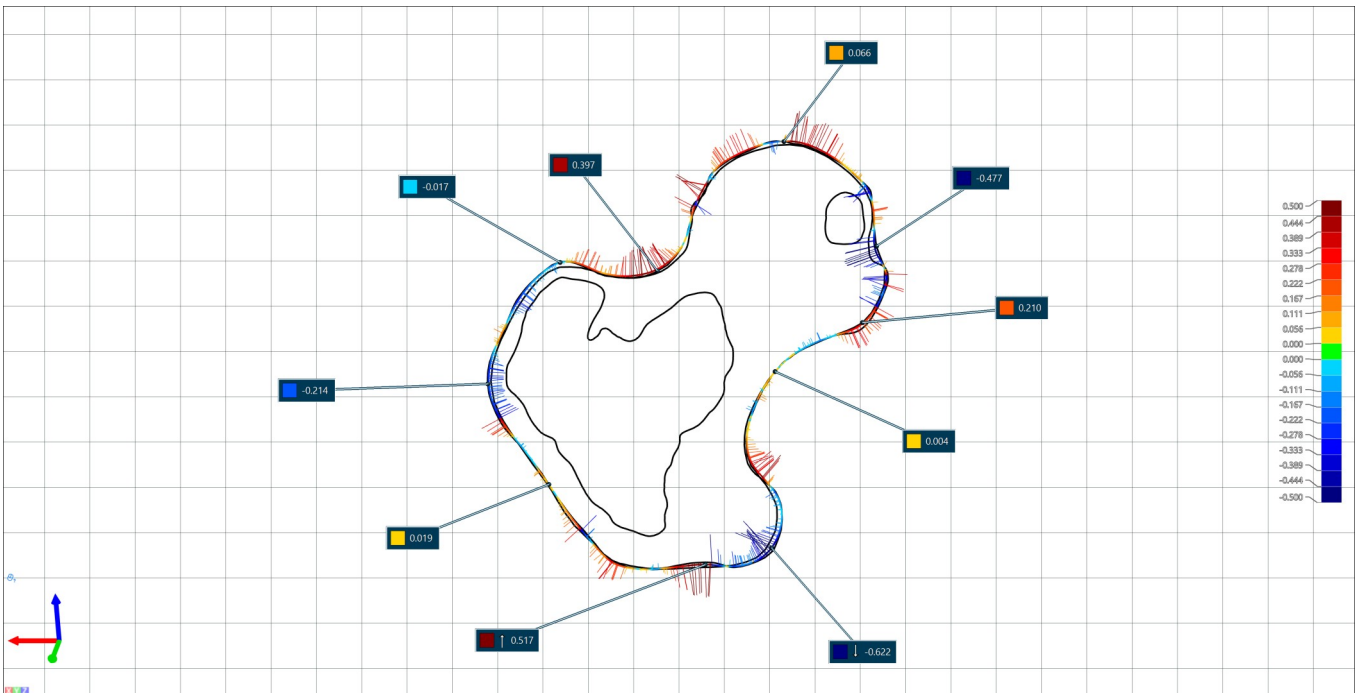
### Snapshot 3



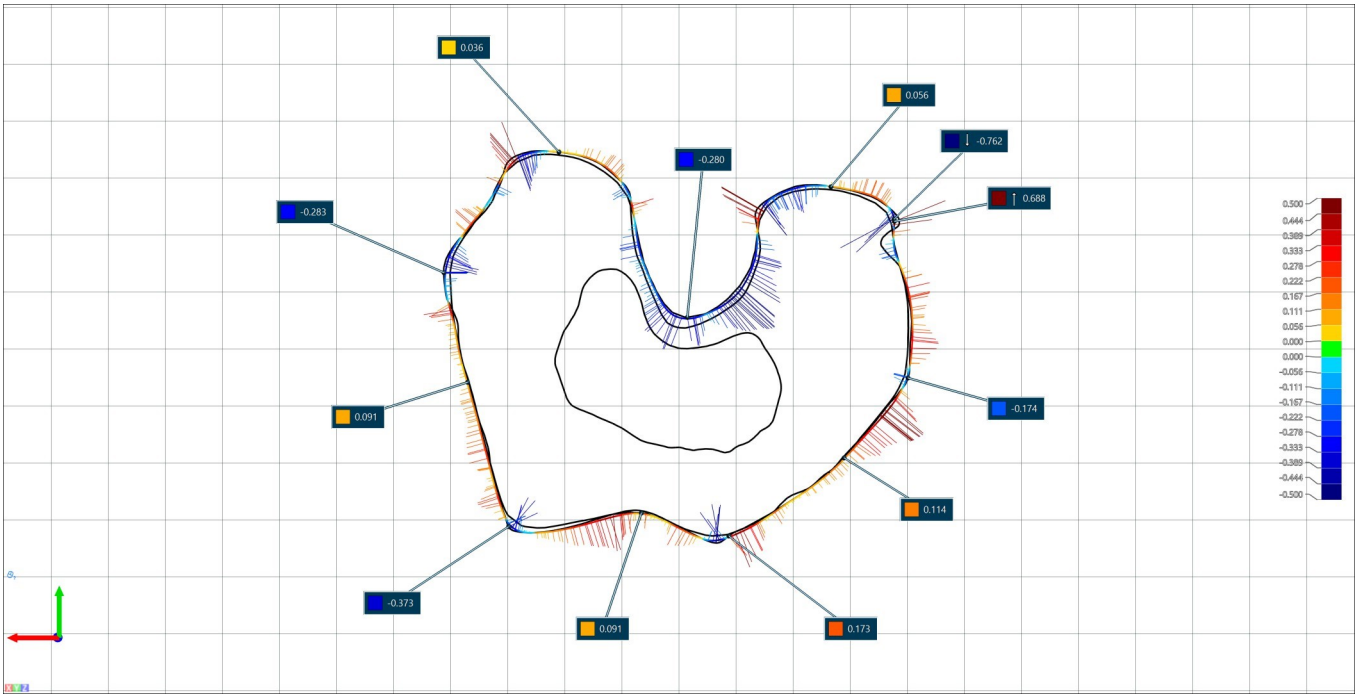
### Snapshot 4



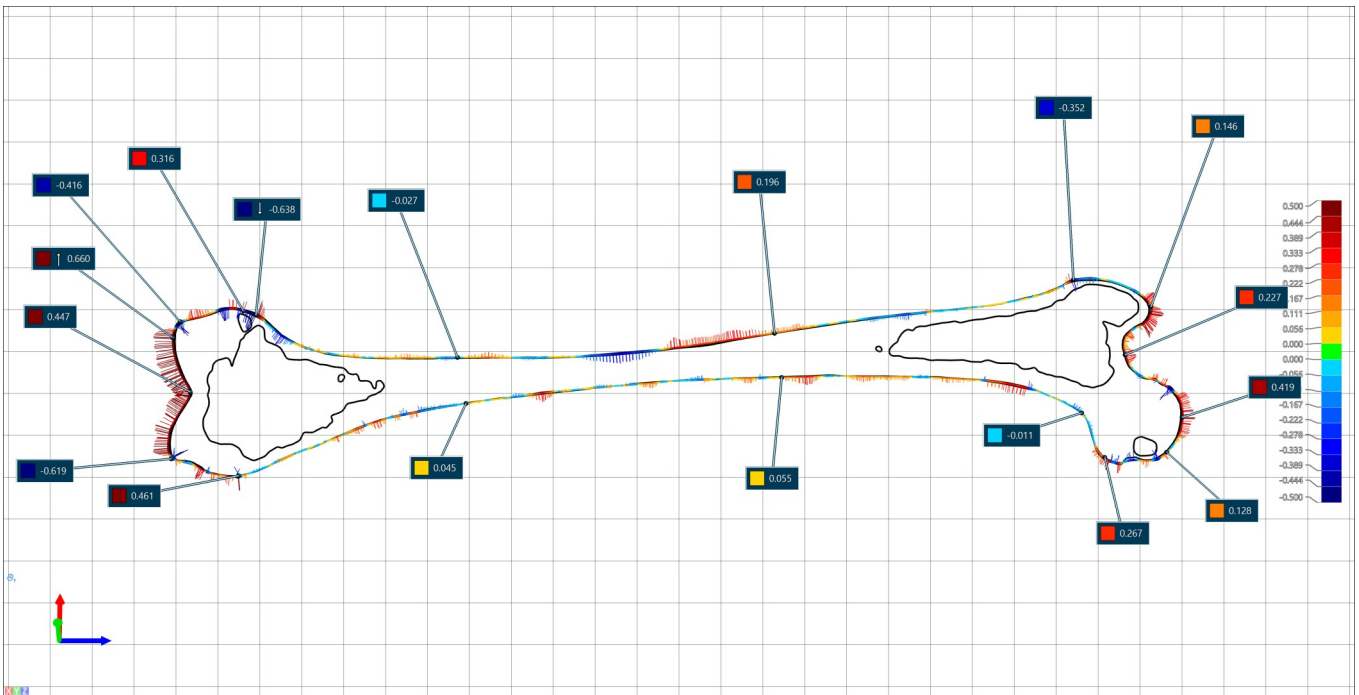
## Snapshot 5



## Snapshot 6



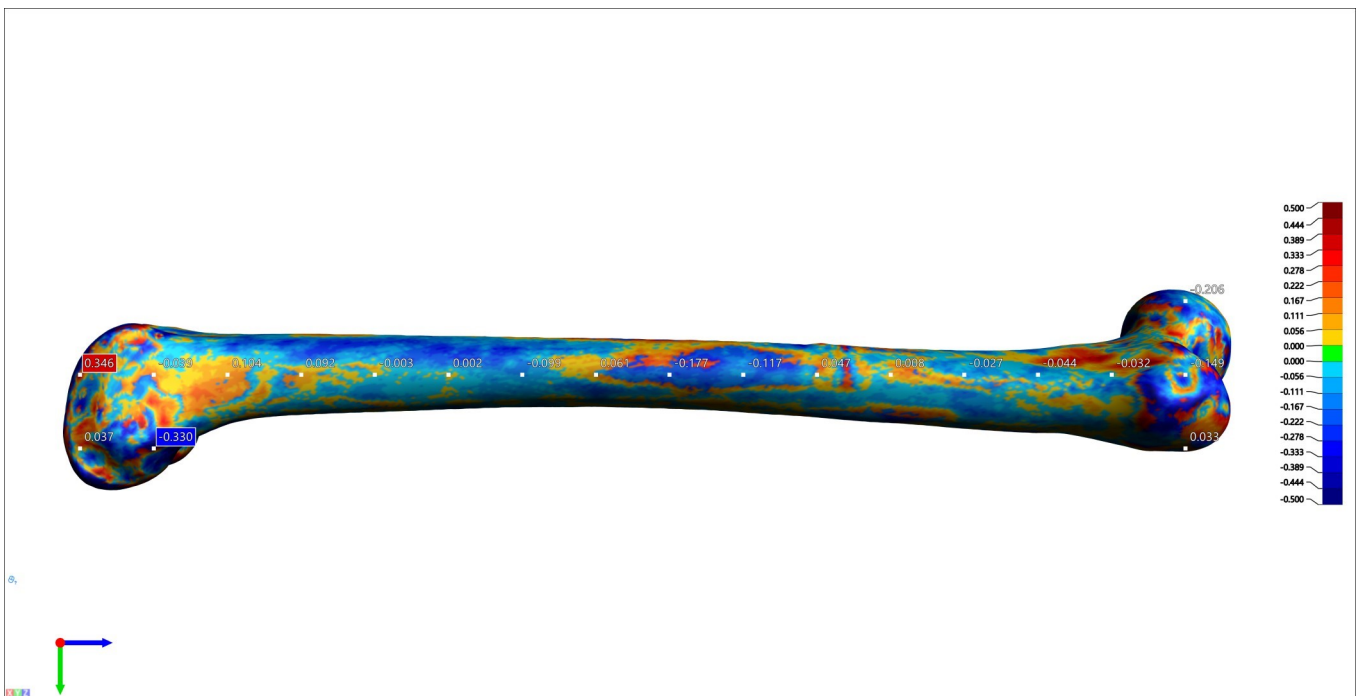
## Snapshot 7



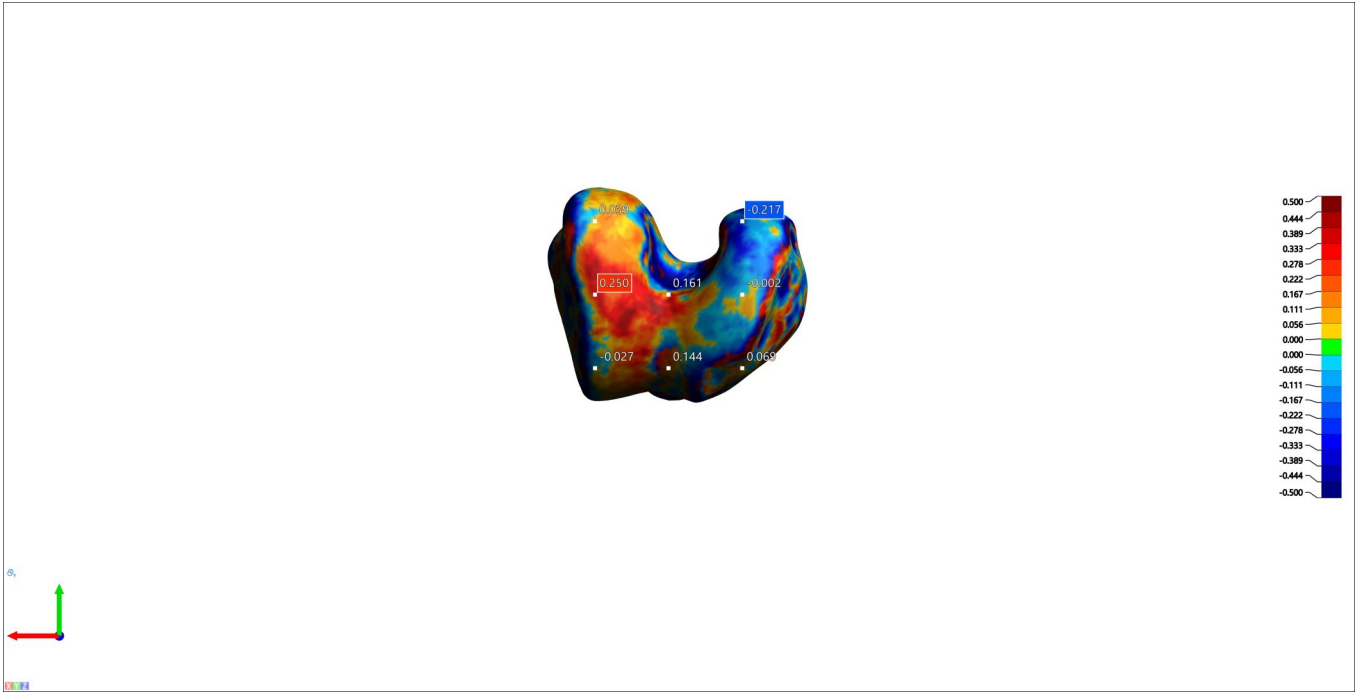
# APPENDIX B

## Handyscan femur models

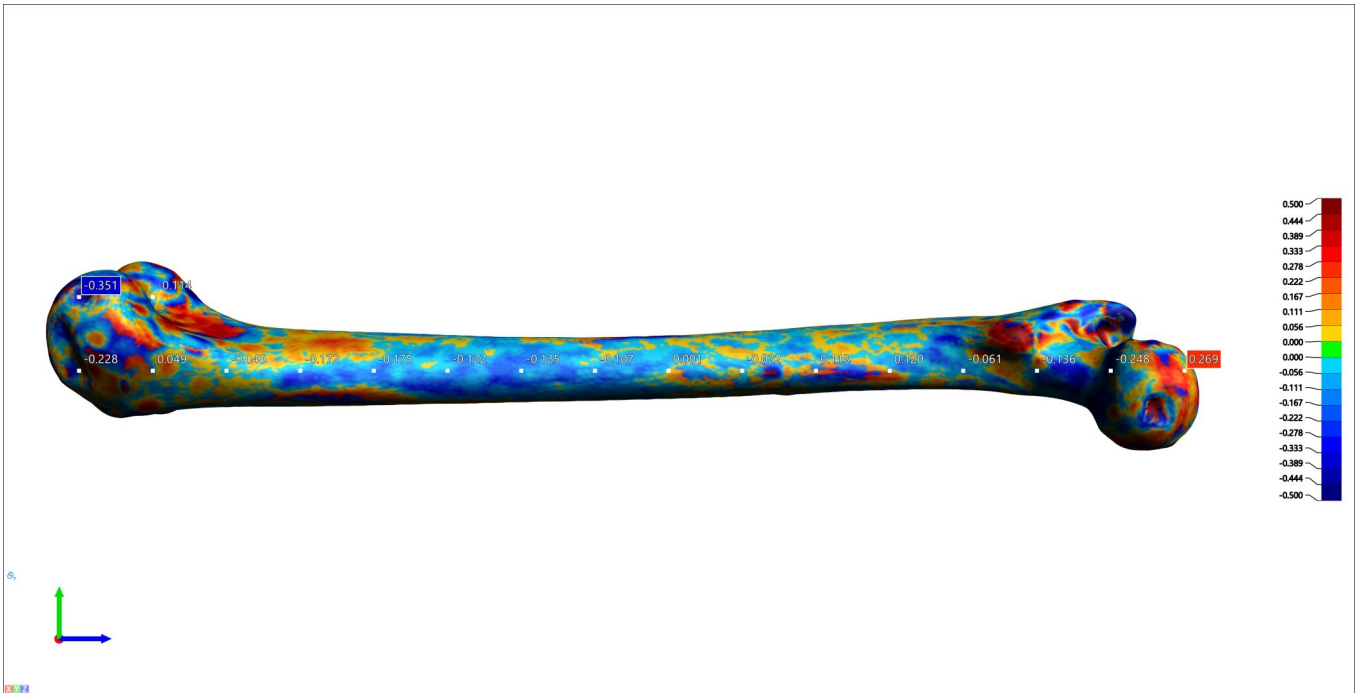
### Snapshot 1



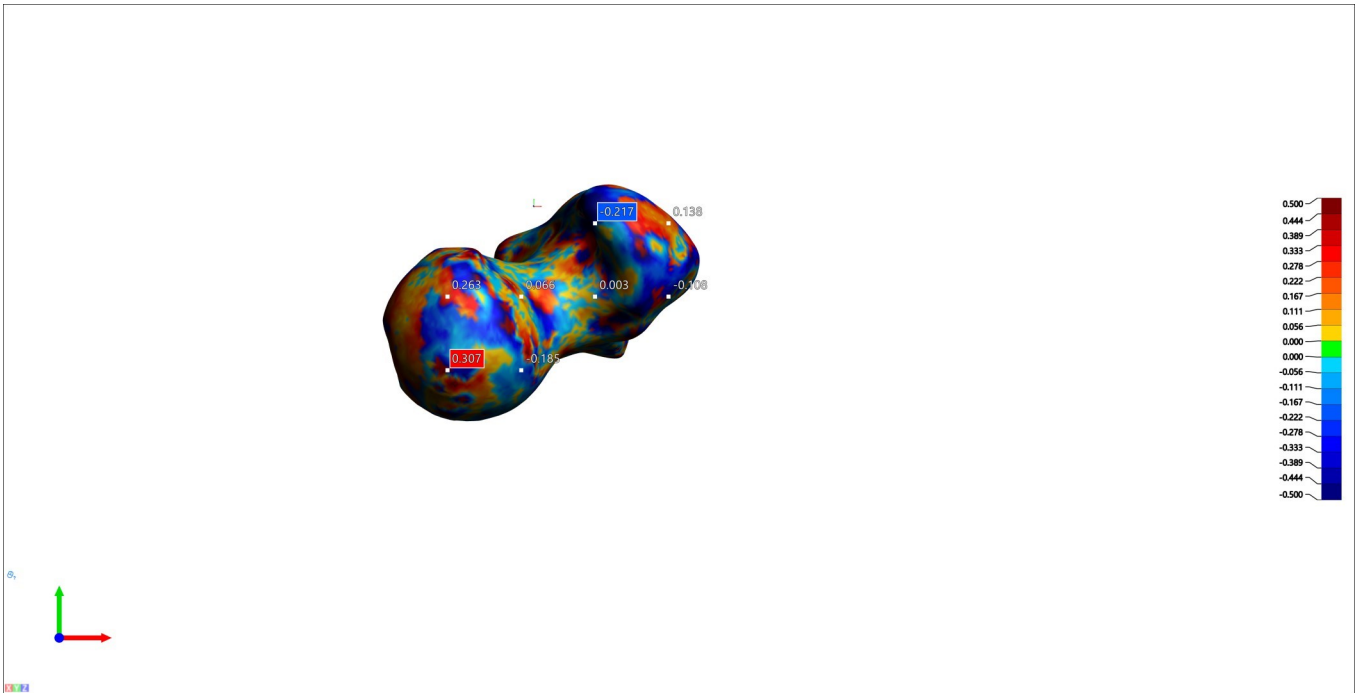
### Snapshot 2



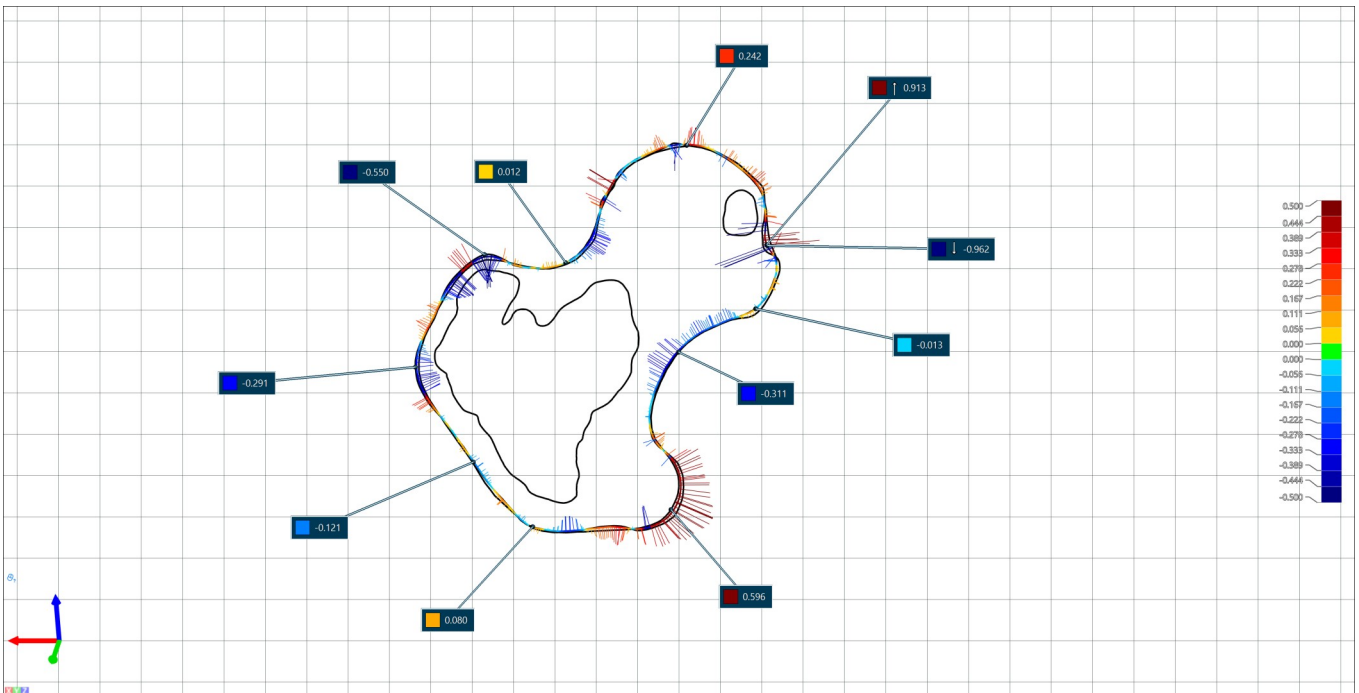
### Snapshot 3



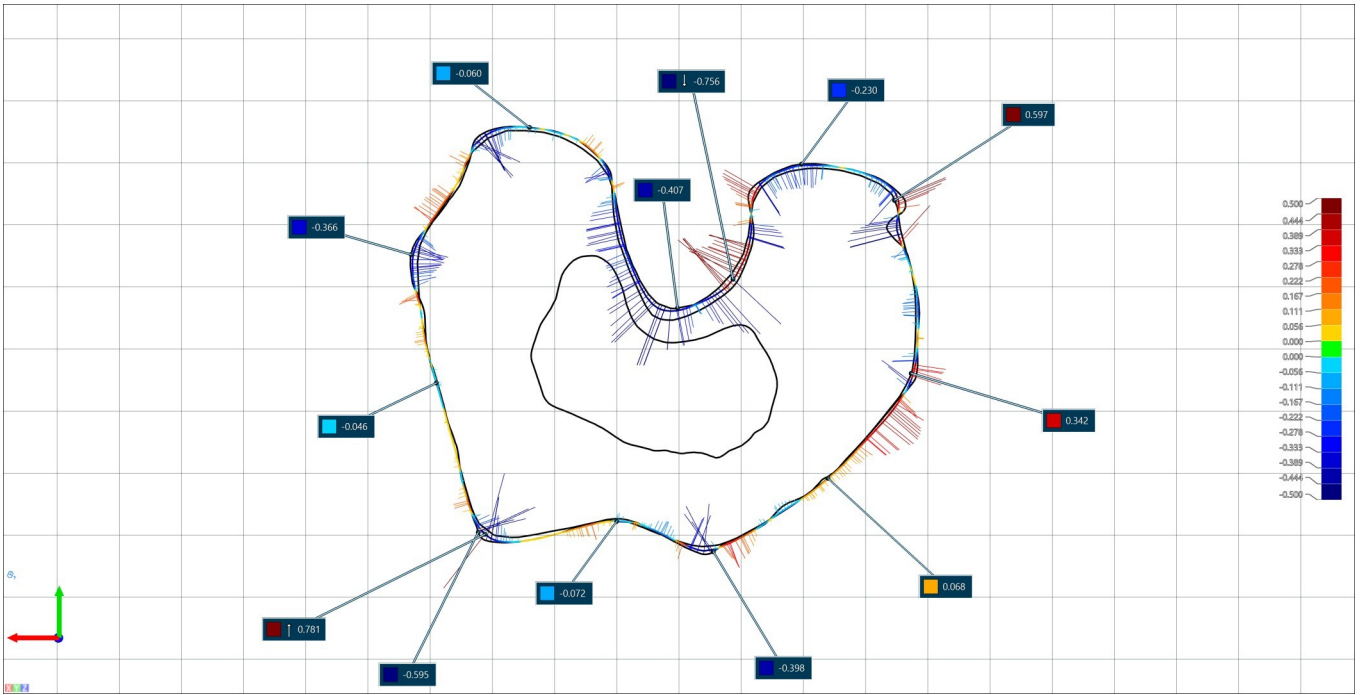
### Snapshot 4



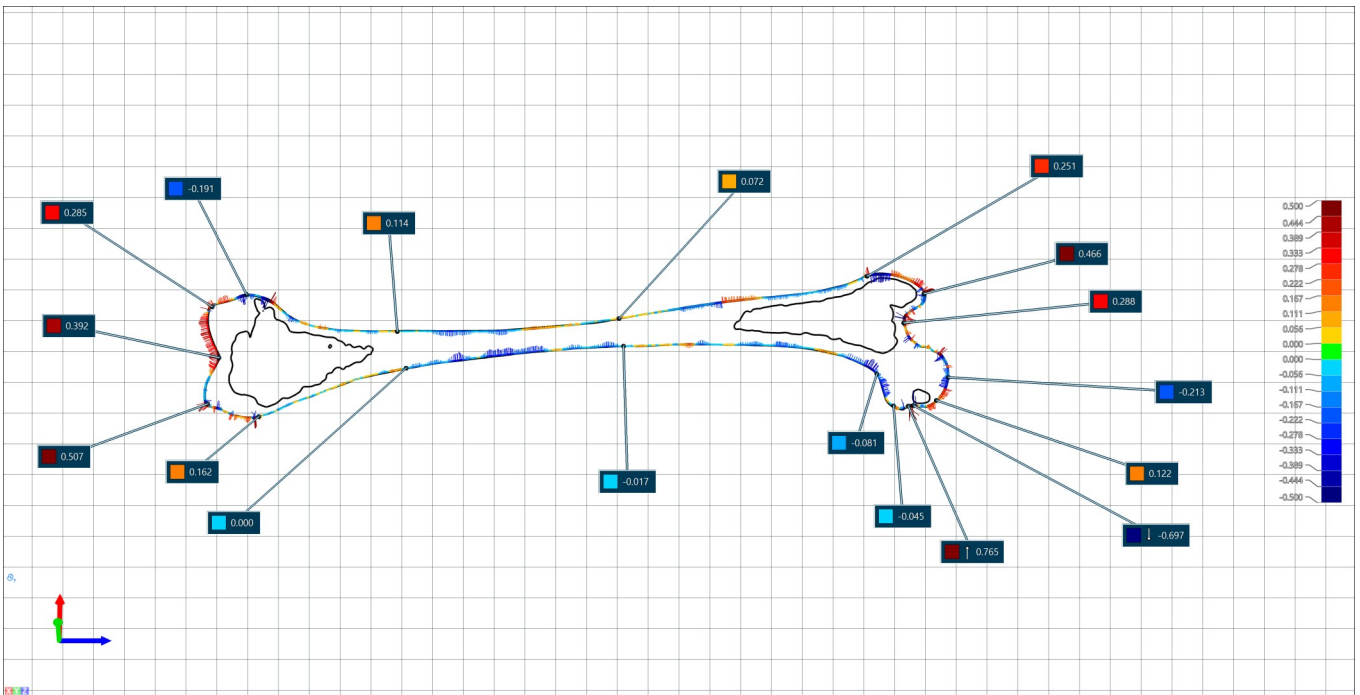
## Snapshot 5



## Snapshot 6



## Snapshot 7





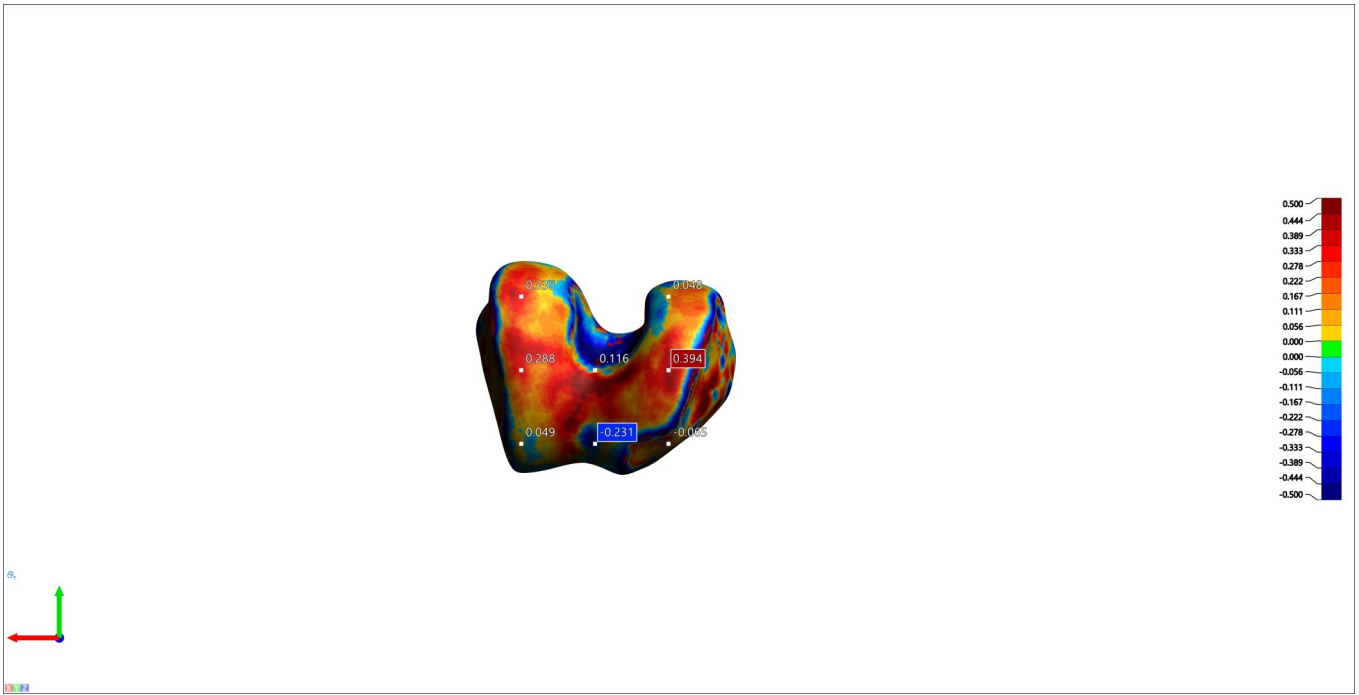
# APPENDIX C

## Artec EVA-M femur models

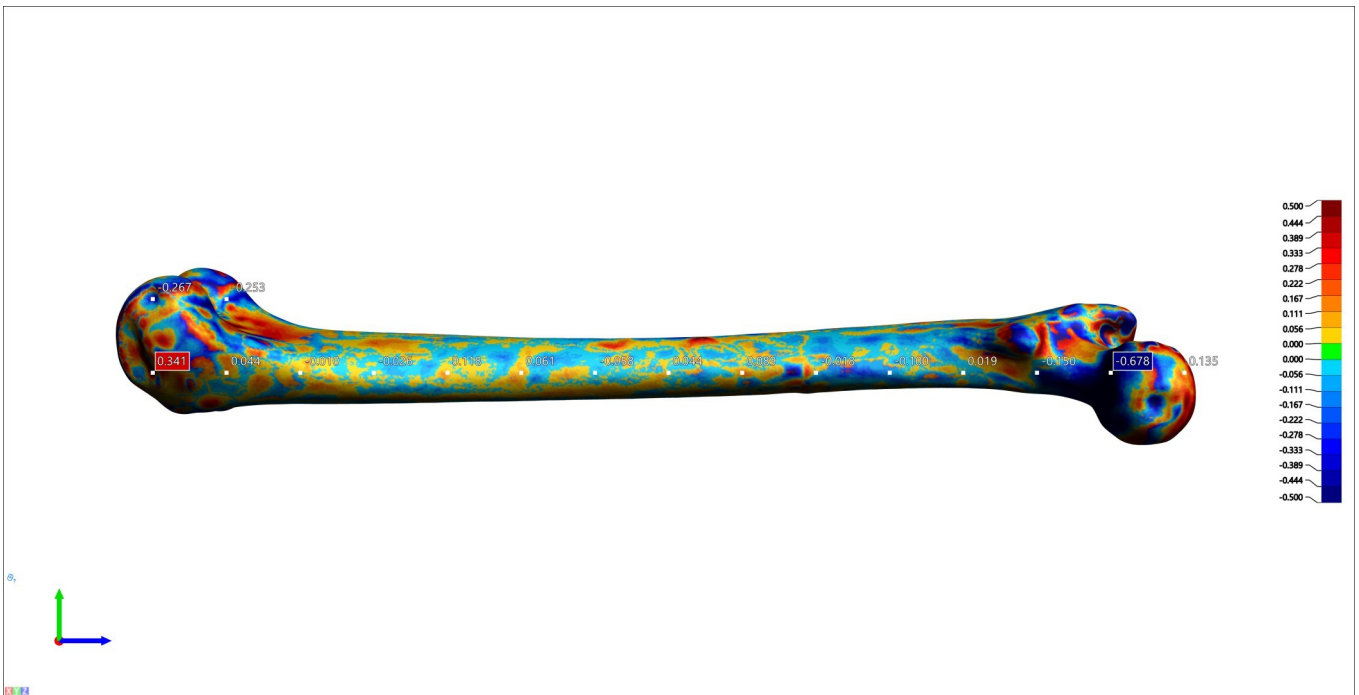
### Snapshot 1



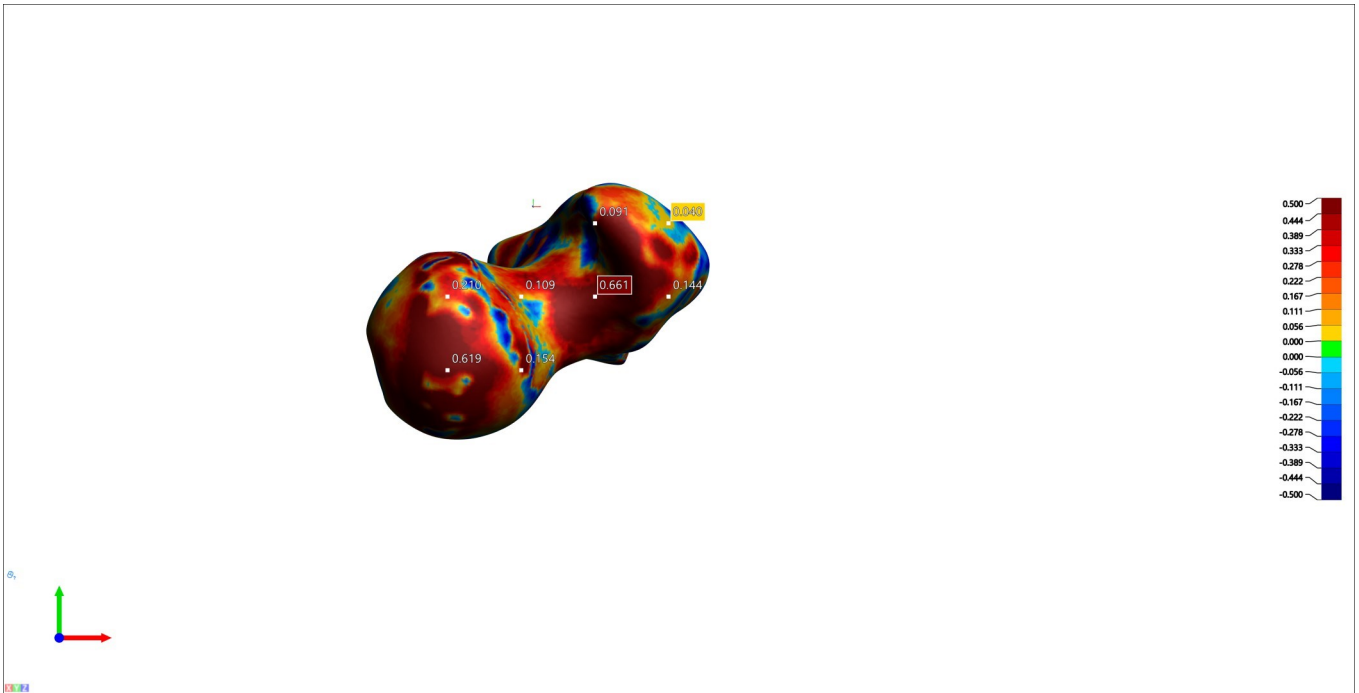
### Snapshot 2



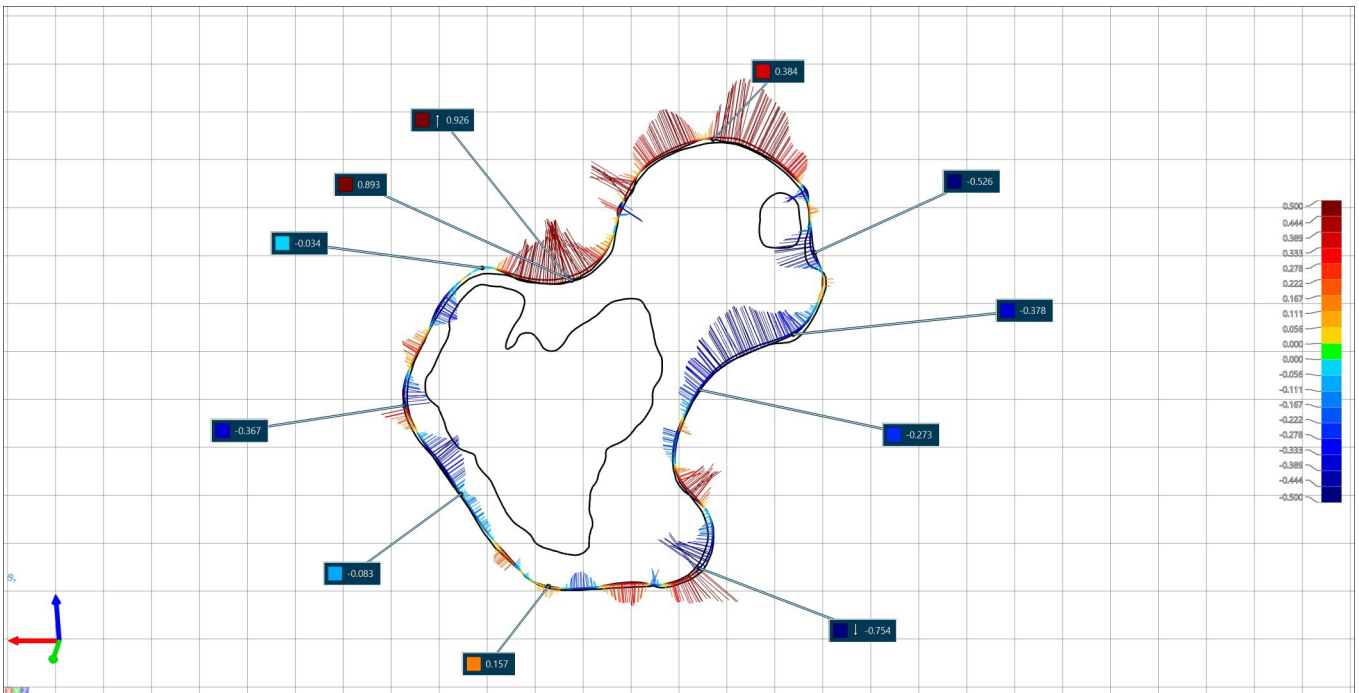
### Snapshot 3



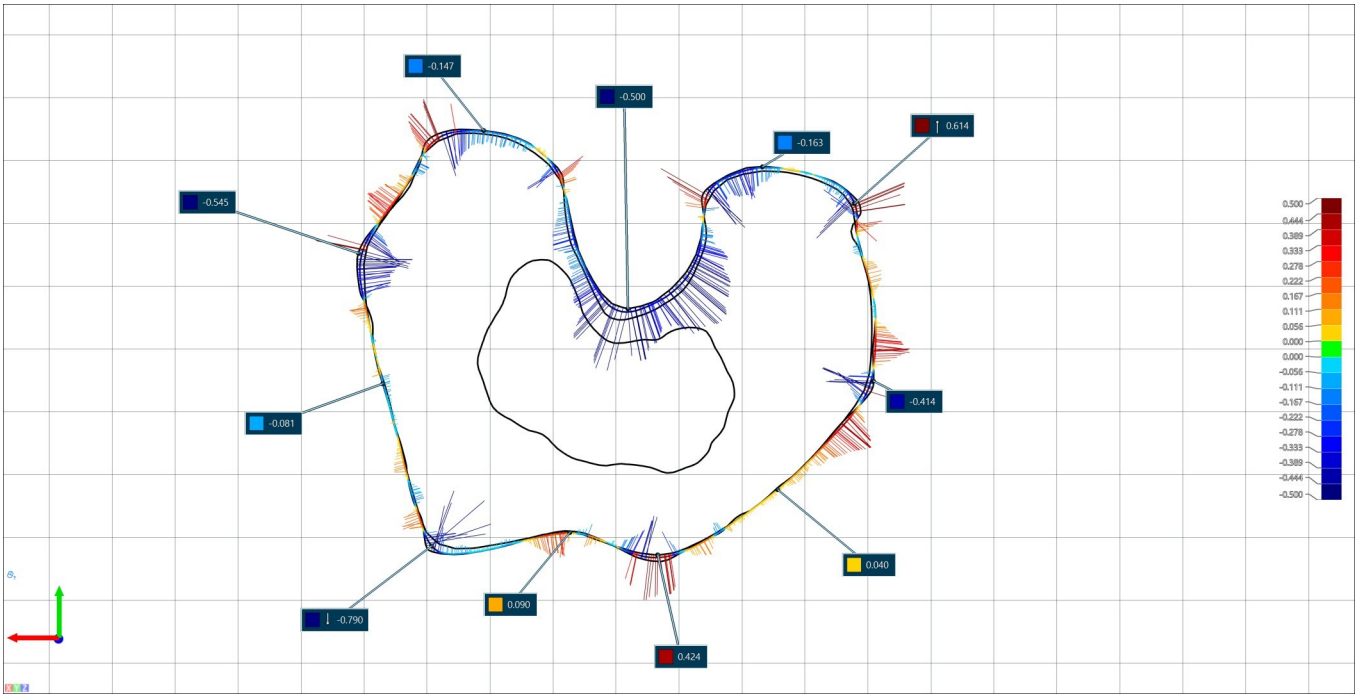
### Snapshot 4



## Snapshot 5



## Snapshot 6



## Snapshot 7

